SYNTHESIS AND BIOLOGICAL EVALUATION OF NOVEL ANTI-TUMOUR (*E*)-STYRYLSULFONYL METHYLPYRIDINES

TIANGONG LU, BSc.

Thesis submitted to the University of Nottingham
for the degree of Doctor of Philosophy

DECEMBER 2014

Abstract

ON01910.Na (Rigosertib, Estybon®), a styryl benzylsulfone, is a Phase III stage anti-cancer agent. This non-ATP competitive kinase inhibitor has multi-targeted activity, promoting mitotic arrest and apoptosis. Extensive Phase I/II studies with ON01910.Na, conducted in patients with solid tumours and haematological cancers demonstrate excellent efficacy. However, issues remain affecting its development. These include incomplete understanding of anti-tumour mechanisms, low oral bioavailability and unpredictable pharmacokinetics.

In an attempt to improve drug-likeness and ADME properties of ON01910.Na analogues, a novel series of (E)-styrylsulfonyl methylpyridine derivatives was designed and synthesised. The SAR of this novel series is discussed. The lead compounds TL-68, TL-77, and AH-123 are highly potent mitotic inhibitors. Their selective cytotoxicity to cancer cells was identified in the screening cascade. Impressively, TL-77 possesses excellent pharmaceutical properties, with improved oral bioavailability when compared to ON01910.Na.

The detailed cellular mechanisms of TL-77 were further investigated in comparison with ON01910.Na. TL-77 exhibits potent anti-proliferative activity against a wide range of human tumour cell lines, and demonstrated > 2 fold greater potency in cancer cell lines over normal cells.. Cell cycle analyses reveal that TL-77 evokes profound G2/M cell cycle arrest at $\geqslant$ 6 h in cancer cells, followed by the onset of apoptosis. In cell-free conditions, TL-77 as well as ON01910.Na potently inhibits tubulin polymerization. Mitotically arrested cells display multipolar spindles and misalignment of chromosomes, indicating

TL-77 interfere mitotic spindle assembly in cancer cells. These effects are accompanied by induction of DNA damage, inhibition of Cdc25c (Ser198) phosphorylation [indicative polo-like kinase 1 (Plk1) inhibition], and downstream inhibition of cyclin B1. However, kinase assays failed to confirm the inhibition of Plk1. Non-significant effects on PI3K/AKT signal transduction are observed after TL-77 treatment. Analysis of apoptotic signalling pathways reveals that TL-77 down-regulates expression of B-cell lymphoma 2 (Bcl-2) family proteins [Bid (BH3 interacting-domain death agonist), Bcl-xl (B-cell lymphoma-extra large) and Mcl-1 (induced myeloid leukaemia cell differentiation protein)] and stimulates caspase activation. These effects are comparable to those elicited by ON01910.Na. Unlike ON01910.Na, however, TL-77 causes preferential toxicity in cancer cells when compared to normal cells and mediates rapid mitotic inhibitory effects.

In summary, selective in vitro anti-tumour activity and multi-faceted mechanisms of action of a novel molecule TL-77 have been identified, presenting a strong rationale for further development of (E)-styrylsulfonyl methylpyridine derivatives as therapeutic agents for cancer.

Acknowledgements

First and foremost, I would like to express my sincerest gratitude to my two supervisors, Dr. Charles Laughton and Dr. Tracey Bradshaw. I appreciate all their supervision, encouragement, and immense knowledge that enabled me to develop an understanding of the subject throughout my Ph.D, and their assistance in writing reports (i.e., year reports, journal manuscript and this thesis).

I heartily thank my previous supervisor, Prof. Shudong Wang for offering me this research project and her kindly guidance. I also appreciate her help for providing the results of biopharmaceutical assessment and pharmacokinetic studies in this thesis.

I would like to thank all of my colleagues in chemistry corridor, C57 and A31/32 in CBS for their friendship and for providing an enjoyable working atmosphere. I particularly want to thank Dr. Shiliang Huang, Dr. Hilary Collins, Dr. Xiangrui Liu, Dr. David Foley, Dr. Abdullahi Abbas, Dr. Osama Chahrour, Dr. Xiaoxia Guo and Vijay Raja for their help and invaluable advice.

My time at Nottingham was made enjoyable in large part due to many friends who have become a part of my life. I am grateful for time spent with roommates and friends. During the final stages of study, my time was also enriched by the Nottingham Archery Society and Latin, Ballroom and Salsa Society.

Finally, this work could not have been possible without the faith and support of my families. I would like to take this opportunity to thank my parents, who raised me with a love of science, supported me in all my pursuits and always be proud of me. My greatest thanks go to my husband and best friend, Shan Huang, who is such a wonderful supporter through this whole exciting “journey”, and whose companion for me until midnight in the lab is so appreciated. Thank you!

This thesis is dedicated with love to my parents.

Abbreviations

ADME	Absorption, distribution, metabolism and excretion
Akt	Protein Kinase B (PKB)
AML	Acute myeloid leukemia
aPKs	Atypical Protein Kinases
ATP	Adenosine triphosphate
Bax	Bcl-2-associated X
Bcl-2	B-cell CLL/Lymphoma 2
Bid	BH3 interacting-domain death agonist
BSA	Bovine serum albumin
CDK	Cyclin-depend Kinase
DCM	Dichloromethane
DMF	N, N-dimethylformamide
DMSO	Dimethyl sulfoxide
DNA	Deoxyribonucleic acid
ECL	Enzymatic chemiluminescence
ePKs	Eukaryotic Protein Kinases
ER	Oestrogen receptor
EtOAc	Ethyl acetate
EtOH	Ethanol
FBS	Foetal bovine serum
FITC	Fluorescein isothiocyanate
G1 phase	Gap phase I
G2 phase	Gap phase II, pre-mitotic phase of cell cycle
GI_{50}	The concentration required to achieve 50% growth inhibition
H2AX	H2A histone family, member X

HCl	Hydrogen chloride
HER2	Human Epidermal Growth Factor Receptor 2
HUVEC	Human umbilical cord vein endothelial cell;
K_2CO_3	Potassium carbonate
Mcl-1	Induced myeloid leukemia cell differentiation protein
M phase	Mitosis cell cycle phase
MDS	Myelodysplastic syndrome
MeOH	Methanol
$MgCl_2$	Magnesium chloride
m.p.	Melting point
MS	Mass spectrometry
mTOR	Mammalian target of rapamycin
MTT	3-(4,5-dimethylthiazol-2-yl)-2,5-diphenyltetrazolium bromide
NaOH	Sodium hydroxide
NBS	N-Bromosuccinimide
NMR	Nuclear magnetic resonance
ON01910.Na	(E)-2-((2-methoxy-5-(((2,4,6-trimethoxystyryl)sulfonyl)methyl)phen-yl)amino)-acetate, sodium salt
PARP	Poly (ADP-ribose) polymerase
PBD	Polo box domain
PBS	Phosphate Buffered Saline
PD study	Pharmacodynamic study
PDK	Phosphoinositide-dependent protein kinase
PE	Petroleum ether
PI	propidium iodide
PI3K	PI 3-Kinase, phosphatidylinositide 3-kinases
PK	Protein kinase

PK study	Pharmacokinetic study
Plk	Polo-like kinase
PRAS40	Proline-rich Akt substrate of 40 kDa
PTEN	Phosphatase and tensin homolog
Rb	Retinoblastoma protein
RNA	Ribonucleic acid
RNAi	RNA interference
r.t.	Room temperature
SAR	Structure-activity relationship
Ser	Serine
TBS	Tris Buffered Saline
THF	Tetrahydrofuran
TL-77	(E)-N-(2-methoxy-5-((2,4,6-trimethoxystyrylsulfonyl)methyl)pyridin-3-yl)methanesulfonamide.
TLC	Thin layer chromatography

Contents

Table of Figures

Table of Tables

Table of Schemes

1 Introduction

1.1 Cancer

Cancer is a global concern. In 2012, about 14.1 million people were diagnosed with cancer worldwide, leading to 8.2 million deaths from cancer in the same year. (WTO media report, 2014) According to the latest statistics from Cancer Research UK, cancer has been and still is the major cause of death in England and Wales.[1]

Cancer is a genetic disease that occurs when the information in cellular DNA is altered and subsequently leads to aberrant patterns of gene expression.[2] The process of cancer development, carcinogenesis, generally involves three essential stages: initiation, promotion, and progression. Initial changes in carcinogenesis are irreversible genetic changes. By generating a DNA adduct formation, initiators cause either activation of proto-oncogenes or loss of tumour-suppressor genes, giving proliferative advantage. In the next stage, tumour promotion is induced by tumour promoters that enhance the selective clonal expansion of initiated cells. Tumour promoters are generally non-mutagenic; however, they can reduce the latency period for tumour formation, enhance proliferation or improve the sensitivity of cells to an initiator. During the third stage, progression, further genetic and epigenetic mutations selecting for increasingly aggressive disease occur due to the malignant conversion. Cells progress to malignant tumour with further degrees of independence, invasiveness, eventually invade adjacent tissue / vessels, and metastasis to distant sites seeding secondary tumours and metastatic disease.[3]

1.1.1 Hallmarks of Cancer

The major goal of cancer research is to understand the causation of malignancy, and translate this knowledge into the development and improvement of cancer treatments.[4, 5] In two landmark reviews "The Hallmarks of Cancer" in 2000 and 2011, Douglas Hanahan and Robert A. Weinberg summarized the essence of several biological capabilities acquired during the multistep development of human malignancies.[6, 7] The hallmarks of cancer provide a solid foundation for understanding the biology of cancer and are described in turn below.

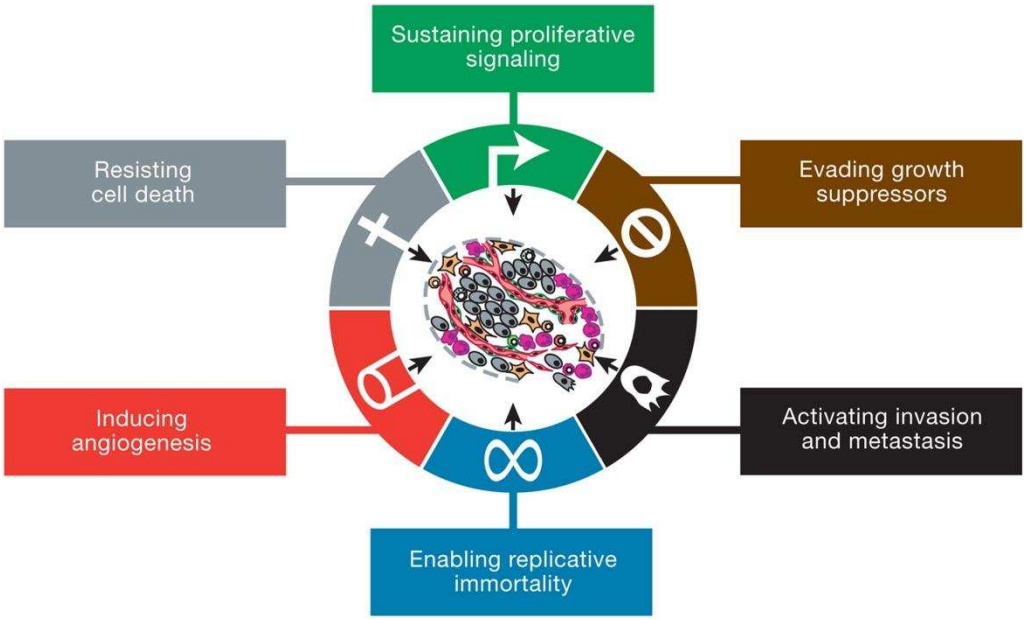

Figure 1.1 The six hallmarks of cancer[7]

1.1.1.1 Sustaining Proliferative Signalling

Mitogenic growth signals (GS) stimulate cell proliferation by directly controlling the initiation of cell cycle. In normal tissues, the production and release of growth-promoting signals are strictly controlled to maintain a homeostasis of cell population and functions.[7] However, the growth signalling pathways are suspected to suffer deregulation in all human tumours.[6] Cancer cells can sustain proliferative signalling by mimicking normal growth

signalling. They deregulate these signals and achieve autonomy through several molecular strategies;[6, 7]

- producing growth factor ligands themselves, resulting in autocrine proliferative stimulation;
- stimulating signals normal cells within the tissue to induce expression of growth factors;
- increasing cells' sensitivity to growth factors by overexpressing or structurally altering surface receptor proteins;
- activating components of intracellular circuits operating downstream of these receptors.

1.1.1.2 Evading Growth Suppressors

In normal cells, cell proliferation is a highly regulated process wherein multiple anti-proliferation signals operate to maintain cellular quiescence and tissue homeostasis. These anti-proliferation signals can block proliferation in two ways; by forcing a proliferative cell out of cycle into quiescence (G_0) phase, or by entering into a post-mitotic state, which usually involves terminally differentiation of the cell.[6] (For cell cycle, please refer to Figure 1.2)

Most cancer cells circumvent normal growth suppressors in order to sustain their proliferative capacity. p53 and retinoblastoma protein (pRb) operate the two key complementary tumour-suppressor pathways that control cellular responses of apoptosis and cellular senescence, and are most commonly dysregulated in cancer cells.[7, 8] The Rb protein is a critical gatekeeper of the cell cycle, maintaining cell division at a healthy pace. Stress signals such as oncogenes induced INK4 (Inhibitors of CDK 4) and Cip/Kip (CDK interacting protein/Kinase inhibitory protein) family proteins, which specifically inhibit

the activity of CDKs (Cyclin-Dependent Kinases) and thereby prevent the phosphorylation of Rb.[8, 9] When in a hypophosphorylated state,, Rb blocks entry of cells into S phase by sequestering and altering the function of the eukaryotic transcription factors (E2Fs), which regulate the transcription of many genes essential for progression from G1 to S transition.[8] Cancer cells evade the anti-proliferative signals by disrupting the pRb pathway.

While the Rb pathway receives antigrowth signals, mainly from outside of the cell, p53 is activated by intracellular operating systems. In response to DNA damage and cellular stresses, p53 functions as a central regulator causing cell-cycle arrest, and triggers apoptosis.[7] Loss of p53 allows propagation of damaged DNA and aberrant cell cycle progression.

1.1.1.3 Resisting Cell Death

The population expansion of cancer is determined by the rate of both cell proliferation and cell attrition. Apoptosis, autophagy and necroptosis are the three main types of programmed cell death. Apoptosis, as a major source of cell attrition, becomes a critical barrier to cancer development.[7]

Apoptosis is triggered and regulated through at least two principal pathways at many levels. The intrinsic pathway (mitochondrial pathway) is primarily regulated by Bcl-2 family proteins in response to the signals of survival factors, cell stress and injury. In the Bcl-2 family, a balance is established between two kinds of regulators, the anti-apoptotic proteins (Bcl-2, Bcl-xL, Bcl-w, A1 and Mcl-1,), which prevent programmed cell death by guarding mitochondrial integrity and regulating the activation of several caspases, and the pro-apoptotic proteins (Bax family and BH3-only family), which block the protective effect of apoptosis inhibitors and initiate apoptosis. This balance

arbitrate the life-or-death decision.[10] Apoptosis is triggered when the protective buffer of anti-apoptotic proteins and pro-apoptotic proteins is breached. The mitochondria are permeabilized and damaged, causing the release of pro-apoptotic factors. The most important factor, cytochrome c, interacts with the cell-death adaptor Apaf-1 (apoptotic protease-activating factor 1), subsequently activate caspase-9.

The extrinsic pathway (death receptor pathways), on the other hand, is induced by receiving and processing extracellular death-inducing signals. For instance, the death receptors on the cell surface, such as Fas ligand, are ligated with their cognate ligands, Fas receptor, forming the 'death-inducing signalling complex' (DISC). This complex subsequently activates caspase-8.

By activating two "gatekeeper" caspases (caspase-9 and -8, respectively), each pathway initiates a cascade of downstream effector caspases (caspase-3, and -7) to induce the multiple cellular changes associated with the apoptotic programme.[7, 11, 12]

Cancer cells can evade apoptosis through various strategies. Mutation and the consequent inactivation of p53 is one of the most common and occurs in more than 50 % of human tumours. For instance, the PI3K-AKT/PKB pathway, which transmits anti-apoptotic signals, is hyper-stimulated in a substantial fraction of cancers.[6] In addition, it is found that all the Bcl2 pro-survival proteins can promote tumorigenesis, and certain pro-apoptotic members can act as tumour suppressors.[10] The multiple apoptosis-avoiding mechanisms that found in tumour cells include: over-expression of pro-survival family members or down-regulation of pro-apoptotic factors to increase expression of survival signals and evade the extrinsic ligand-induced pathway.[11]

1.1.1.4 Enabling Replicative Immortality

The concept of the Hayflick limit has been widely accepted. It indicates normal cells have a finite replicative capacity in vivo, after which they reach the state of senescence or crisis.[7, 13] Cancer cell, on the other hand, acquires unlimited replicative potential giving rise to macroscopic tumours.[7]

It has been indicated that telomeres and telomerase are centrally involved in the capability for unlimited proliferation and tumorigenesis.[7, 14] Telomeres are composed of tandem hexanucleotide repeats and protect the end of the chromosome from recombination and degradation activities.[15] Due to the end-replication problem, telomeres progressively lose telomeric DNA sequences coupling to cell division in non-immortalized cells. This shortening eventually results in the eventual loss of telomere protection and leads to chromosomal instability, after which cells progress into senescence.[7, 15]

Telomerase is an enzyme that adds repetitive nucleotide sequences to the ends of DNA strands in telomere regions. Many observations indicate that the expression of telomerase is an essential requirement for cellular immortalization and unlimited proliferation characteristic of cancer cells.[14] Almost all human tumours (approximately 90%) have detectable telomerase activity, which is sufficient for the escape of proliferation barriers.[16] By aberrantly up-regulating telomerase, tumour cells can prevent telomere loss and maintain the replicative immortality.

1.1.1.5 Inducing Angiogenesis

The formation of new blood vessels helps tumour tissues to obtain essential nutrients and oxygen, as well as evacuate metabolic wastes. Therefore, this progress is critical for sustained tumour growth and metastasis. Tumour

angiogenesis is induced by a continually activated “angiogenic switch” in tumour cells, which is regulated by the balance of the anti- and the pro-angiogenic factors.[17] Vascular endothelial growth factors (VEGF), pro-angiogenic factors, are generally overexpressed by oncogene signals during an early stage of the development of invasive cancers.[7]

1.1.1.6 Activating invasion and metastasis

Tissue invasion and metastasis represent a multistage process of cancer cells escaping from the primary site and disseminating into distant organs. Pioneer cancer cells from an aggressive primary mass acquire the ability to penetrate the walls of lymphatic and/or blood vessels, circulate through the bloodstream, seed at distant sites by forming small nodules of cancer cells, continue to multiply, and eventually colonize to generate macroscopic tumour.[7, 18, 19] The process of tissue invasion and metastasis is not fully understood. Up to now, E-cadherin, a key cell-to-cell adhesion molecule, is the best characterized antagonist of invasion and metastasis. Down-regulation and mutation of E-cadherin are frequently detected in human carcinomas.[7]

1.1.1.7 Emerging hallmarks and characteristics

The continuous conceptual progress for understanding the biology of cancer has presented two emerging hallmarks: reprogramming of energy metabolism and evasion of immune destruction.

The anomalous characteristic of cancer cell energy metabolism was first observed by Otto Warburg.[7] Glycolysis is a major metabolic program for cancer cells. By increasing uptake and utilization of glucose (even in the presence of oxygen), leading to ‘‘aerobic glycolysis’’, cancer cells can reprogram their glucose metabolism, and thus their energy production to

support tumour growth more effectively.[20] The second emerging hallmark describes the ability of cancer cells to evade immunological destruction by T/B lymphocytes, macrophages or natural killer cells. However, these two emerging hallmarks still need to be fully generalized and validated.[7]

In addition, genome instability and tumour-promoting inflammation facilitate the acquisition of both main and emerging hallmarks and thus are endowed with two enabling characteristics.[7]

1.1.2 Targeting cell cycle progression

As reviewed in the previous session, aberrant regulation of the cell cycle leading to uncontrolled proliferation is one of the hallmarks of cancer. Over the decades, considerable effort has been expended to understand the molecular mechanisms driving the cell cycle, thereby aiding identification of potential targets for cancer therapeutics.[21]

1.1.2.1 The mammalian cell cycle

Maintaining genetic integrity, as the most important condition for the survival of species, is tightly controlled during the cell cycle. Orchestration of cell cycle progression involves a critical network that governs the DNA division and duplication (replication) to produce daughter cells, as well as integration of external and cellular pro- and anti-proliferative signals.[22, 23]

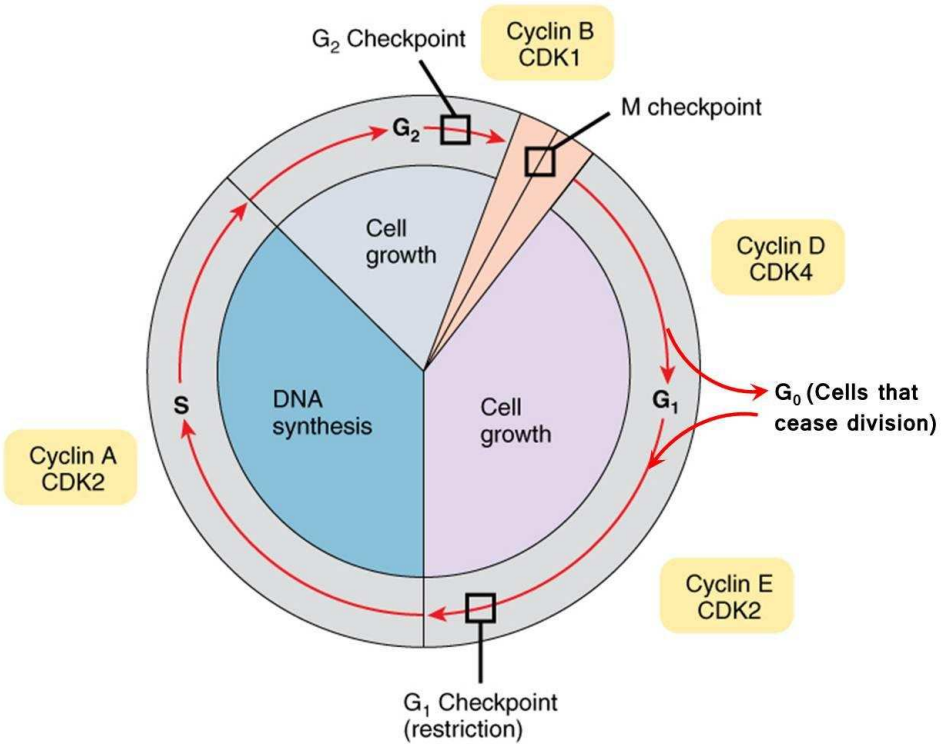

Figure 1.2 The mammalian cell cycle with cyclins and checkpoints

Progress in the eukaryotic cell cycle is driven by periodic activation of CDKs. The mammalian cell cycle consists of four phases: S-phase, M-phase, G1 and G2 phase. The different cyclins, specific for the G1-, S-, or M-phases of the cell cycle, accumulate and activate CDKs at the appropriate times during the cell cycle and then are degraded, causing kinase inactivation. The illustration is adapted from Wikimedia Commons "0332 Cell Cycle With Cyclins and Checkpoints".

There are four phases in the mammalian cell cycle (Figure 1.2): DNA-synthesis (S) phase, during which the genome is duplicated; mitosis (M) phase, a highly complex multi-stage process that segregates the chromosomes into two new nuclei in preparation for cell division or cytokinesis. These two phases are separated by two "Gap" phases, called G1 and G2. In G1 phase, cells are prepared to ensure proper intracellular changes and DNA replication occurrence for entering into S phase, while G2 phase is a period for protein synthesis and rapid cell growth before the entry of M phase. G0 denotes the quiescent state in which cells have withdrawn from the active cell cycle.

The cell cycle is controlled temporally by discrete transcriptional programs. Cyclins and CDKs are the key drivers of the cell cycle. Different cyclins, specific for the G1-, S-, G2- or M-phases of the cell cycle, bind to and activate

the subunits of CDKs at the appropriate times. Therefore, activated cyclin-CDK complexes drive the cell forward through the cell cycle (Figure 1.2).[22, 23]

The surveillance mechanisms that ensure the proper spatial and temporal order of cell cycle events are termed cell cycle checkpoints.[24] Like in all signalling pathways, the regulation of cell division is achieved through reversible phosphorylation of regulatory components by protein kinases and phosphatases.[22] To date, several families of protein kinases that control the cell cycle regulation have been characterized, including CDKs, polo-like kinases (Plks), and Aurora kinases.

Considering the high relevance to this project, the G2/M DNA damage checkpoint and spindle assembly checkpoint will be reviewed in detail here.

1.1.2.1.1 G2/M checkpoint (DNA damage checkpoint)

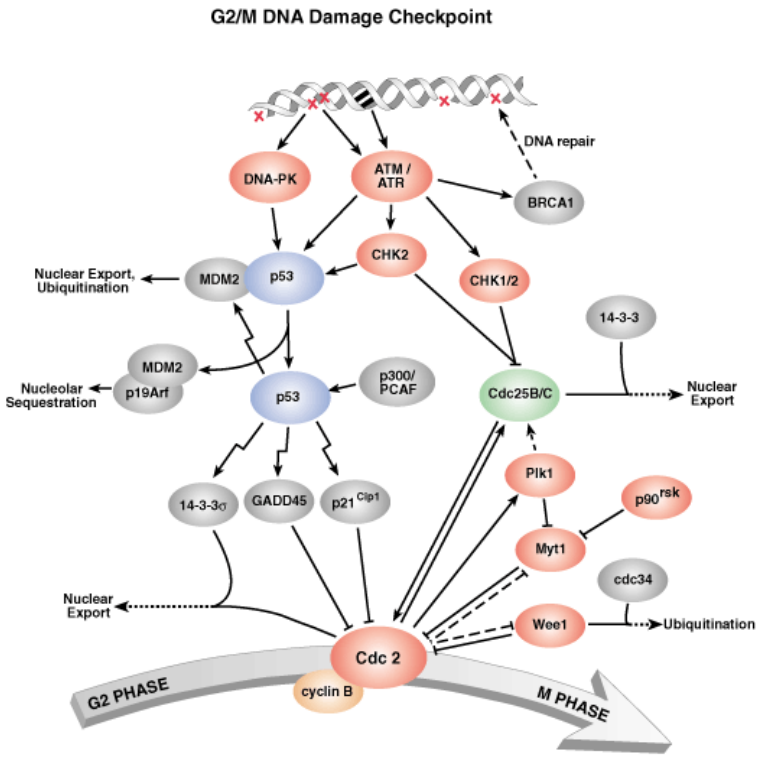

Figure 1.3 Cell cycle G2/M DNA damage signalling pathway.

Illustration is adapted from of Cell Signaling Technology, Inc. (www.cellsignal.com) with permission.

The G2/M DNA damage checkpoint prevents cells containing damaged DNA from entering mitosis by inducing several cellular responses. In general, the entry into mitosis is promoted by activated CDK1(Cdc2) bound to cyclin B or by accumulation of the CDK1/cyclin B complex in the nucleus.[25]

CDK activity is regulated by phosphorylation on the catalytic subunit. This involves phosphorylation at Thr 161 by Cyclin Activating Kinase (CAK, or CDK7) and removing two inhibitory phosphate groups at Thr14 and Tyr15, which are added by Wee1 and Myt1 and removed by Cdc25 phosphatases (Cdc refers to cell division cycle).[26] Therefore, CDK1 activity is competitively regulated by Wee1 and Myt1 (negatively) and Cdc25c phosphatase (positively). As cells approach the G2/M boundary, Bora and the aurora kinase A cooperatively activate polo-like kinase 1 (Plk1).[27] Plk1 in turn activates the Cdc25c, down-regulates Wee1 and Myt1, and subsequently activates CDK1/cyclin B. Alternatively Plk1 can directly phosphorylate cyclin B to block export of cyclin B1 from the nucleus. Hence, Plk1, Cdc25c, and CDK1/cyclin B form a feedback loop to positively regulate each other's activity and drive the cell into mitosis.[28, 29]

DNA damage signals activate the sensory DNA-PKcs / ATM / ATR kinases, which initiate G2/M DNA damage checkpoint signalling and relay two parallel cascades. In the first cascade, the key checkpoint kinases CHK1 and CHK2 are rapidly activated, which in turn phosphorylate and deactivate Cdc25 phosphatases through phosphorylation at Ser216. Once phosphorylated by CHKs, Cdc25c is stimulated to bind to 14-3-3 proteins, and the resulting complex is sequestered in the cytoplasm, which prevent Cdc25c to dephosphorylate Cdc2, leading to the G2 arrest. In the slower second parallel cascade, phosphorylation of p53 promotes the dissociation between p53 and

MDM2, resulting in p53 stabilization. Activation of p53 leads to cell cycle arrest and apoptosis, in part through the CDK inhibition via $p21^{Waf1}$, and the induction of several pro-apoptotic proteins, including Bax, PUMA (p53 upregulated modulator of apoptosis), PIG3 (proapoptotic human p53-inducible quinone oxidoreductase), and NOXA (Phorbol-12-myristate-13-acetate-induced protein 1).[22, 28, 30]

1.1.2.1.2 Mitosis and spindle assembly checkpoint

The spindle assembly checkpoint (SAC) delays the metaphase-anaphase transition until each chromosome is properly attached to the spindle apparatus. Generally, SAC is activated and maintained through two steps. Firstly, SAC negatively regulates Cdc20, thereby preventing polyubiquitylation mediated by anaphase-promoting complex/cyclosome (APC/C) on two key substrates, cyclin B and securin, which delays mitotic exit. A mitotic checkpoint complex (MCC) that contains a series of proteins has been proved to be a SAC effector.[31] Prior to anaphase, SAC proteins bind unattached kinetochores, which facilitate the creation of MCC and production of inhibitory complexes to maintain the SAC activity. The proper attachment of all kinetochore and chromosome congression negatively regulates the SAC signal and promotes the mitotic exit.[22, 31]

Several kinases have key roles in regulating SAC. Centrosome maturation is critical for cell division to occur and is regulated by several kinases including Plk and aurora kinase.[23] Kinases such as MPS1, BUB1, BUBR1, Plk1, NEK2, MAPK and aurora-B kinases play the key role in recruiting SAC proteins to kinetochores and maintaining SAC activity.[31] Deregulation of these kinases are found in a wide spectrum of cancers in humans.

1.1.2.2 Targeting the cell cycle for cancer therapy

Perturbations in the cell cycle are described commonly in carcinogenesis and are mainly caused by genetic alterations of tumour suppressor genes (inactivation), such as pRb and p53, and proto-oncogenes (mutation).[23, 25] This dysregulation occurs through mutations of genes, which encode proteins at different phases of cell cycle, including CDK, cyclins, CDK-activating enzymes, CKI, CDK substrates, and checkpoint proteins, such as CHKs, WEE kinases, aurora kinases and Plks.[22, 25, 32] Therefore, the enzymes that mediate reversible phosphorylation of cell cycle regulation, especially kinases, are currently being pursued as drug targets.[22]

The rationale for targeting the cell cycle for cancer therapy is based on the frequency of perturbations in cell cycle in human malignancy and the observation that cell cycle arrest could induce apoptosis. This rationale led to the development of CDK inhibitors (CDKI) as novel antitumor agents. These compounds can inhibit CDKs by directly inhibit the catalytic subunit of CDK, or by indirectly target regulatory pathways to govern the CDK activity. To date, the most successful strategy is the direct inhibition of CDK.[23] About 25 of them have reached clinical trial, such as AT7519, CYC202 (R-roscovitine), and Flavopiridol, and all of which interact with the catalytic active site of Cdk and are ATP-competitive inhibitor.[23, 33] Strategies for developing the indirect CDKI include overexpression of cyclin-dependent kinase inhibitor (CKI), decrease of cyclin levels and using small peptides mimicking the effects of endogenous CKI.[25, 34]

In addition, targeting the deregulation of cell cycle checkpoint machinery presents another attractive therapeutic strategy. Cell cycle checkpoints regulate the quality and rate of cell division. Mutations of checkpoint proteins are

frequent in all types of cancer.[25] In contrast to healthy cells, tumour cells are unable to stop at predetermined points of the cell cycle because of loss of checkpoint integrity.[23] Therefore, this rationale led to the development of agents that destruct the cell-cycle checkpoints. Candidates currently under the development either abrogate or arrest the checkpoints.[35] Abrogation of G2/M DNA damage checkpoint allow damaged cells enter mitosis and thus undergo apoptosis. A number of reported compounds override G2/M checkpoint and have shown enhanced cytotoxicity.[36, 37] On the other side, increasing G2/M DNA damage arrest have also been associated with enhanced cytotoxicity and apoptosis. This has been proven by many agents, such as flavopiridol and silibinin.[35, 38]

1.2 Protein kinases as an important class of cancer drug targets

In 1954, Krebs and Fischer first discovered the key role protein kinases play in regulating diverse biochemical signalling pathways.[39] Since then, the protein kinases have come to be recognised as critical catalysts in cellular energy supply and regulators activating almost all cellular processes.

1.2.1 The structure and regulation of protein kinases

Protein kinases are one of the largest gene families in eukaryotes. They catalyse the transfer of ATP γ-phosphate to specific hydroxyl groups of serine/ threonine or tyrosine residues of protein substrates.[39] Hence, they are broadly divided into serine/threonine kinases and tyrosine kinases. To date, 518 human genes encoding protein kinases have been identified, of which 478 are human eukaryotic protein kinases (ePKs) and 40 are atypical protein kinases (aPKs).

Based on the various gene sequences and structure, they are classified into 10 subsets as shown in Figure 1.4.[40-42]

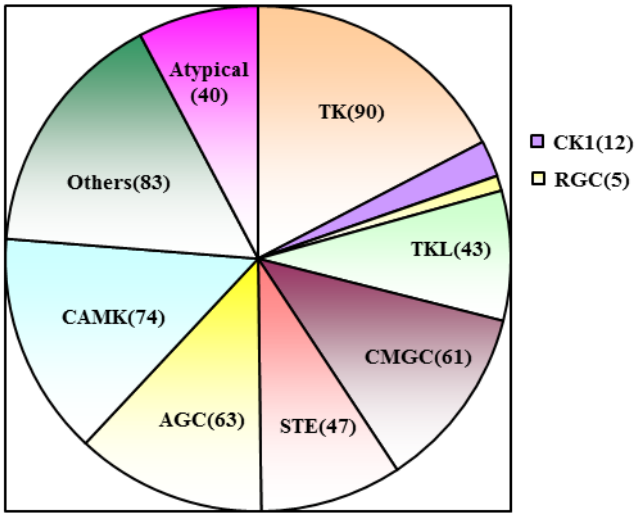

Figure 1.4 Classification of human kinases[39, 42]

Different protein kinase subsets are denoted in various colours with the number of protein kinases in each subset in parenthese. AGC: PKA, PKG and PKC; CAMK: Ca^{2+}/calmodulin-dependent protein kinase; CK1: casein kinase 1; CMGC: CDKs, MAPKs, GSKs and CLKs; RGC: receptor guanylate cyclase; STE: homologues of sterile 7, 11 and 20 kinases; TK: tyrosine kinase; TKL: tyrosine kinase-like; others: kinases have no sufficient close sequence similarity.

Due to conservation in sequence, protein kinases share a homologous catalytic core (Figure 1.5). The catalytic domain of protein kinases is formed as two lobes, which consists of a small N-terminal lobe (mainly of β-sheets and long α-helix) and a larger C-terminal lobe of predominantly α-helices. At the junction of the two lobes, an activation cleft is formed, which is a key element of the ATP nucleotide binding site.[43, 44] A short polypeptide chain named the hinge region is located in this cleft.[44] All kinases have a conserved activation loop, which is important in regulating kinase activity. When the activation loop folds back and exhibits as a substrate mimic, the active site is disrupted and the kinase remains inactive.[45]

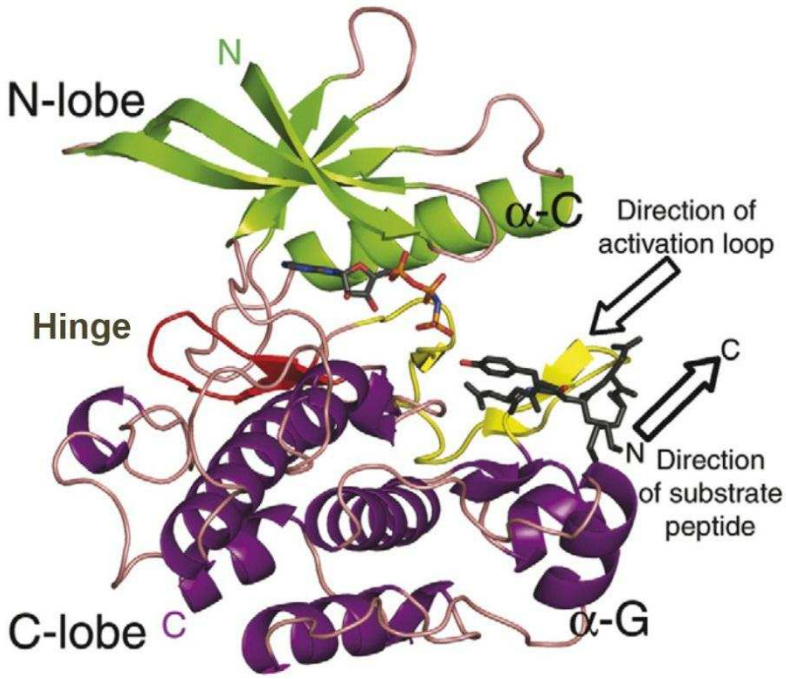

Figure 1.5 Global features of a protein kinase catalytic domain based on the structure of insulin receptor kinase (IRK).[45]

The N-lobe is coloured in green, the C-lobe is in purple and the activation loop is shown in yellow. An ATP (in black) binds at the junction between the two lobes. The α helix-C contains residues critical for catalysis and the α helix-G is involved in docking protein substrates.

Protein kinases are involved in almost all cellular processes. In human cells, the accumulation of signalling molecules is a key feature of biochemical signalling cascades. In these clusters with high concentration of signalling effectors, diverse protein-protein interactions are promoted by utilizing specialized domains. Through reversible phosphorylation, protein kinases activate themselves and other proteins, therefore, mediating the whole cellular processes.[45] Most protein kinases are involved in multiple regulatory mechanisms, playing diverse biological roles with individual properties relating to various residues, loops or insertions in different families.[46-47]

1.2.2 Targeting cancer with kinase inhibitors

Given that protein kinases mediate most of cellular processes, it is apparent that mutations and dysregulation of protein kinases play causal roles in human diseases, especially cancer.[39, 42] Thus, protein kinases have attracted significant

attention as important targets for cancer drug discovery. Several outstanding small molecule inhibitors have been approved for the treatment of cancer and more are currently undergoing clinical evaluation.

1.2.2.1 ATP-competitive inhibitors

The majority of kinase inhibitors to date interact with the ATP binding pocket of target kinases. These kinase inhibitors, named as type I kinase inhibitors, directly bind to the adenine region of ATP binding site and do not require a three-residue motif, Asp-Phe-Gly (DFG), in the activation loop, generating a "DFG-in" conformation (Table 1.1). These inhibitors usually form 1-3 hydrogen bonds with the hinge region of the kinase, thus mimicking the hydrogen bonds formed by the adenine ring of ATP.[48, 49]

However, several challenges have arisen along with the development of second generation type I kinase inhibitors. Due to the highly conserved ATP binding site in protein kinase family, it is difficult for inhibitors to specifically identify the target kinase.[40] This has been demonstrated by a recent study, which evaluated the selectivity of previously characterized 38 kinase inhibitors against a panel of 317 kinases.[50] Additionally, it is challenging for inhibitors to target with high-affinity to the kinase competing with high intracellular ATP concentrations (typically 1–10 mM). The low selectivity ATP-competitive inhibitors have exhibited undesirable toxicities (lack of selectivity, e.g. CDK inhibitors) and drug resistance (due to the mutations in the ATP binding site, e.g. imatinib), which have limited their clinical use as drugs.[51]

1.2.2.2 Non-ATP-competitive inhibitors

Accumulating efforts are focusing on developing new types of non-ATP-competitive inhibitors, which could be an alternative strategy to overcome the

cross-reactivity of ATP-competitive inhibitors. As presented in Table 1.1, there are three types of non-ATP-competitive reversible kinase inhibitors based on their mechanism of action.

Table 1.1 Comparison between the different types of reversible kinase inhibitors[48, 52]

Kinase Inhibitors	Type I	Type II	Type III	Type IV
Binding site	ATP site	ATP site and DFG pocket	Allosteric (by ATP pocket)	Allosteric (substrate binding domain)
ATP-competitive	Yes	Yes, indirectly	No	No
Selectivity	Usually low, but very selective inhibitors have been identified	High	Very high	Very high
Representative inhibitors	Gefitinib, Erlotinib, Sunitinib	Imatinib, BIRB796	GNF-2, GNF-5, selumetinib	ON012380, ON01910.Na

1.2.2.2.1 Type II kinase inhibitors

Type II kinase inhibitors occupy a hydrophobic site that is directly adjacent to the ATP binding pocket. This site is made by the DFG motif of the activation loop being moved away from the kinase active conformation (form“DFG-out” conformation).[48, 49] Type II inhibitors typically have more potent cellular activity and a higher degree of selectivity compared with type I kinase inhibitors, this is benefit from their lipophilic interactions with the DFG pocket. However, on the other hand, binding to the hydrophobic DFG pocket leads to the production of compounds with undesired properties for druggability, such as high MW and clogP.[52] Although the allosteric site provides Type II kinase inhibitors another handle for improving kinase selectivity, drug resistance issue due to their high sensitivity to the mutations in the ATP binding site as well as mutations located in regions that affect the kinase conformation is still a disadvantage affecting their development (e.g. imatinib).[48, 49]

1.2.2.2.2 Allosteric Inhibitors

Type III kinase inhibitors, also named as allosteric inhibitors, bind in the regulatory regions modulating the activity of the kinase in an allosteric manner. Inhibitors belonging to this class tend to show relatively high kinase selectivity because they bind sites that are unique to a particular kinase family.[52]

1.2.2.2.3 Substrate Directed Inhibitors

Substrate directed inhibitors, or the fourth type of kinase inhibitor, are small molecules that present a reversible interaction at the substrate binding site in an ATP-independent manner.[52] To ensure signalling fidelity, protein kinase must recognize and act only on a defined subset of cellular targets. Due to this exquisite specificity in the interactions between kinase and substrate, a high degree of selectivity could be achieved by targeting substrate binding regions of kinases with substrate competitive inhibitors.

ON01910.Na is a Phase III clinical non-ATP competitive inhibitor with multi-targeted activity. It inhibits Plk1 (9 - 10 nM) by binding to the substrate binding sites of Plk1. At higher concentrations (20 - 260 nM), the activities of several kinases, such as BCR-ABL, PDGFR, FLT-1, PI3K, Fyn and Plk2 as well as CDK1, are influenced by ON01910.Na.[53] Whether the efficacy of ON01910.Na in inhibiting tumour growth is the direct result of inhibiting Plk1 or other protein kinases remains a controversial issue that requires further investigation. Due to its broad spectrum of anti-cancer activity, excellent efficacy and safety profile, ON01910.Na has become a promising compound for the treatment of cancer.

1.3 Preclinical cancer drug discovery, design and development

1.3.1 Integrated preclinical cancer drug development

The discovery of modern anti-cancer agents is a time-consuming and expensive process, which consists of preclinical discovery and clinical development. Success in discovering a drug requires a creative interplay between the essential disciplines of biology/pharmacology and medicinal chemistry.[54] A typical preclinical cancer drug discovery and development with biological test cascade is shown in Figure 1.6.

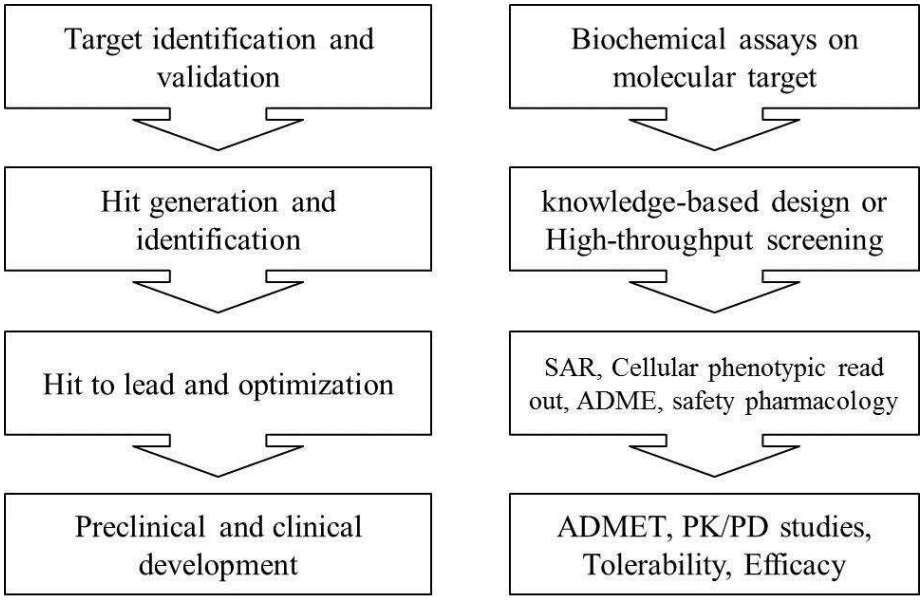

Figure 1.6 Stages of drug discovery and development with biological test cascade.[54]

Abbreviations: SAR, structure activity relationship; ADME, absorption, distribution, metabolism, and excretion; ADMET, absorption, distribution, metabolism, and excretion - toxicity in pharmacokinetics; PK/PD studies, Pharmacokinetics and pharmacodynamics studies.

Selecting the right molecular target is crucial to success in developing a new drug. A good target should be 'druggable', while a good drug should be efficacious, safe, meet clinical and commercial needs. The best approach to develop anti-cancer drugs is acting upon the hallmark traits of cancer (refer to Figure 1.1). In support of this notion, most drugs that have been approved for

clinical use throughout the past century target one of the six classic hallmarks.[55] Targeting the cell cycle, by inhibiting key regulatory kinases, and interfering with mitotic spindle assembly, is observed after exposure of cancer cells to TL-77 described in this project. This may address the proliferative dysregulation and induce apoptosis in cancer cells.

Once a target is chosen, one or more "hit" molecules with preliminary biological activity against the target must be generated.[56] Several hit generation approaches have successfully been developed and can be used either individually or in combination. These approaches include, but are not limited to high-throughput screening, fragment screening, focused screening, virtual screening, physiological screening, NMR screening, structural aided drug design and knowledge-based design.[57, 58]

Once a number of hits have been identified, the next job is to define which compounds justify future investigation. Intensive structure–activity relationship (SAR) studies and primary assays to generate target dose–response curves will compare activity and selectivity of each compound. For compounds with similar core structure hitting specific classes of targets (such as kinases), focused or knowledge-based screening is a cheaper and effective method.[58] In chapter three, SAR and cell-based screenings are described, which are able to identify compounds with improved potency and drug-like properties compared to reported compounds.

The hit-to-lead and optimization processes are iterative cycles of chemical synthesis and biological evaluation. Extensive modification of compounds is required. Optimizations in key parameters include: potency and understanding molecular mechanism(s) of action, pharmaceutical properties (absorption, distribution, metabolism, and excretion), tolerability and efficacy against

cancer tumour in vivo. Each cycle provides feedback to allow further optimization of new compounds to improve properties.[56] In formulation and toxicology studies, if successful, one or more candidates are nominated for clinical development, clinical evaluation and ultimately be a marketed drug.

1.3.2 Analogue-based drug design

In addition to ligand-based and structure-based drug design, analogue-based drug design, which is the process of using existing drugs as leads, has been an efficient and reliable strategy to synthesize new drugs.

Analogue-based drug design possesses considerable advantages. Firstly, developing a pioneer drug can be extraordinarily unpredictable and risky, because the therapeutic use has not yet been validated clinically. One may argue that this would be an attractive challenge of drug discovery, but it is true that one can avoid a major uncertainty from the overall risk of success by starting with an established drug with proven therapeutic use. Secondly, developing a pioneer drug can be extraordinarily costly and time-consuming. An existing drug may have been developed with validated target and well-established biomedical assays. Research team can shorten the research cycle and expenses by directly focusing on the iterative improvements of compounds. Moreover, ongoing improvement in understanding of the drugs mechanism of action and in vivo behaviour provide opportunities for improved drug analogues.

Analogue-based drug design is based on the improvement and optimization of existing drugs, for example reducing the side effects, improving the target selectivity, or developing a better dosage form. It is important to identify an analogue with expected clinical advantage over the established drug. The aim,

therefore, must be to prove the improvement of new compounds compared with the lead drug.[56]

Lovastatin is a convincing example to illustrate the success of analogue-based approaches on improvement of drug-likeness properties. Lovastatin (Mevinolin, Merck) is potent inhibitor of 3-hydroxy-3-methylglutaryl-coenzyme A (HMG-CoA) reductase for hypercholesterolemia treatment. The disclosure of biological efficacy of Lovastatin opened opportunities for the discovery of therapeutic analogues. This led to the success of Rosuvastatin, which is the most recent approved HMG-CoA reductase inhibitor. By replacing a pyrimidine to lower ring system of statins and introducing the methanesulfonamide to optimize physical properties, Rosuvastatin shows greater potency and superior efficacy.[56, 59]

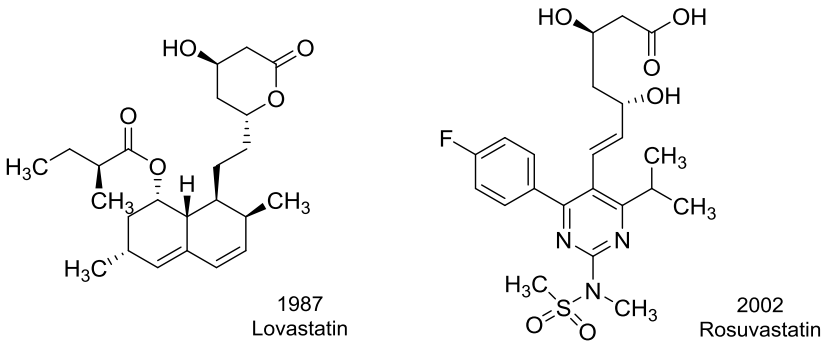

Figure 1.7 Structures of selected HMG-CoA reductase inhibitors.[56]

1.4 Discovery and development of ON01910.Na

1.4.1 ON01910.Na

ON01910.Na (also referred to as Estybon™, Rigosertib) is a novel anti-cancer agent currently undergoing clinical trials for various solid tumours and hematologic malignancies. This compound is selected from a class of (E)-styrylbenzylsulfones developed by Dr. E. P. Reddy's research team and currently supported by Onconova Therapeutics®, Inc.[60] The chemical

composition of ON01910.Na is $C_{21}H_{24}NNaO_8S$ (MW= 473.47 Da), sodium (E)-2-((2-methoxy-5-(((2,4,6-trimethoxystyryl)sulfonyl)methyl)phenyl)amino)acetate (Figure 1.8).

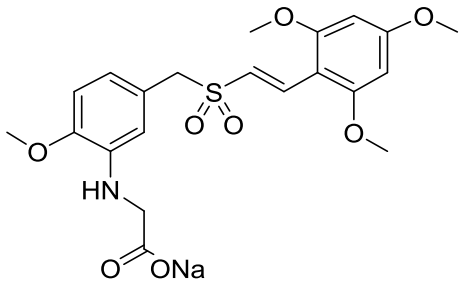

Figure 1.8 Structure of ON01910.Na.

1.4.1.1 Pre-clinical studies

ON01910.Na exhibits a broad spectrum of anti-cancer activity with an IC_{50} value range from 50 to 250 nM against more than 100 cell lines, including numerous drug-resistant cell lines.[53] Statistical comparison using the NCI algorithm COMPARE confirmed that ON01910.Na is a mitotic blocker of cancer cells. The finding that such a large range of cancer cell lines are sensitive to this compound suggests that its targets are essential for cancer cell proliferation and survival.[61] Meanwhile, strong synergistic effects were observed when ON01910.Na therapy was combined with other anti-cancer agents including oxaliplatin, doxorubicin, and gemcitabine.[62]

The pharmacokinetic profile (PK) of ON01910.Na was evaluated across several species such as mice, rats and dogs. This compound exhibited extensive plasma protein binding and displayed a rapid distribution with a prolonged elimination phase. [63, 64] Half-lives ($t_{1/2}$) less than 2 hours were observed in rat, dog, and human plasma following single dose administration.[62] Because of the short half-life and the rapid clearance, ON01910.Na was suggested to be administered as a continuous intravenous (IV) infusion for cancer treatment.[62]

There has been limited evidence of drug metabolism in in vitro and in vivo experiments, and studies in mice and rats so far identified that ON01910.Na exhibited extensive liver uptake, and is mainly eliminated through biliary excretion.[62] In a steady-state study in orthotopic U87 glioma xenograft model, ON01910.Na exhibited low brain (5%) and brain tumour (14%) distribution. The limited access of ON01910.Na to the brain is perhaps attributed to its low lipophilicity (predicted logD value of −1.07) and influenced by high plasma protein binding (93–95%).[62, 63] Toxicology studies using rats and dogs by Gumireddy et al showed a very desirable safety profile for ON01910.Na; no evidence for hamatologic, hepatocellular or neurotoxicity was detected and only slight toxicity was observed until drug levels were as high as 1200mg/m^2 in rats.[53]

1.4.1.2 Clinical Studies

On the basis of the encouraging results from the preclinical stage, ON01910.Na is currently under clinical assessment as a single agent (oral and parenteral formulations) and in combination with conventional chemotherapy (Figure 1.9). In advanced Phase I and Phase II clinical trials, the compound has been tested in patients with both solid tumours and haematological cancers.

Clinical studies of ON01910.Na in patients with solid tumours showed good tolerability across a range of dosing schedules by IV infusion.[65] In the clinical trials with MDS patients, ON01910 was infused IV at 800−1500 mg/m^2, and the maximum tolerated dose (MTD) was 800 mg/ (kg·m^2·d) infused for 5 days every other week.[66] A patient with refractory ovarian cancer had an objective response after four cycles and remained progression-free for 24 months.[64] Recent phase I studies with B-cell chronic lymphocytic leukaemia

demonstrated that ON01910.Na selectively induced apoptosis and reduced Plk1 activity in the leukaemia cells.[65]

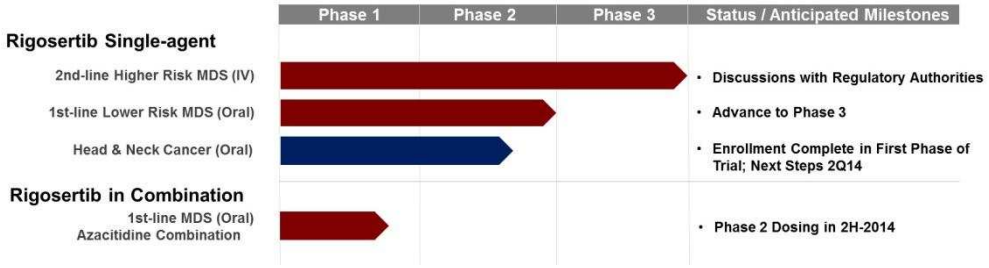

Figure 1.9 Clinical development of ON01910.Na (Rigosertib).

The figure is adapted from Onconova Therapeutics, Inc. homepage (http://www.onconova.com/).[67]

ON01910.Na is also being investigated for the treatment of myelodysplasia (MDS) due to its inhibitory effect on cyclin D1 accumulation and selective toxicity towards trisomy 8 cells and is currently in Phase I/II/III trial in MDS patients with refractory anamia. (Figure 1.9)[63] Four Phase I/II clinical studies were conducted to assess the efficacy and safety of intravenous ON01910.Na in 48 higher risk MDS/AML patients, and increased overall survival after the treatment of ON01910.Na was reported.[68-70] ON01910.Na appeared to be well-tolerated and no significant myelosuppression, hamatologic toxicities or drug accumulation (repeatedly treated) was noted. Most common drug-related side effects included fatigue, anorexia, nausea, dysuria and abdominal pain.[71] These encouraging results led to the initiation of a pivotal Phase III ONTIME trial of intravenous rigosertib (ON01910.Na) in patients with secondary MDS who have failed prior therapy with hypomethylating agents. On 19th Feb. 2014, however, Onconova announced that the Phase III ONTIME trial failed to meet the primary endpoint of overall survival.[72]

Oral formulation of ON01910.Na has entered phase II to treat patients with MDS and advanced solid malignancies.[73, 74] The recommended MTD of oral rigosertib is 560 mg (1120 mg/d) twice daily given continuously. The

permeability studies found ON01910.Na displayed medium permeability with absolute bioavailability of 10–15%.in rats (10 and 20 mg/kg, 1h infusion).[75] More recently, a new oral formulation of ON01910.Na (in PEG400 and PEG4000) showed a modest improvement in oral bioavailability (F=∼34.9% fasting vs ∼13.8% fed) at MTD levels.[73] However, only at a higher dose of 700 mg did ON01910.Na achieve a C_{max} value of 3-4 μM, while the minimum pharmacodynamically relevant level required for its biological activity is 4-7 μM (by measuring cyclin B1, p-CDK1, and p-H3 in plasma). The poor and variable oral availability of ON01910.Na is further complicated by its efflux by P-gP and MRP membrane transporters.[75, 76] Clearly, the pharmacological properties of ON01910.Na are not satisfactory.

1.4.2 Cellular mechanism of action of ON01910.Na

ON01910.Na is a multi-targeted kinase inhibitor promoting selective mitotic arrest and apoptosis in cancer cells. According to studies to date, ON01910.Na causes three major abnormalities leading to the loss of cancer cell viability: (a) abnormal cell division by interfering chromosomal segregation and cytokinesis;[64] (b) irregular centrosome and spindle localization, subsequently followed by G2/M arrest and apoptosis; and (c) decreased expression of phosphatase Cdc25c.[77]

ON01910.Na's complex mechanism of action involves suppression of two important cellular signalling pathways, Plk and phosphatidylinositide 3-kinase (PI3K), both of which are frequently overexpressed in cancer cells. In HeLa cells, ON01910.Na inhibited the Plk1 activity, creating spindle abnormalities and mitosis dysregulation.[53] Recent studies indicated ON01910.Na modulates the PI3-K/Akt pathway to promote apoptosis in cancer cells.[78] This multi-

targeted mechanism of action makes ON01910.Na effective in killing cancer cells with various anti-apoptotic and drug-resistance mutations.

1.4.2.1 ON01910.Na targets Plk1

1.4.2.1.1 What is Polo and what are Plks?

Plks belong to the family of serine/threonine kinases and play key roles during multiple stages of cell cycle progression.[79] In the 1980s, polo, the founding member of the Polo kinase family, was first discovered in Drosophila melanogaster to encode a protein kinase whose mutation resulted in abnormal spindle poles.[80] Since then, five mammalian Plk family members have been identified so far, Plk1(STPK13, serine-threonine kinase 13), Plk2 (SNK, serum inducible kinase), Plk3 (CNK, connector enhancer of KSR; FNK, FGF-inducible kinase; and PRK, proliferation-related kinase), Plk4 (SAK, Snk/Plk-akin kinase; and STK18, serine-threonine kinase 18) and Plk5.[81]

All Plks share the similar topology with a catalytic kinase domain at the N-terminus and a regulatory C-terminal region, known as Polo-box domain (PBD). PBD is unique to the Plk family. Plk1, Plk2, Plk3 and Plk5 have a PBD consisting of two polo boxes, while Plk4 possesses only one polo box.[29] The general structure of Plk families is depicted as in Figure 1.10.The kinase domains are very highly conserved among all Plks, and most closely resemble those in aurora kinases and calcium/ calmodulin-dependent kinases.

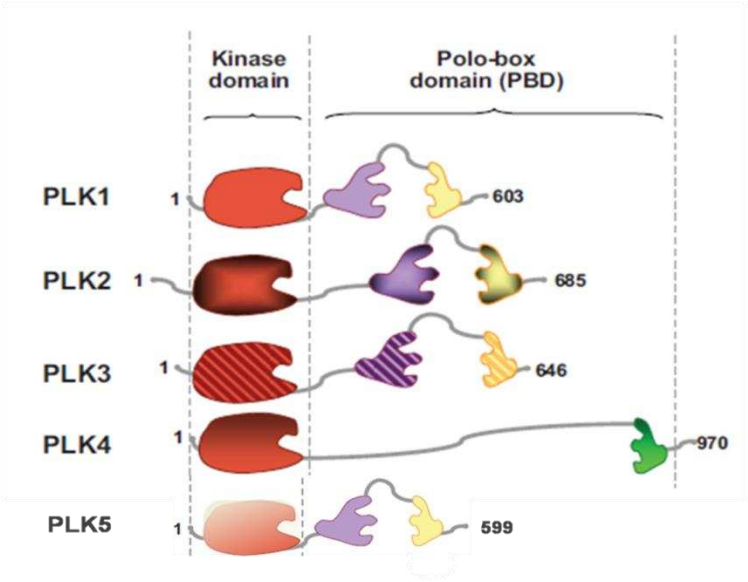

Figure 1.10 General structure of Plk proteins

The kinase domain is shown in the left region while the PBD is shown to right. The number of protein residue in each Plk member is also presented. [65, 81]

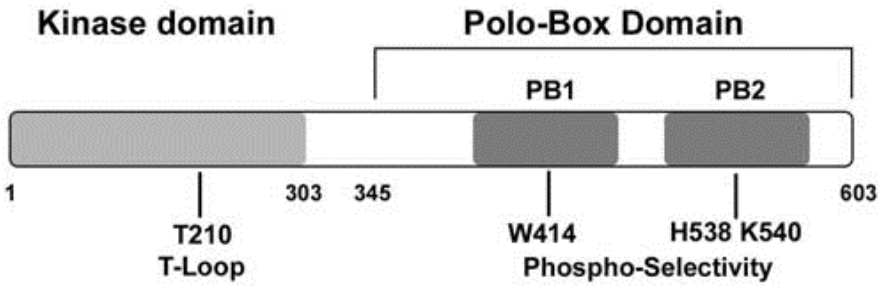

Figure 1.11 Domain structure and key features of Plk[79]

The key structural features of Plks are shown in Figure 1.11**.** The kinase domain holds the regulatory phosphorylation site, the activation loop (T-loop) and an ATP-binding site, and is responsible for phosphorylation. Phosphorylation of Thr-210, which located in the T-loop is required for the activation of Plk1.[81] The polo-box domain functions as a protein-protein interaction motifs containing three binding sites (Trp414, His538 and Lys540).[29] Localization of Plks is governed by docking of the PBD to specific motifs (phosphothreonine/phosphoserine)-(proline/X) that have been primed by phosphorylation.[82] Early reports indicated that Plks activity is negatively regulated by the PBD.[83] In the absence of phosphorylated ligands, the PBD blocks the kinase domain's substrate docking sites, thereby inactivating Plks.

Once the PBD is bound by the phosphopeptide to its ligands, the catalytic domain is released and activates Plks. Simultaneously Plks localize to specific subcellular structures and initiate subsequent downstream effects.[65, 79]

1.4.2.1.2 The multiple functions of Plk1 in cell cycle

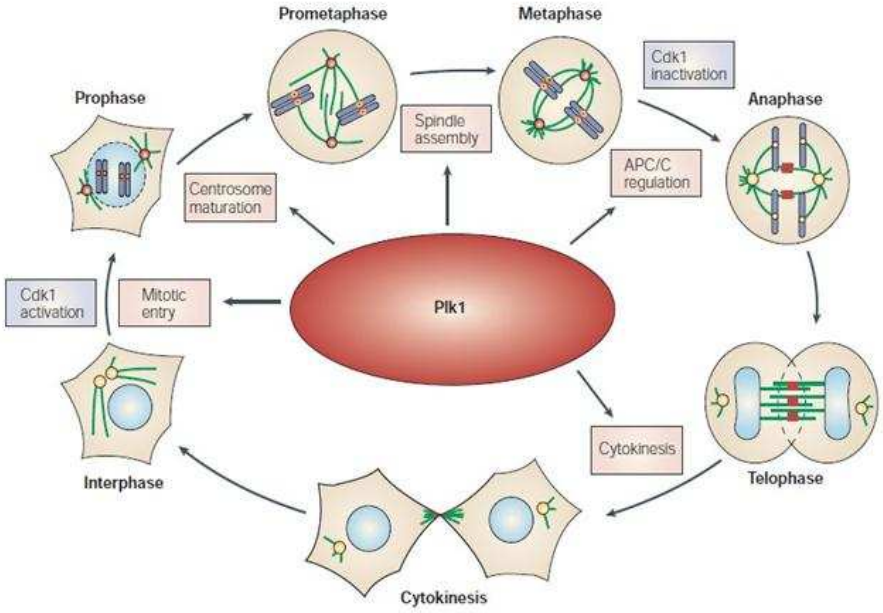

Figure 1.12 Functions and localization of Plk1 in the cell cycle[29]

Among all family members, Plk1 is best characterized. In human cells, it is expressed primarily during G2/M phases and controls critical steps in the cell cycle.[84] (Figure 1.12)

In human cells, Plk1 positively triggers the entry and progression of mitosis and, therefore, is suggested as a marker for proliferation.[84] As reviewed in previous session, Plk1 controls the rate of mitotic entry by phosphorylating Cdc25c, which in turn activates CDK1/cyclinB. When cells enter mitosis, Plk1 is involved in recruiting γ-tubublin and facilitates the centrosome's microtubule nucleating activity.[23] Mutation or depletion of Plk1 results in aberrations in mitotic spindle formation and unstable chromosome alignments.[29, 85] Sister-chromatid separation and mitotic exit are coordinated through the anaphase-promoting complex/cyclosome(APC/C)-dependent ubiquitylation.[29] By

activating certain functions of APC, which in turn triggers the proteolysis of cyclin B, Plk1 allows mitotic exit.[53]

1.4.2.1.3 Plk1--- An attractive drug target for cancer treatment

As with the important role in cell proliferation, Plk1 is found to be a major driving force in oncogenesis of many cancers.[86] Cancer is regarded as a proliferative disorder; targeting the cell cycle, therefore, has become a potent strategy for new anti-cancer agents.[87]

Substantial evidence supports Plk1 is an attractive candidate molecule for anti-cancer therapy. Firstly, about 80% of human tumours with diverse origins overexpress Plk1 transcripts, which correlate with a poor outcome.[65] Plk1 overexpression leads to enhanced proliferation and induce genetic instability (chromosomal instability (CIN), DNA aneuploidy and centrosome amplification), thus promoting oncogenic transformation.[88] Secondly, constitutive expression of Plk1 is able to transform mouse NIH-3T3 cells and induces tumour growth in nude mice.[89] Many studies have identified that targeted interference of Plk1 activity using antibodies or small interfering RNA results in mitotic arrest with subsequent induction of apoptosis in numerous cancer cell lines.[53, 90-93] Notably, interference with Plk1 function was reported to selectively induce apoptosis in tumour cells but not in non-transformed cells. A series of Plk1 hypomorphs were generated by the lentivirus-based RNAi approach. Hela cells with strong Plk1 hypomorph underwent serious mitotic catastrophe, exhibiting significant delayed mitotic entry and complete mitotic block. In contrast, non-transformed hTERT-RPE1 and MCF10A cells with Plk1 depletion exhibited no apparent cell proliferation defect or cell cycle arrest.[93] Moreover, Plk1 possesses two regions as potential targets, the kinase domain and the polo-box domain. Interfering with Plk1 function could be not

only via targeting the kinase domain, but also by interfering with PBD binding to docking proteins, which increase the potential for discovery and design of selective and specific inhibitors. Several small-molecule Plk1 inhibitors, such as BI2536, GSK-461364, are presently in clinical trials and exhibit potent and specific effect in cancer.[39, 65]

1.4.2.1.4 ON01910.Na affects microtubule dynamics by inhibiting Plk1

Among the Plk1 inhibitors, ON01910.Na increasingly gains attention in view of its potent inhibitory activity. Studies of the inhibitory effects of ON01910.Na on a panel of 29 serine/threonine and tyrosine kinases showed that Plk1's activity was influenced most with an IC_{50} of 9 - 10 nM, suggesting it might be one of the primary targets (Table 1.2).[53] Steady-state analysis on the effects of increasing concentrations of ATP or substrate (recombinant casein and Cdc25c) on the Plk1 (recombinant) inhibitory activity of the compound revealed that ON01910.Na targets Plk1 activity in an ATP-independent and substrate-dependent manner: the velocity of substrate phosphorylation was unaltered in the presence of increasing concentrations of ATP, while increasing the concentration of the substrate resulted in increased substrate phosphorylation.[53]

The mitotic microtubule abnormalities induced by this agent activate apoptotic pathways leading to cancer cell death and have been clarified by many comparative analyses.[94] ON01910.Na treated cells exhibited profound abnormalities in spindle formation in G2/M. The multipolar spindles then led to misalignment of chromosomes, which was similar to the appearance observed in Plk1-depleted cells.[95] Moreover, Plk1 siRNA as well as ON01910.Na treatment exhibited growth inhibitory effects on HS766T cells, while mild additive effects were observed when Plk1 siRNA and ON01910.Na

were given together.[96] This indicates that Plk1 knockdown- and ON01910.Na-mediated effects may impinge on both parallel and connected pathways in mitotic progression. Phosphorylation of Cdc25c at Ser198 was suggested to serve as a reliable marker to monitor Plk1 activity.[24] ON01910.Na has been shown to induce stark G2/M arrest and suppress cell cycle effectors downstream of Plk1, including phospho-Cdc25c (Ser198) and cyclin B1.[53, 64] To date, the molecular modelling of ON01910.Na in complex with Plk1 has not been resolved, thus the exact binding mode is still undefined. It has been reported that a range of kinases without PBDs are also inhibited by ON01910.Na. Meanwhile, ON01910.Na shows inhibition of tyrosine kinases as well as CDK1 (Table 1.2).[53] These clues suggest that ON01910.Na may interfere with the kinase domains by binding to the peptide binding sites, rather than target the polo-box domain of Plk1.[95]

Table 1.2 Kinase inhibitory activity of ON01910.Na.

Inhibitory activity of ON01910.Na against a panel of serine/threonine and tyrosine kinases reported by Gumireddy et a. (Reported experimental procedures is discribed in Appendix I).[53]

Protein Kinase	**IC_{50} (nM)**
Akt1/PKBα	>10,000
Aurora A	>10,000
Aurora B	>10,000
BCR-ABL	32
BTK	>10,000
Cdk1	260
Cdk2	>10,000
Cdk4	>10,000
Cdk5	>10,000
Cdk6	>10,000
Cdk9	>10,000
Chk1	>10,000
Chk2	>10,000
ErbB-2	>10,000
EGFR	>10.000

ERK	>10,000
Flt1	42
Fyn	182
FGFR	>10,000
IGFR	>10,000
JNK	>10,000
Lyn B	>10,000
MEK1	>10,000
Plk1	9
Plk2	260
Plk3	>10,000
PDGFR	18
ROS	>10,000
Src	155

Although the antimitotic activity of ON01910.Na was deemed as the consequence of Plk1 inhibition, continuative studies did not support a direct effect on Plk1. However, previous kinase inhibitory results of ON01910.Na on Plk1 could not be reproduced by other scientists.[97, 98] Several lines of experimental evidence suggested that ON01910.Na is an inhibitor of tubulin polymerization rather than a Plk1 inhibitor. The compound effectively blocks cell proliferation, however, cellular effects caused by this compound resembled the phenotype that is caused by treatment with microtubule depolymerizing agents rather than Plk1 RNAi.[97, 99] When treated with higher doses (≥2.5μM) of ON01910.Na, depolymerisation of microtubules was visible in interphase cells. Moreover, in vitro kinase assays indicated that ON01910.Na does not show obvious Plk1 inhibition in until concentrations of 30 μM have been reached.[97] Overall, it seems that the mechanism for ON01910.Na on Plk1 activity has not yet been completely established. Improved understanding of the specific interactions between ON01910.Na and Plk1 are critical.

1.4.2.2 ON01910.Na targets PI3K/Akt pathway

Since its discovery in the 1980s, Phosphatidylinositol 3-kinases (PI3 kinases, PI3Ks) have been found to be play key roles in regulating many cellular processes.[33] The PI3K/Akt pathway is a key signal transduction system linking multiple receptors, as well as oncogenes, to essential cellular processes and is activated in cancers.[100] Thus, this pathway presents both an opportunity and a challenge for cancer drug disoverers.[33] Recent studies reported that the PI3K/Akt pathway was affected by ON01910.Na.

1.4.2.2.1 Structure and function of PI 3-kinases

1.4.2.2.1.1 Structure of PI 3-kinases

PI 3-kinases are a lipid kinase family characterized by their capability to phosphorylate inositol lipids on the 3-position of the inositol phospholipids.[101] To date, eight PI3K isoforms have been identified in mammals and are subdivided into three classes (Class I, Class II, and Class III). (Figure 1.13 A)

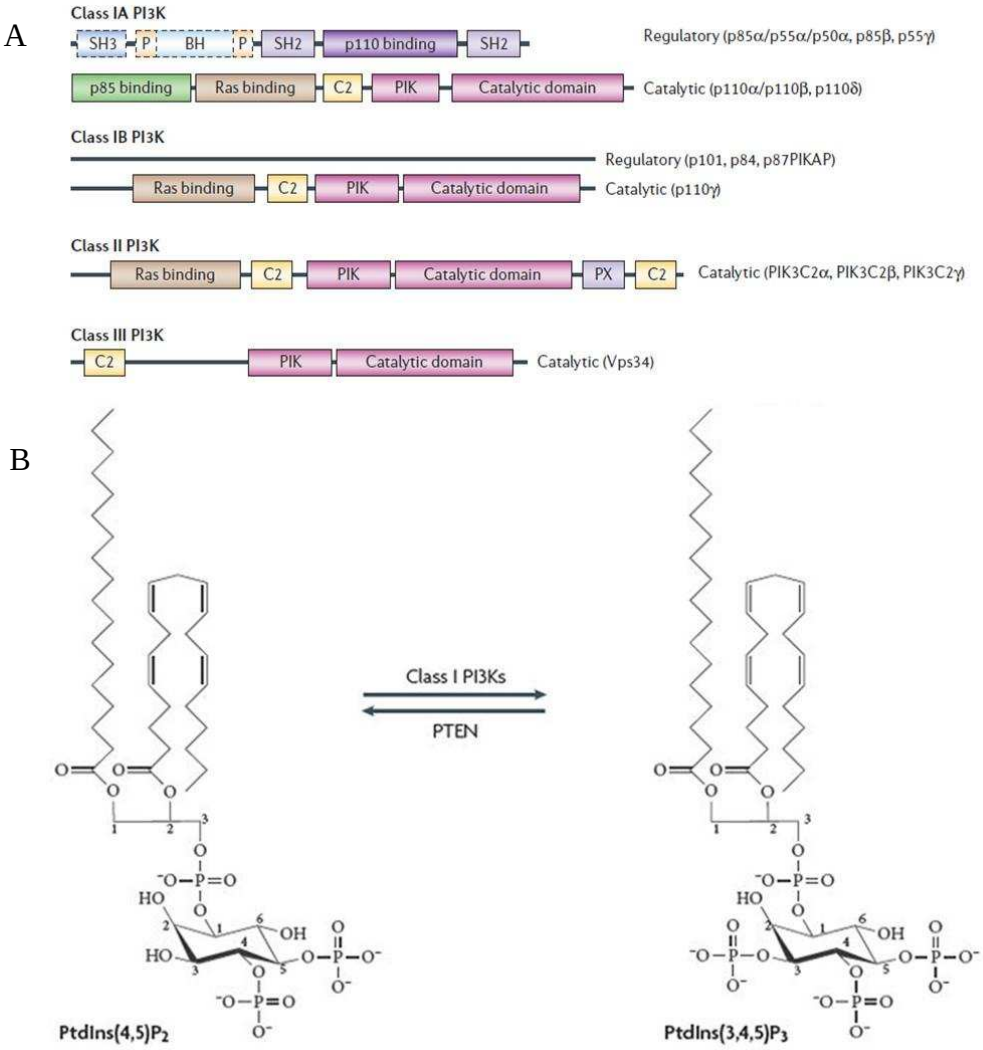

Figure 1.13 The members of the PI3K family[33, 100]

(A) PI3Ks have been divided into three classes according to their structural characteristics and substrate specificity. (B) The level of phosphatidylinositol-3,4,5-triphosphate, $PI(3,4,5)P_3$, is regulated by Class I PI3K and PTEN.

Among major classes of PI3K, class I PI3Ks (named as PI3Kα, PI3Kβ, PI3Kγ and PI3Kδ) have shown to be involved in cancers, and so have drawn the majority of attention in research.[102] Class I PI3Ks are heterodimers consisting of a regulatory subunit and a 110 kDa catalytic subunit. Based on different mechanisms of activation, this class is further divided into two subgroups: class Ia (p110α, p110β, and p110δ) and class Ib (p110γ). They phosphorylate the inositol lipids to generate the same lipid product phosphatidylinositol-3,4,5-triphosphate ($PtdIns(3,4,5)P_3$) (Figure 1.13 B).[33, 103] Interestingly, class I PI3K could also function as serine/threonine protein kinases.[104]

1.4.2.2.1.2PI3K/Akt signalling pathway

The signalling network defined by PI3K, Akt and mTOR controls most hallmarks of cancer, including cell cycle, survival, metabolism, motility and genomic instability.[103] The PI3K/Akt signalling pathway is depicted in Figure 1.14.

Activated by receptor tyrosine kinases (RTKs) and Ras at the membrane, PI3K generates phospholipids (second messengers) and initiates a series of intracellular signalling pathways. The production of key second messenger phosphatidylinositol-3, 4, 5-trisphosphate (PtdIns(3,4,5)P_3) from the substrate phosphatidylinositol-4,5-bisphosphate (PtdIns(4,5)P_3) is tightly regulated by the opposing activity of PI3K and PtdIns(4,5)P_2 phosphatases (PTEN).[101, 105, 106] PTEN (Phosphatase and tensin homolog) is an important tumour suppressor, and acts as a major negative regulator of PI3K/Akt signalling. Loss of PTEN activity leads to unrestrained PI3K/Akt pathway activation leading to cancer.[33]

Through providing docking sites for signalling proteins with pleckstrin-homology (PH) domains, PtdIns(3,4,5)P_3 then recruits a subset of signalling proteins to the plasma membrane, including Akt and its activator PDK1 (3-phosphoinositide-dependent kinase 1).[101] Akt, also known as protein kinase B, is a serine/threonine kinase phosphorylated by both PDK1 (on Thr308) and mTOR2 (on Ser473). It is the primary receptor of PI3K-initiated signalling and controls essential cellular activities through phosphorylation of a number of downstream effectors.[102, 107]

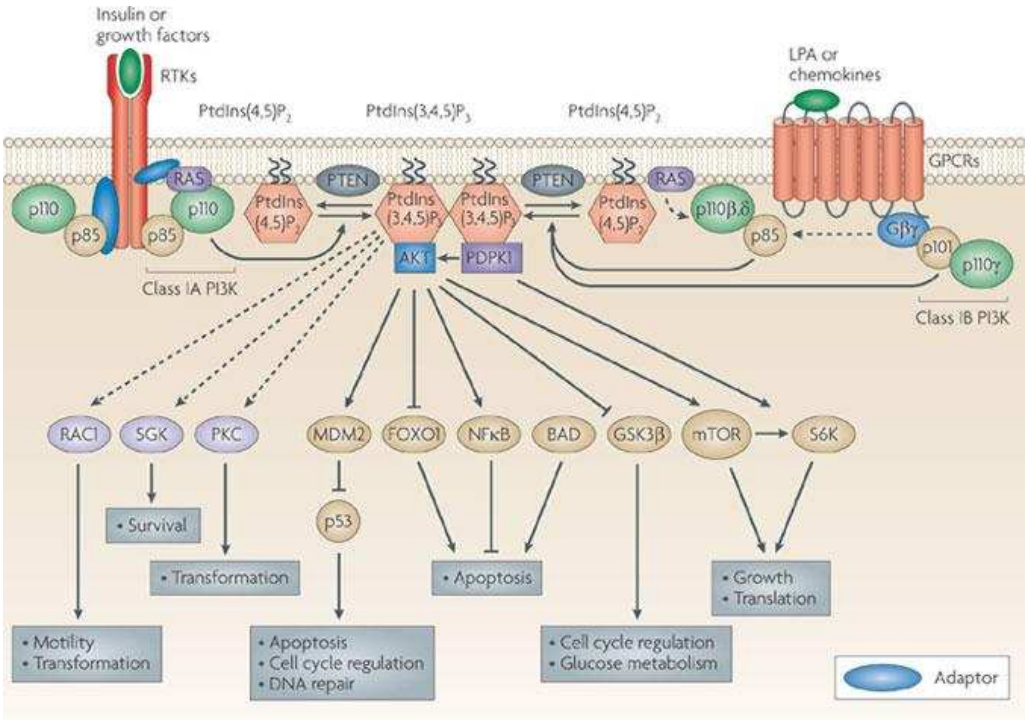

Figure 1.14 The class I PI3K signalling pathway[33]

One of the key downstream effector of Akt is mTOR. The serine/threonine protein kinase mTOR belongs to a group of the PI3K family referred to as class IV PI3Ks. It functions at two distinct nodes in the pathway: mTOR complex 2 (mTORC2) phosphorylates key residues to activate Akt and other kinases, while mTORC1 is a central regulator of cellular metabolism and biosynthesis.[103] Akt activate mTOR by phosphorylating both PRAS40 and TSC2 (tuberous sclerosis complex) to release their inhibitory effects on mTORC1. The best characterized downstream targets of mTORC1 are S6K1 (p70S6 kinase) and 4E-BP1 (4E-binding protein), both of which are critically involved in the regulation of protein synthesis.[33]

1.4.2.2.1.3PI3K/Akt signalling on cell cycle and apoptosis

PI3K/Akt pathway regulates cell growth signalling pathways and determines the rate of cell cycle progression. PI3K and its downstream effector Akt control cell cycle entry by inactivating the FOXO (Forkhead Box, subgroup O) transcription factors. PI3K/FOXO work as a complementary switch: when

PI3K is active, FOXO transcription factors are inactive. The switch is turned on and off at different phases of the cell cycle, thus regulating cell cycle progression.[108] During the G1/S cell cycle progression, Akt inactivates GSK-3β, leading to increased cyclin D1 and $P21^{Cip1}$ phosphorylation.[107] Meanwhile, it inhibits tumour suppressor tuberin (TSC2), leading to the reduction of $p27^{(Kip1)}$.[109] Thus, Akt positively regulates G1/S cell cycle progression and prolongs cell survival. Recent studies have also shown that constitutive activation of PI3K pathway induced by DNA damage led to a substantial decrease in Chk1 kinase activity.[110] Inactivation of Chk1 therefore mediated Cdc25c phosphorylation and prevent the inhibition of cyclin B1/Cdc2 leading to resistance to DNA damage mediated G2/M arrest.

PI3K/Akt pathway is one of the major anti-apoptotic pathways operating in cells and Akt mediates PI3K-dependent survival. Anti-apoptotic effects mediated by Akt include modulating the activity of Bcl-2 family members, down-regulation of death receptors, and enhancement of the glycolytic rate.[109] Akt phosphorylates pro-apoptotic Bad, which in turn dissociates from Bcl-2, consequently inducing cell survival and preventing apoptosis.[107]

1.4.2.2.1.4Linking the PI3K pathway to human cancers

The discovery that the tumour suppressor PTEN worked by antagonizing PI3K established the first direct link between PI3K activation and human cancer.[33] Recent human cancer genomic studies suggest that the PIK3CA gene (encoding the PI3K catalytic isoform p110α) is the second most frequently mutated oncogene and multiple components of the PI3K pathway are frequently mutated or altered in common human cancers.[33, 103] As described above, activation of the PI3K signalling pathway contributes to cellular processes responsible for all important aspects of tumourigenesis.

For these reasons, PI3 kinase and other key components in this pathway become one of the most attractive targets for therapeutic intervention in cancer. Gradually deepening understanding about the PI3K/Akt signalling pathways is emerging and helping to provide a platform for novel drug discovery. From the first-generation inhibitors (LY294002 and Wortmannin) to the latest clinical candidate (GDC-0941), numerous PI3K inhibitors have shown promising results in cancer therapy.[100, 107]

1.4.2.2.2 ON01910.Na inhibits the PI3K/Akt pathway

A recent study by Prasad et al reported the molecular mechanism of ON01910.Na in mantle cell lymphoma (MCL) cell lines.[78] ON01910.Na down-regulates cyclin D1 by suppressing cyclin D1 mRNA translation through inhibiting PI-3K/Akt/mTOR/eIF4E-BP signalling pathway, and induces apoptosis via the mitochondrial pathway.

1.4.2.2.2.1ON01910.Na down-regulates cyclin D1

MCL is a subtype of B-cell lymphoma. Uncontrolled over-expression of cyclin D1 is the main characteristic of MCL. Many studies with ON01910.Na treatment both in vitro and in vivo have indicated that ON01910.Na may affect the translation of cyclin D1 through the PI3K/Akt/mTOR/eIF4E-BP signalling pathways.[74, 78, 111]

ON01910.Na modulates post-transcriptional regulation of cyclin D1, which is supported by the observation in cells that expression of cyclin D1 was significantly inhibited, while the mRNA levels of cyclin D1 were minimally affected.

In cancer cells, activated Akt phosphorylates and activates mTOR protein on Ser2448, which in turn phosphorylates eIF4E-BP (eIF4E-binding protein). The

phosphorylated eIF4E-BP releases eukaryotic translation initiation factor 4E (eIF4E), which simultaneously binds to the mRNA 7-methyl-guanosine cap and initiates translation of cyclin D1.[112] It has been shown that eIF-4E overexpression leads to an increase in cyclin D1 protein through both transcriptional and post-transcriptional regulatory pathways.[113] eIF4E enhances the transport of the cyclin D1 mRNA from the nucleus.[114]

ON01910.Na inhibited phosphorylation of Akt (Ser473), mTOR, eIF4E-BP and reduced the cap binding activity of eIF4E, indicating ON01910.Na negatively regulates the Akt/mTOR/eIF4E-BP/eIF4E pathway. However, the expression of PTEN was not affected, suggesting that PI3K was the direct target of ON01910.Na. This is confirmed by in vitro kinase inhibition assays using the recombinant PI-3Kα, β, γ and δ isoforms. ON01910.Na inhibited the kinase activity of PI-3Kα and β isoforms between concentrations of 1 and 10 mM in vitro.[78] The proposed mechanism of ON01910.Na blocking the PI3K/Akt/mTOR pathway is shown in Figure 1.15.

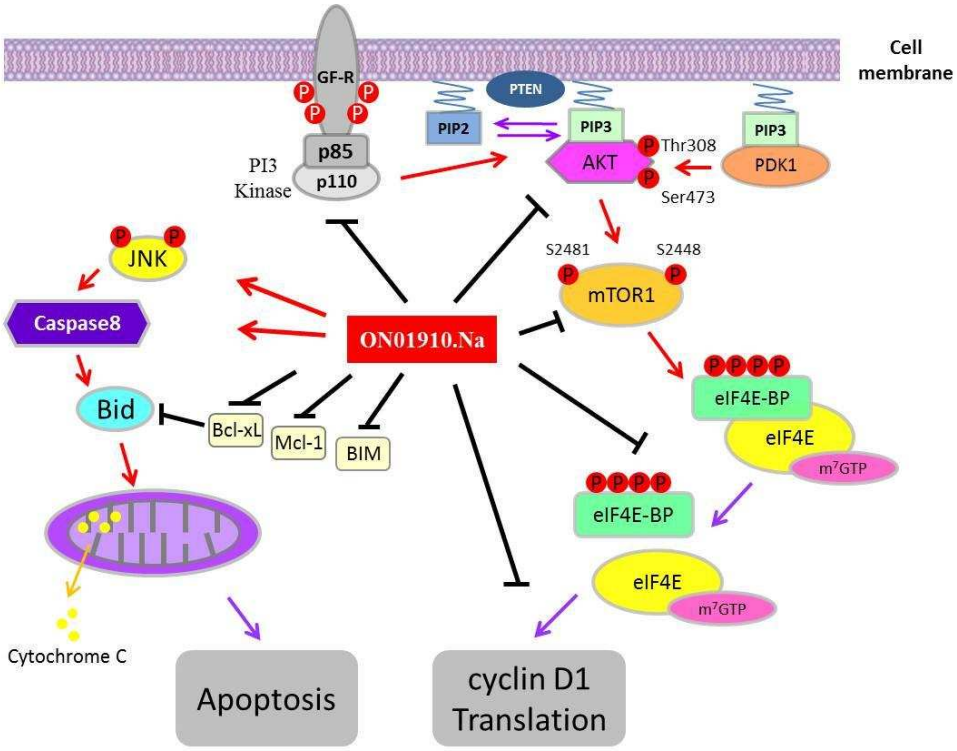

Figure 1.15 Proposed mechanism of action of ON01910.Na on blocking the PI3K/Akt/mTOR/eIF4E-BP pathway and inducing apoptosis.

Stimulatory (red) and inhibitory (black) interactions with ON01910.Na are shown.[78, 112, 115, 116]

1.4.2.2.3 ON01910.Na induces mitochondrial apoptosis

ON01910.Na was reported to induce apoptosis through mitochondrial pathways.[78] Analysis of the Bcl-2 family revealed that ON01910.Na down-regulate the expression of Bid, Bcl-xL and Mcl-1, while Bax and Bad are not affected. Recently ON01910.Na was found to inhibit another anti-apoptotic factor, BIM, which is targeted and phosphorylated by Akt.[115] Bid plays the key role in releasing cytochrome c from mitochondria.[116] Existing as an inactive precursor in the cytosol, Bid is activated following cleavage by caspase-8. Subsequently, Bid translocates to the mitochondria and induces cytochrome c release, followed by mitochondrial damage.[117]

The caspase-8 independent cleavage of Bid involves JNKs (c-Jun N-terminal kinases), members of MAP-kinases which play important roles in both death receptor (DR) and mitochondrial-mediated apoptotic pathways.[118]

ON01910.Na increases the phosphorylation of JNKs. Afterwards, JNKs induce cleavage of Bid and release cytochrome c to form the apoptosomes.[118] Studies show that after ON01910.Na treatment caspase-3 and -7 also generate the cleaved product and lead to apoptosis.[78]

1.4.2.3 Other possible targets of ON01910.Na

ON01910.Na has also been reported to target other signalling pathways. A study demonstrated that ON01910.Na induced apoptosis in chronic lymphocytic leukaemia B-cells without significant toxicity against T-cells or normal B-cells.[119] Gene expression profiling revealed two main mechanisms of action: inhibition of PI3K/Akt and induction of an oxidative stress response through AP-1 (activator protein 1), JNK and ATF3 (Cyclic AMP-dependent transcription factor) that culminated in the up-regulation of NOXA. Induction of cell cycle arrest by ON01910.Na has also been shown to correlate with the level of hyper-phosphorylation of Ran GTPase-activating protein.[119]

1.4.3 Issues affecting ON01910.Na's development as an anti-cancer agent

Despite ON01910.Na presenting efficacious activity against a wide range of cancers together with an attractive safety profile, a number of key issues remain that are affecting its development; these include an incomplete understanding of its anti-tumour mechanisms, its low oral bioavailability and unsatisfactory pharmacological properties.

1.4.3.1 Incomplete understanding of anti-cancer mechanisms

ON01910.Na is regarded as a multi-target kinases inhibitor. To date, although hypotheses regarding mechanism of action have been put forward, limited

findings have been reported and the precise mechanisms still need to be established. Besides, the crystal structure or molecule modelling for ON01910.Na in complex with any target kinase is not available yet, therefore the precise binding mode is difficult to predict, which holds back lead optimization of molecules with improved druggable properties.

1.4.3.2 Unsatisfactory pharmacological properties

In preclinical data, the plasma half-life of ON01910.Na was less than 2 hours in rat, dog, and human plasma.[120] Due to its short plasma half-life and rapid clearance, a continuous IV infusion is recommended. This issue will limit the option for dosage forms and schedule, and more importantly, will increase unwanted toxicities.

Both oral and parenteral formulations of ON01910.Na are under clinical investigation. However, low lipophilicity of ON01910.Na was observed with $LogD_{pH\ 7.4}$ = 0.83. This would reduce the extent of drug absorption as well as limiting its administration. Moreover, failure to broadly metabolize ON01910.Na in vivo limits the drug exposure and must be compensated by higher drug concentrations.[62] It is a fact that ON01910.Na exhibits extensive protein binding which impairs drug distribution to the tissue, further resulting low drug bioavailability (10–15%.in rats).[75]

2 Aims and objectives

(E)-Styrylbenzylsulfones exhibit broad spectrum of anti-tumour activity in vitro while exhibiting relatively mild toxicity to normal human cells.[68] In view of the limitations identified during the development of ON01910.Na, the styrylbenzylsulfones pharmacophore was intended to be optimized by implementing an analogue-based design approach and develop a novel series of anti-cancer agents. The aim of the research project described hereinafter is to design, synthesise and biologically evaluate a novel class of 5-((styrylsulfonyl)methyl)pyridin-3-amine with improved efficacy and drug-like properties using ON0910.Na as a lead compound.

To achieve this major aim, the research project was undertaken with the following specific objectives:

1) Design and synthesis of a class of 5-((styrylsulfonyl)methyl)pyridin-3-amine as novel anti-cancer agents. A synthesis strategy will be developed for 5-((styrylsulfonyl)methyl)pyridin-3-amine and its derivatives.
2) Understand the SAR of new compounds, based on their effects on proliferation. The new SAR will enrich previously reported SAR and help to verify the variation of certain features, including efficacy, selectivity and drug like properties of the molecule. Furthermore, these SAR relationships in turn may guide to predict the activity of new analogues.
3) Develop a cell-based screening cascade for evaluating biological activities of new compounds, including the effects on proliferation, cell cycle regulation and apoptosis. This cascade could then be used to identify favoured compounds to go forward to in vitro and in vivo testing, such as assessment of drug like properties.

4) Investigate the detailed cellular mechanism of action of favoured compounds in comparison with ON01910.Na.

   During the middle-stage of the project, TL-77 as well as ON01910.Na was subjected to the kinase activity test. Although ON01910.Na was originally considered to be a novel Plk1 inhibitor, lacking Plk1 kinase inhibitory activity was observed in both compounds treatment. Thus, it became one of the major goals of this project to identify the mechanism of action and could be addressed through the following strategy:

   - In-depth analysis the effects of lead compound TL-77 on cell cycle regulation. Effect of TL-77 on DNA damage signalling regulators will be primarily identified.
   - Probe the potential target molecules on PI3K/AKT signal transductive pathway.
   - Examine the effect of TL-77 on tubulin polymerization and inducing microtubule abnormalities.
   - Identify the molecule mechanism of TL-77-induced apoptosis.

This project involves the synthesis phase, in vitro biological evaluation and preliminary mechanistic study of these small molecule inhibitors. Broad spectra of biological and chemical techniques are employed, which are critical in the early stages of drug discovery.

3 Synthetic Chemistry

3.1 Introduction and rationale of design

Definitions of "drug-likeness" have been wildly published based on the analysis of molecular properties of successful drugs. These rules correlate simple molecular properties with successful drug development.[121] The optimization of drug-like properties, such as absorption, distribution, metabolism, excretion, and toxicity (ADME/Tox) properties is an integral element of drug discovery studies.[122] The primary guide to this approach is pioneered by Lipinski's Rule of Five.

Based on an extensive analysis of the structures of orally active drugs candidates, Lipinski and colleagues set up an absorption - permeability alert procedure to guide the development of an orally active compound.[123] According to the Rule of Five, good absorption or permeation is more viable for a chemical when hydrogen bond donors are ≤ 5; hydrogen bond acceptors ≤ 10; molecular weight ≤ 500; and Log P ≤ 5 (octanol-water partition coefficient).[123] Lipinski's Rule of Five provided the original framework for the development of orally bioavailable drug candidates and it has been widely used for the assessment of drug-likeness.[124, 125] In addition to the molecular properties discussed by Lipinski, other properties have been proposed as oral bioavailability parameters, such as the number of rotatable bonds (NROT), lipophilicity, polar surface area, and number of aromatic rings.[126-128] An example of those extensions of the rule is the adjustment of the optimal molecular lipophilicity. Lipophilicity significantly influences ADME/Tox properties and can be valued by partition or distribution coefficient (Log P or

Log D). Compounds with moderate lipophilicity (Log D 0-3, optimal Log D ~2) generally possess good balance between solubility and permeability, and is optimal for drug development.[129] Moreover, in an attempt to improve the predictions of drug-likeness, the rule of five has also been extended to the rule of three based on the 'fragment-based' discovery to define lead-like compounds.[124]

Reddy et al. have pioneered the development of a novel group of anti-tumour agents with general structure of (E)-Styrylbenzylsulfones to inhibit the cell cycle progression and induce apoptosis in cancer cells (Figure 3.1).[61] A molecule with the amino group in third position on benzene ring, ON01500 (Figure 3.1), showed the highest potency; however, it has very low solubility. In order to enhance the drug-likeness and the hydrophilicity, the amino group in third position was converted to glycine as ON01910, which was further made into its water-soluble sodium ON01910.Na (Figure 3.1). The presence of sodium glycine in ON01910.Na did not affect the potency against cancer cell lines, but improved aqueous solubility, which is critical for intravenous administration.[61]

ON013100 (Figure 3.1), a structural analogue of ON01910.Na, is another potent anti-tumour candidate and was selected by in silico and in vitro screening for evaluation in a preclinical brain tumour model. Given the lipophilic nature of ON013100 (predicted logD=2.53), its structure was further modified to achieve favourable lipophilicity values and facilitate intravascular administration. An aqueous soluble form, ON013105 (Figure 3.1) was then developed by introducing a disodium phosphate group at 3-hydroxyl position on the benzene ring.[63]

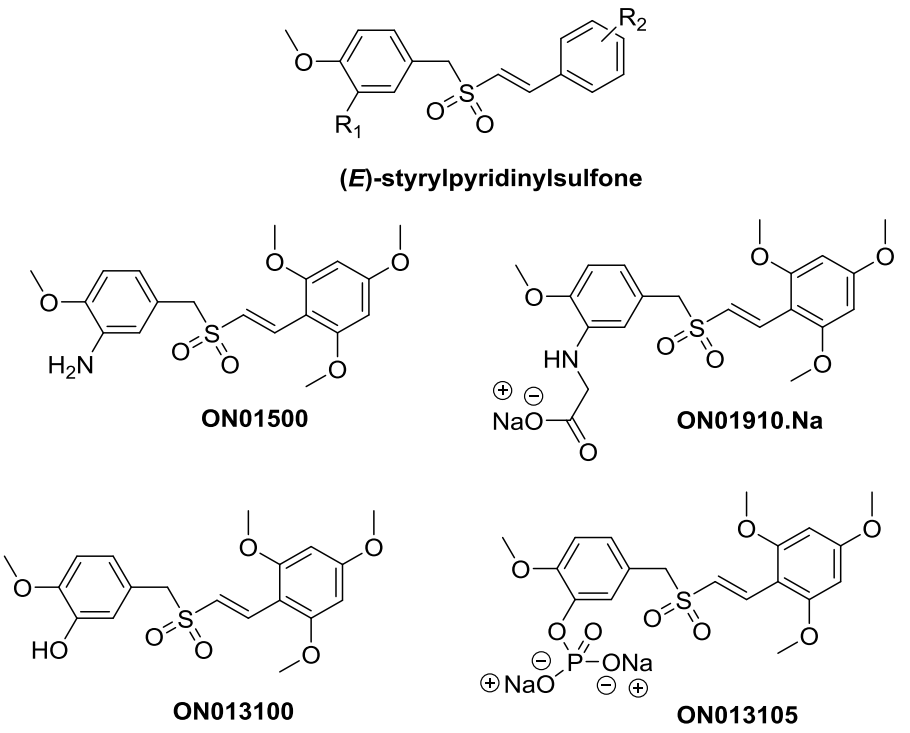

Figure 3.1 The styrylpyridinylsulfone pharmacophore and drug-like candidates.

Introduction of an ionized moiety into (E)-Styrylbenzylsulfones improved aqueous solubility of drug candidates ON01910.Na and ON013105. However, failing to keep the balance between solubility and permeability, low lipophilicity of both ON01910.Na (predicted logD = −1.07 [63]; $logD_{pH\ 7.4}$ = 0.83 [125]) and ON013105 (predicted logD = −2.45 [63]) were observed. The solubility of ON01910.Na is 95 mg/mL (200 mM) in vitro and 30 mg/mL (Saline) in vivo.[130] Such hydrophilic compounds are not expected to show desirable drug-like properties or oral bioavailability. Poor permeability, low BBB penetration for CNS drug and high renal clearance - shortening the half-life - are big concerns with such compounds. The preclinical in vivo pharmacokinetics study of ON01910.Na confirmed this issue and recommended the administration of ON01910.Na by continuous IV infusion due to its short half-life and rapid clearance.[120] Meanwhile, low bioavailability with 10-15% of ON01910.Na (10 and 20 mg/kg, 1 h infusion) in rats was observed.[75]

In an attempt to improve drug-likeness and ADME properties of ON01910.Na analogues, two novel series of (E)-styrylsulfonyl methylpyridine derivatives was designed (**class I and II,** Figure 3.2).

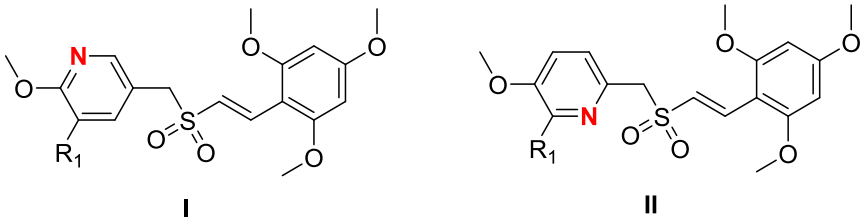

Figure 3.2 The structures of (*E*)-styrylsulfonyl methylpyridine derivatives.

SAR studies have identified that the styrylbenzylsulfonyl moiety is essential for anti-mitotic activity.[68, 131] However, the main scaffold of styrylbenzylsulfone pharmacophore exhibits high lipophilicity (cLog P > 3, PSA < 40, calculated by Chem Office Ultra 13.0), which may lead to non-specific binding, low solubility causing formulation problems, and poor oral absorption. Reddy group intend to increase the drug likeness and the water solubility by introducing ionized functional groups at the 3-position of the benzyl ring for intravenous administration, but the pioneer compounds exhibited undesirable drug likeness properties (high PSA, poor permeability), which have been described previously. Therefore, we intend to modify this pharmacophore to achieve derivatives with improved pharmaceutical properties.

Pyridine replacement from benzene was proposed due to its expected impact on physicochemical characteristics.[132] Pyridine-containing compounds exhibited intermediate solubility and low protein binding.[133] Many examples of bioisosteric replacement of benzene rings with pyridine rings have been described.[134, 135] Preferred compounds demonstrate desirable properties, including improved metabolic stability, aqueous solubility, as well as similar mechanism of action.[134] In this case, by introduction of a polar pyridinyl ring,

two novel chemical classes were generated, which were expected to possess improved pharmaceutical properties (moderate lipophilicity with $logD_{7.4}$ values ~2, desirable aqueous solubility and improved oral bioavailability) when compared to the benzylstyrylsulfonyl series. (Figure 3.2)

Cytotoxic activity of the styrylbenzylsulfones was found to be greatly dependent on the nature and position of the substituents on the two aromatic rings. Substitutions on the styryl ring system were generally found to be tolerated, but a 2,4,6-trimethoxystyryl moiety is important for optimum potency. A recent study has also indicated that the (E)-isomers of styrylbenzylsulfonyl derivatives have superior biological efficacy compared to the respective (Z)-isomers.[136] For these reasons, the 2, 4, 6-trimethoxystyryl section and (E)-configuration was retained.

Meanwhile, structure–function studies have also shown that substitutions at the 3-position of the benzyl ring help to enhance anti-proliferative activity.[68] Therefore, diverse drug-like groups were selected that would modify the 3-positon of the benzyl ring.

3.2 Synthetic strategy

A synthetic strategy to prepare ON01910.Na was reported previously by Reddy et al.[68] Two general methods of synthesizing benzyl styrylsulfone are shown in Scheme 3.1 and Scheme 3.2.

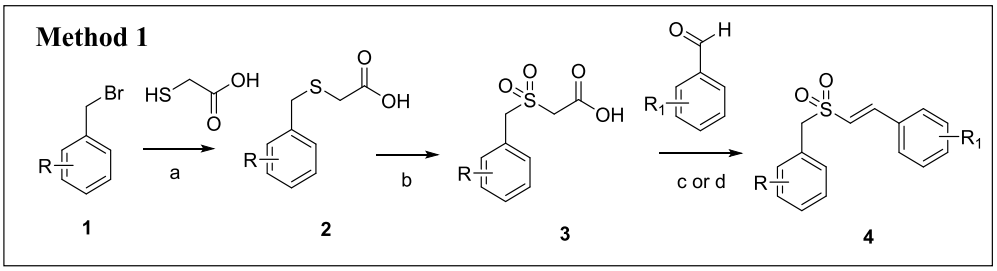

Scheme 3.1 Method 1 of synthesizing benzyl styrylsulfone.[68]

Reagents and conditions: (a) NaOH, MeOH, 4hr, r.t., 94%. (b) 30% H_2O_2, CH_3COOH, 18hr, r.t., 92%. (c) Piperidine, benzoic acid, toluene, 120°C, 2-4h, 48% or (d) CH_3COOH, benzylamine, 118°C, 2-8h, 66%.

In Scheme 3.1, substituted benzyl bromides **1** were initially reacted with thioglycollic acid in mild basic conditions to yield compound **2**. Then **2** was further oxidized in hydrogen peroxide to give **3**. The key step, Knoevenagel condensation between **3** and the aromatic aldehyde followed. This step can be carried out with (c) the aromatic aldehyde in toluene in the presence of catalytic piperidine and benzoic acid or (d) the aromatic aldehyde in glacial acetic acid in the presence of catalytic benzylamine to afford benzyl styrylsulfone **4**.[68]

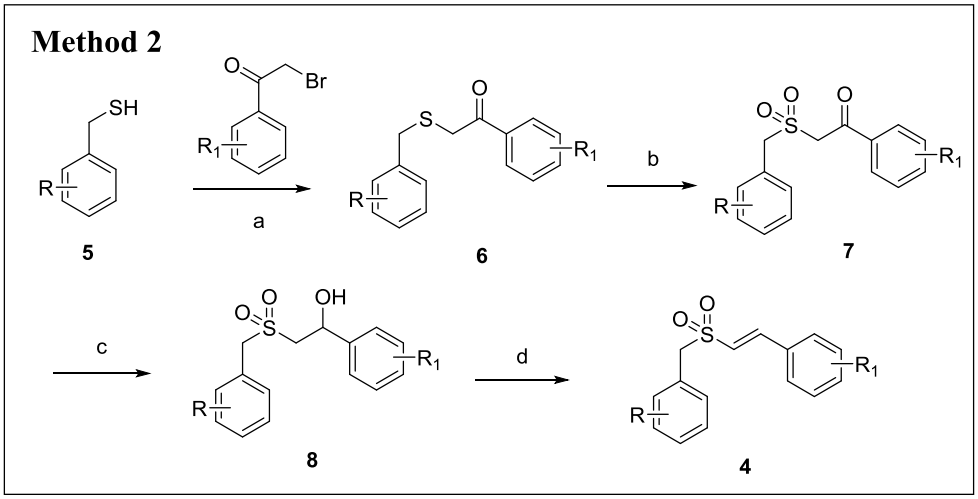

Scheme 3.2 Method 2 of synthesizing benzyl styrylsulfone.[68]

Reagents and conditions: (a) NaOH, MeOH, 4hr, r.t., 93%. (b) 30% H_2O_2, CH_3COOH, 24hr, r.t., 94%. (c) $NaBH_4$, EtOH, 30 min, 0°C, 88%. (d) p-toluenesulfonic acid, C_6H_6, 3h, reflux, 80°C, 65%.

Alternatively, **4** could be prepared through method 2 in Scheme 3.2. Starting from coupling of benzyl mercaptans **5** and α-bromo substituted acetophenones, compound **6** was then oxidized to yield **7**. Sodium borohydride was used to reduce the carbonyl group and give the corresponding alcohol, **8**. Finally, elimination of water from **8** in refluxing solution of p-toluenesulfonic acid in benzene gave benzyl styrylsulfone **4**.[68]

3.2.1 Synthetic strategy of (E)-3-((styrylsulfonyl)methyl)pyridine

Method 1 was adopted in this project. The general synthetic strategy for the production of (E)-2-methoxy-5-(((2,4,6-trimethoxystyryl)sulfonyl)methyl)pyridine intermediates **9-16** is outlined in Scheme 3.3.

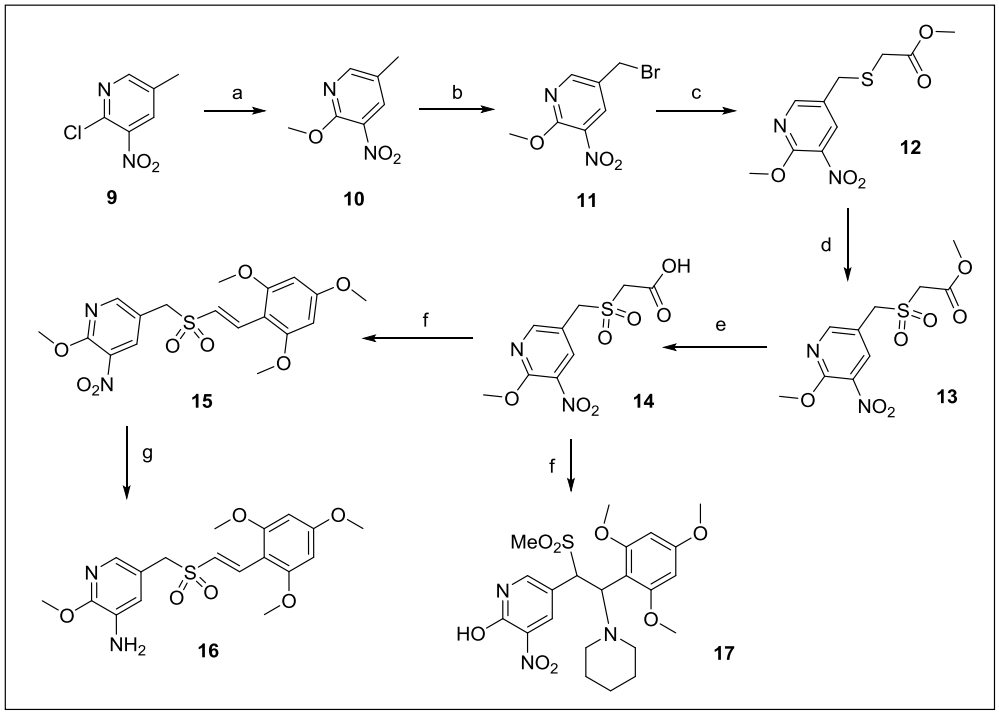

Scheme 3.3 Synthesis of (*E*)-2-methoxy-5-(((2,4,6-trimethoxystyryl)sulfonyl)methyl)pyridin-3-amine.

Reagents and conditions: (a) Na, MeOH, reflux, 4 h, 92%; (b) NBS, benzoyl peroxide, CCl_4, reflux, 48 h, 33%; (c) methyl thioglycolate, Na_2CO_3, MeOH, r.t. 1 h, 74%; (d) H_2O_2, acetic acid, 60 ºC, 6 h, 99%; (e) Na_2CO_3, H_2O/MeOH (1:1), r.t., 4 h, 99%; (f) 2,4,6-Trimethoxybenz-aldehyde, benzoic acid, piperidine, toluene, reflux, 3 h, 41%; (g) Fe, acetic acid/MeOH (3:4), 50 ºC, 2h, 98%.

Starting from commercially available 2-chloro-5-methyl-3-nitropyridine (**9**), methyoxylation (nucleophilic substitution) was carried out with sodium in refluxing methanol to yield 2-methoxy-5-methyl-3-nitropyridine (**10**) in 92% yield. Bromination of 5-methylpyridine **10** with N-bromosuccinimide (NBS) in the presence of benzoyl peroxide obtained **11**. Subsequent nucleophilic displacement of the bromine of 5-(bromomethyl)pryridine (**11**) with methyl

thioglycolate to afford thioether **12**. **12** was then readily oxidised with 30% hydrogen peroxide in glacial acetic acid to give sulfone **13** in excellent yield. Saponification of the latter was performed using sodium carbonate in a mixture of methanol and water to give carboxylic acid **14** in a quantitative yield.

The key step, Doebner - Knoevenagel condensation between **14** and 2,4,6-trimethoxybenzaldehyde, was initially attempted using pyridine as solvent in the presence of piperidine. The desired (E)-2-methoxy-3-nitro-5-(((2,4,6-trimethoxystyryl)sulfonyl)methyl)pyridine **15** was isolated by flash column chromatography in 10% yield along with a piperidine-substituted by-product **17**. The yield of **15** was significantly improved to 41% when the reaction was conducted using toluene in the presence of a mixture of piperidine and benzoic acid. Reduction of **15** to (E)-2-methoxy-5-(((2,4,6-trimethoxystyryl)sulfonyl)methyl)pyridin-3-amine **16** was achieved in a high yield using iron powder in methanol in the presence of mild acid.

3.2.2 Synthetic strategy for (E)-3-((styrylsulfonyl)methyl)pyridine 3C-amino derivatives

To assess the influence of substitution at the 3-positon on the heterocyclic ring on the anti-proliferative activity, a series of 3C-amino derivatives of **16** were synthesised by the chemistry shown in Scheme 3.4. Substitution reaction of **16** with methanesulfonyl chloride or acetyl chloride in the presence of an appropriate base afforded the corresponding sulfonamide **18a** (R = $NHSO_2Me$) or acetamide **18b** (R = NHCOMe) in good to excellent yields. **18b** was further treated with iodoethane in THF in the presence of strong base resulting in N, N-disubstituted acetamide **18c** (R = N(Et)COMe). Treatment of **16** with ethyl 2-bromoacetate in DMF in the presence of base obtained ethyl acetate **18d** (R =

$NHCH_2CO_2Et$). Subsequently hydrolysis of **18d** in an alkaline solution afforded carboxylic acid **18e** (R = $NHCH_2CO_2H$), while **18d** was also reacted with ammonia to afford amide **18f** (R = $NHCH_2CONH_2$) in 98% yield.

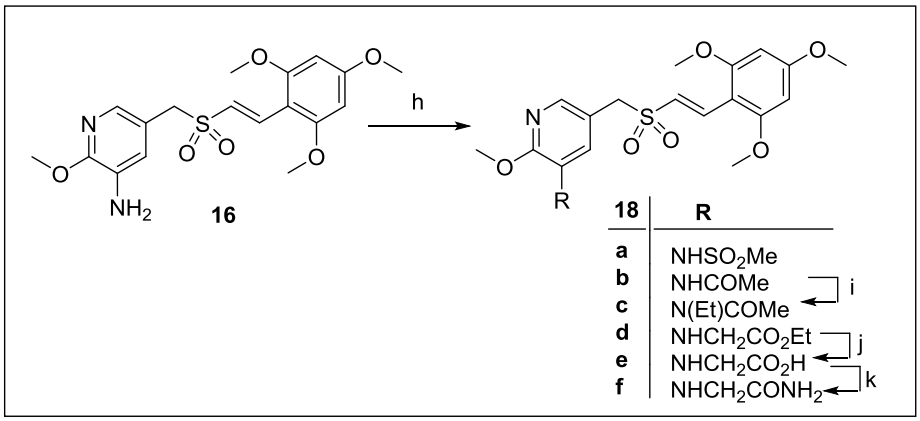

Scheme 3.4 Synthesis of (*E*)-2-methoxy-5-(((2,4,6-trimethoxystyryl)sulfonyl)methyl)pyridin-3C-amine derivatives.

Reagents and conditions: (h) 18a*:* methanesulfonyl chloride, pyridine, 0 ºC to r.t., 12-13 h, 76%; 18b: acetyl chloride, pyridine, 0 ºC to r.t., 12 h, 43%; 18d: ethyl bromoacetate, K_2CO_3, DMF, 60 ºC, overnight, 73%; (i) NaH, 18b, THF, iodoethane, r.t., 4.5 h, 70%; (j) NaOH, 18d, THF/H_2O (1:1) r.t. 1 h, 69.5%; (k) NH_3 (7*N* in MeOH), 18d, H_2O, 60 ºC, o/n, 98%.

3.3 Discussion

3.3.1 Bromine free radical substitution of 2-methoxy-5-methyl-3-nitropyridine

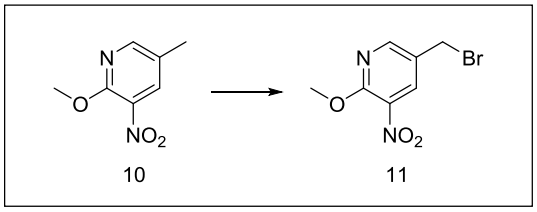

Scheme 3.5 Synthesis of 5-bromomethyl-2-methoxy-3-nitropyridine.

Reagents and conditions: NBS, benzoyl peroxide, CCl_4, reflux, 48 h, 33%.

Benzylic brominations with NBS producing excellent yield of benzyl bromides were reported previously.[137, 138] Most widely used conditions are refluxing a solution of NBS in CCl_4 in the presence of a suitable initiator i.e. UV, benzoyl

peroxide, azo-bis-isobutyronitrile (AIBN).[138] In this case, Benzoyl peroxide was used to effect radical initiation.

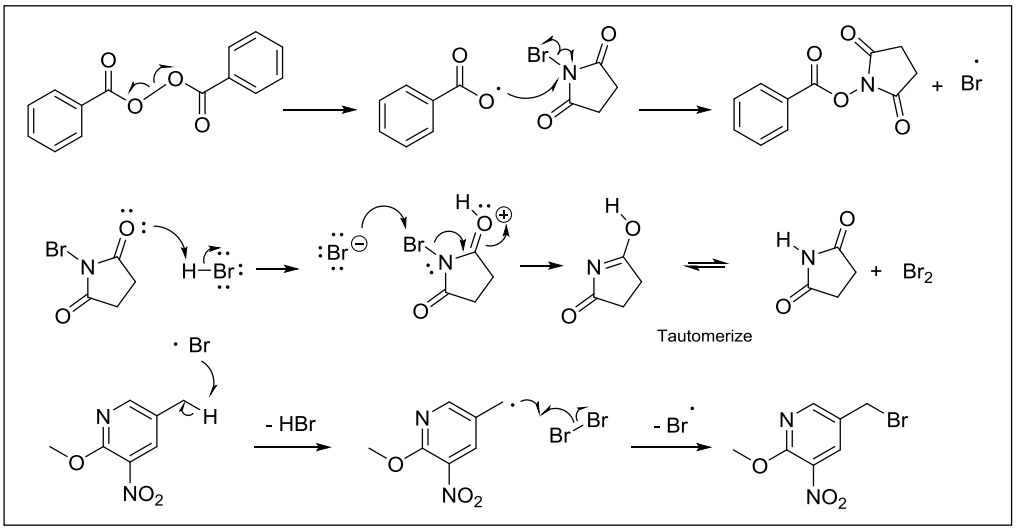

Scheme 3.6 Proposed reaction mechanism of 5-bromomethyl-2-methoxy-3-nitropyridine.

The bromination of **10** followed free-radical chain mechanism. The proposed reaction mechanism is shown in the Scheme 3.6. Benzoyl peroxide ($(PhCOO)_2$) generates benzoyloxyl radicals (PhCOO•), which attack NBS to produce the free bromide radicals (Br•). The free bromide radical attacks the 5-methyl of the molecule to produce the free radical intermediate and HBr. At the same time, the new generated HBr reacts with another molecule of NBS and maintains the high concentration of Br_2. Therefore, the reaction is driven forward by the participation of the second molecule of Br_2.

During the reaction, dibromide compound would be formed as the majority side product. Chloroform was suggested as a possible solvent, since it is a more general and relatively lower toxic solvent for organic compounds. However, CCl_4 was proved to have the optimal characteristics for this reaction, resulting in a lower level of dibromide production and a relatively high yield of the desired product. Alternatively, the generation of dibromide compound could be decreased by strictly controlling the equivalence of NBS: starting material to

1:1. Following these optimizations, the yield could be improved from 33% to 42%.

3.3.2 Formation of pyridine-3- methyl sulfonyl acetic acid

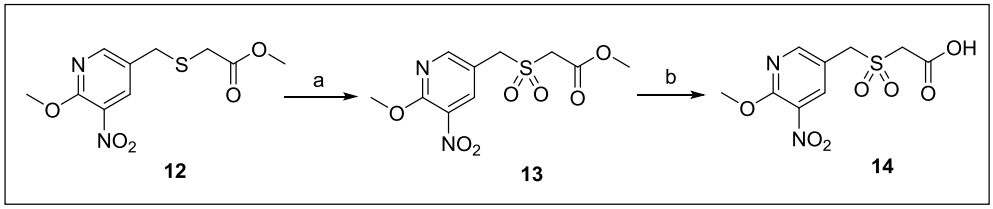

Scheme 3.7 Synthesis of 2-(((6-Methoxy-5-nitropyridin-3-yl)methyl)sulfonyl)acetic acid.
Reagents and conditions: (a) H_2O_2, AcOH, 60°C; (b) Na_2CO_3, H_2O, MeOH, r.t.

Pyridine methylsulfonyl acid **14** was prepared according to the route shown in the Scheme 3.7. The proposed reaction mechanism of oxidation and hydrolysis were detailed in Scheme 3.8 and Scheme 3.9.

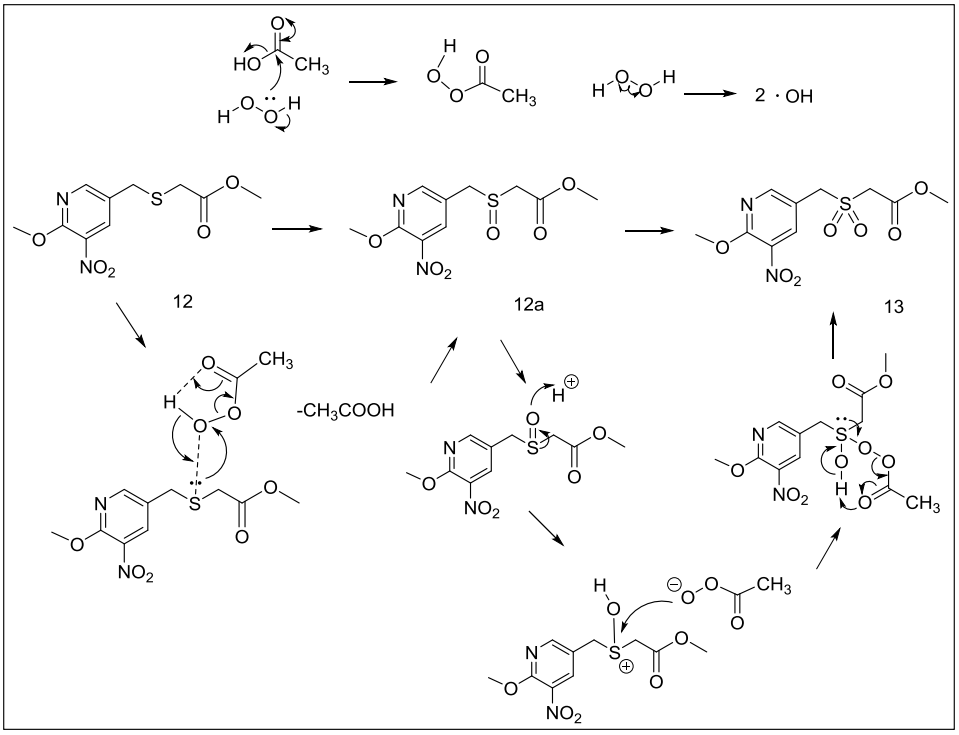

Scheme 3.8 Proposed reaction mechanism of 2-((6-methoxy-5-nitropyridin-3-yl)methylsulfonyl)acetate.

The chemoselective oxidation of **12** is proposed to be a free radical reaction. Firstly, hydrogen peroxide is capable of forming ethaneperoxoic acid in the presence of acetic acid. At the same time, it can generate hydroxide radicals.

Then ethaneperoxoic acid promotes the formation of the sulfinyl bond to generate intermediate **12a**, which is subsequently attacked by the hydroxide radical, thus forming compound **13** with the sulfonyl function group.

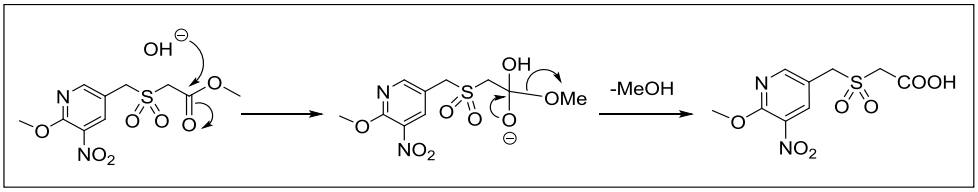

Scheme 3.9 Proposed reaction mechanism of 2-((6-methoxy-5-nitropyridin-3-yl)methylsulfonyl)acetic acid.

As shown in Scheme 3.9, the hydrolysis is a base-catalysed hydrolysis reaction. In base, the hydroxide nucleophile (OH^-) attacks the electrophilic C of the C=O bond in acetate ester, forming a tetrahedral intermediate. Subsequently, as a better leaving group, alkoxide picks up H^+ and leaves as a methanol molecule to generate the acid **14**.

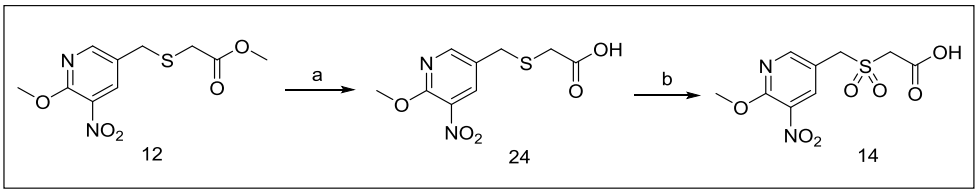

Scheme 3.10 Alternative method of synthesising 2-(((6-Methoxy-5-nitropyridin-3-yl)methyl)sulfonyl)acetic acid.

Reagents and conditions: (a) Na_2CO_3, H_2O, r.t.; (b) H_2O_2, AcOH, 60°C.

Alternatively, 2-((6-methoxy-5-nitropyridin-3-yl)methylsulfonyl)acetic acid **14** could be prepared by hydrolysis of **12** followed by the oxidation of 2-(((6-methoxy-5-nitropyridin-3-yl)methylthio)acetic acid **24** (Scheme 3.10). However, compared to the route detailed in Scheme 3.7, this method was proved not only hard to be monitored by Thin Layer Chromatography (TLC) but also brought difficulties to the purification procedure.

3.3.3 Doebner-Knoevenagel condensation

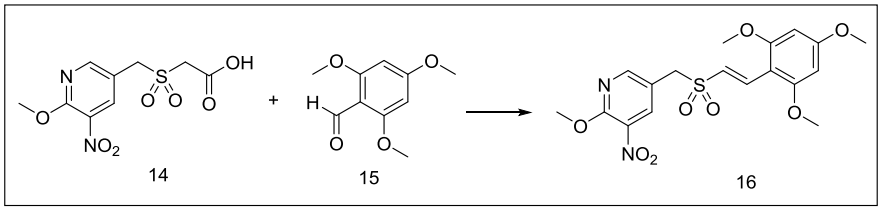

Scheme 3.11 Synthesis of (*E*)-2-methoxy-3-nitro-5-((2,4,6-trimethoxystyrylsulfonyl)methyl)pyridine.

Reagents and conditions: benzoic acid, piperidine, toluene, reflux, 3 h, 41%.

A key step reaction of this project, the Doebner-Knoevenagel condensation between **16** and 2,4,6- trimethoxybenzaldehyde aims to introduce the styryl function group. This reaction is aldol condensation involving the monocarboxylate and the aldehyde. Weak bases are used to avoid side reaction of the aldehydes and ketones. After many trials investigating the reaction conditions, an optimum yield of 41% was achieved when the reaction was conducted using toluene in the presence of a mixture of piperidine and benzoic acid.

Reaction occurs via the deprotonation of the alpha carbon of the methylene at the acetic acid moiety by the piperidine. An enolate intermediate is formed initially as shown below:

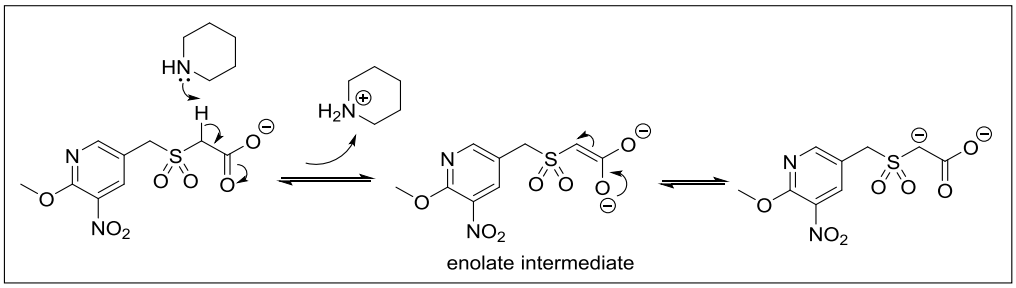

Next, the resulting anion intermediate attacks the aromatic aldehyde, and an aldol is generated. The resulting anion pick up the H on previously generated piperidine cation, and then it undergo subsequent base-induced elimination.

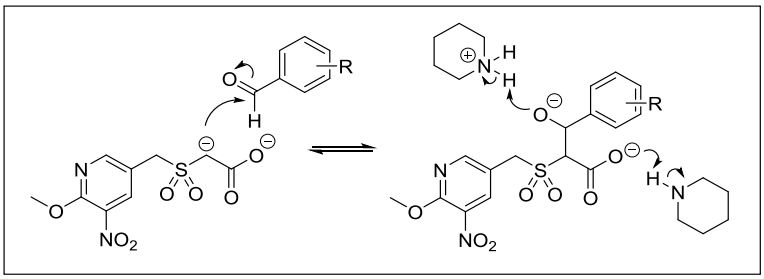

In the final decarboxylation step, the decarboxylation and elimination of H_2O and CO_2 subsequently affords (E)-3-((styrylsulfonyl)methyl)pyridine.

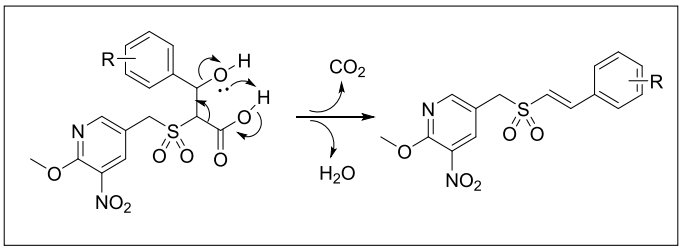

In this reaction, piperidine acts as organocatalyst and involves the corresponding iminium intermediate as an acceptor. Toluene is often used as solvents in these reactions because it forms azeotropes with water. The azeotropes can be measured quantitatively by distillation so as to monitor the reaction.[139] The decarboxylation could give either the E or Z double bond. As the trans isomers are the more stable than cis isomers, you can assume that the elimination reaction is under thermodynamic control and the product has E geometry.

Doebner - Knoevenagel condensation was initially attempted using pyridine as solvent in the presence of piperidine. The reaction gave a complex mixture with many by-products and resulted a yield as low as 10-15%. The purification of the mixture led to the identification of 2-methoxy-5-(1-(methylsulfonyl)-2-(piperidin-1-yl)-2-(2,4,6-trimethoxyphenyl) ethyl)-3-nitropyridine **17** as one of the major by-products (in 14% yield). Its structure was confirmed by X-ray crystallography as shown in Figure 3.3. The proposed reaction mechanism is shown in Scheme 3.12.

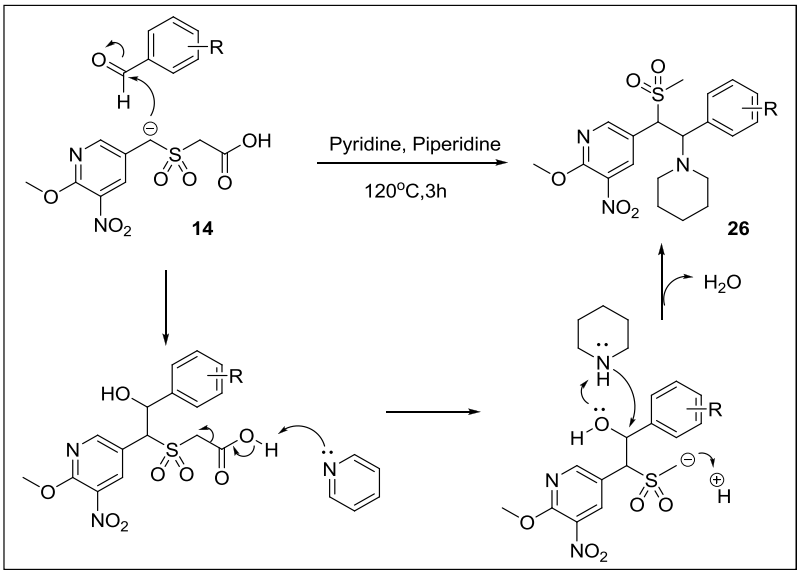

Scheme 3.12 Proposed reaction mechanism of 2-methoxy-5-(1-(methylsulfonyl)-2-(piperidin-1-yl)-2-(2,4,6-trimethoxyphenyl)ethyl)-3-nitropyridine.

3.4 Structure determination

All compounds were characterized fully by ^{1}H-NMR, ^{13}C-NMR and Mass spectrometry as detailed in the Experimental Section. Stereochemistry of the styryl functional group can be signed using ^{1}H-NMR spectroscopy. It is well known that the vicinal coupling constants measured for (E)-isomers are larger (range from 12–18 Hz; typical 15 Hz) than for (Z)-isomers (range from 0–12 Hz; typical 8 Hz). ^{1}H-NMR spectra of the derivatives of 2-((styrylsulfonyl)methyl)pyridine and 3-((styrylsulfonyl)methyl)pyridine gave rise to the vicinal coupling constants J values in a range of 15-16 Hz, indicating (E)-stereochemistry.

As representatives of the series, the molecular structure of compound **18a** was further determined unambiguously by the x-ray diffraction. The data collection and structure is presented in Table 3.1 and Figure 3.3. Compound **18a** crystallizes with a near planar solid-state conformation excepting the sulfonamide group on the pyridine ring and the "step" that occurs for the sulfone and the sp3 methylene (Figure 3.3A).[140] The bond length of C_{18}-C_{19} is

0.134nm, which is confirmed to be a double bond of alkene. The crystal structure of **18a** confirms that the compound is the (E)-isomers as expected from the synthetic approach and on the basis of ^{1}H NMR spectroscopy.

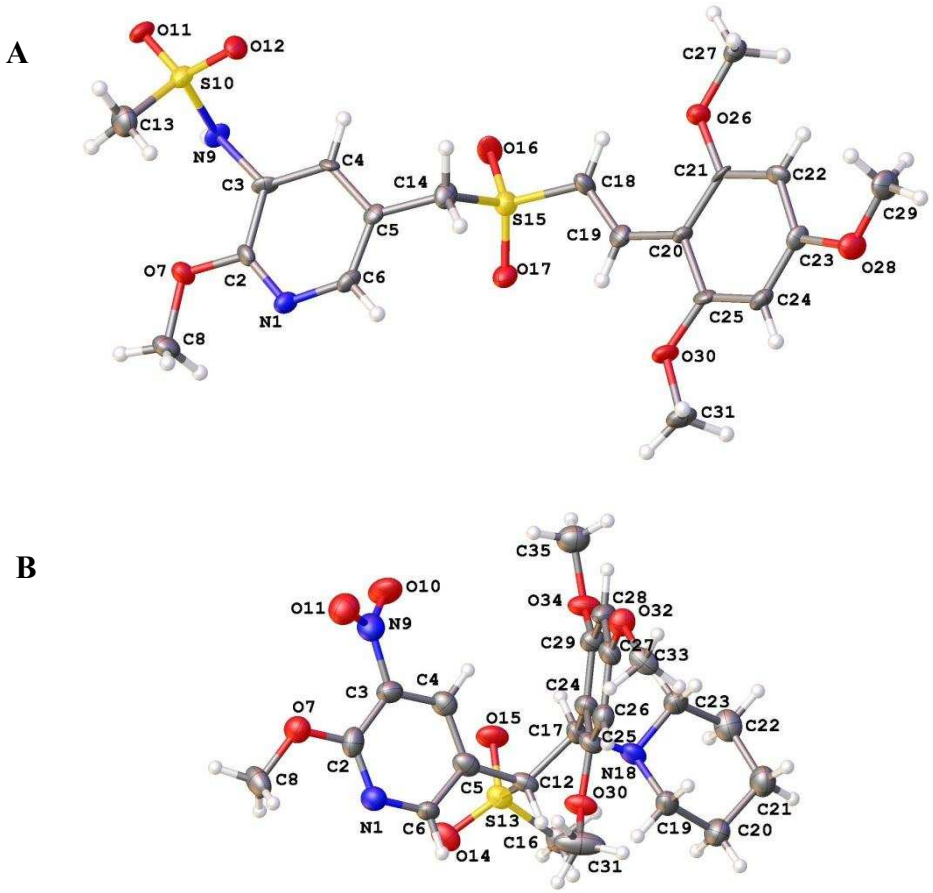

Figure 3.3 Crystal structures of 18a (A) and 17(B) with atomic numbering scheme.

Table 3.1 Crystal and X-ray experimental data for 18a.

Formula: $C_{19}H_{24}N_2O_8S_2$	M = 472.52 gmol^{-1}
Crystal System: Monoclinic	T = 90(2)K
Z = 4	Theta range: $8.16 \leq 2\theta \leq 148.68°$
Unitcell: a = 20.6703(11) Å	
b = 9.6447(5) Å	D_{calc} = 1.453 gcm^{-3}
c = 10.8382(4) Å	
$\alpha = 90.00$, $\beta = 91.021(4)$, $\gamma = 90.00°$	V = 2160.34(18) Å^3

4 Screening and biological evaluation of (E)-styrylsulfonyl methylpyridines

4.1 Introduction

In a programme to identify a novel chemical series of molecules possessing similar potency and modes of action, but improved pharmaceutical properties compared to ON01910.Na, our group have designed and synthesised a series of ON01910.Na analogues, including benzylstyrylsulfones, benzylstyrylsulfines and benzylsulfonyl-N-phenylacetamides.[131]

A cell-based screening was carried out on Class I of (E)-styrylsulfonyl methylpyridines. The principal aims of the biological screening were to assess the in vitro anti-tumour activities of new compounds, as well as determine the effects of different substitution on the potency of the compounds against tumour cells.

4.2 Results and discussion

4.2.1 Anti-proliferation activity

Effective anti-tumour drugs normally induce cancer cell death or inhibit proliferative activity, both of which decrease cancer cell viability. MTT is a water soluble yellow dye which can be converted to insoluble purple crystal formazan by mitochondrial dehydrogenases in viable cells. The anti-proliferative activities of new synthesized (E)-styrylsulfonyl methylpyridine derivatives were first assessed against colorectal carcinoma HCT-116, breast

carcinoma MCF-7, and ovarian carcinoma A2780 using a standard 72 h MTT cytotoxicity assay.[141]

We have chosen to focus the attention on these three cancers because they are among most common malignancies worldwide. These cell lines are all well characterised and are commonly utilized as model systems for studying cancer pathways and for developing new therapeutic approaches.

HCT-116 cells are well characterised by intact DNA damage checkpoint, and normal p53 responses.[142] According to Duldulao et al., up-regulated expression of seven genes responsible for DNA damage signalling was observed in HCT-116, including Cdc25c.[143] In addition, HCT-116 cells were reported to have a high expression and activity of Plk1.[144] Both HCT-116 and A2780 cell lines have been validated in the scientific literature to be the mitotic spindle checkpoint proficient.[145] Whereas, MCF-7 cells are partially defective for the G1 and mitotic spindle checkpoints.[146] Meanwhile, A2780 is confirmed with a biallelic inactivation of PTEN (9bp deletion in exon 5 and 37bp deletion in exon 8).[147] Due to PTEN deletion, PI3K pathway is deregulated in A2780 cells.[148] Since ON01910.Na targets Plk1 and PI3K by interrupting cell cycle division, decreasing expression of Cdc25c and producing multipolar spindles (refer to Chapter One), cytotoxicities of new synthesised compounds were accessed towards these cell lines.

Silencing genes, such as Plk1, in HCT-116 cells in vitro and in vivo have been stably generated.[149] Both HCT-116 and A2780 xenograft models established in nude mice were widely conducted to evaluate inhibitory capacity of Plk1 and PI3K inhibitors.[148, 150, 151] In consideration of both HCT-116 and A2780 cell lines could be well developed as in vitro and in vivo models, these two cell lines were used in this study for investigation of the mechanism of action.

The GI_{50} values (concentration for 50% of maximal inhibition of cell proliferation) of the tested compounds are summarized in Table 4.1. The anti-proliferative activity of the (E)-3-(((2,4,6-trimethoxystyryl)sulfonyl)methyl)pyridines were dramatically influenced by the 3C-substituent (R inTable 4.1) of pyridinyl ring. To analysis the influence of cell growth rates due to the different tissue origin on anti-proliferative activity, the population doubling time of tested cell lines were also provided in Table 4.1. A2780 exhibited a shortest population doubling time (13.5 h), while the doubling time of MCF-7 and HCT-116 are 30 h and 18 h, respectively.

Among the tested cell lines, A2780 cell is the most sensitive to compounds compared with other two cell lines, showing less anti-proliferative with smaller value of GI_{50}s (except ON01910.Na). On the other hand, compounds were generally less active in MCF-7 cells, with GI_{50}s higher than respective GI_{50}s in other two cell lines, except TL-66, TL-81 and AH-123. These differences in sensitivity correlated with population doubling time. For a given set of growth conditions, the cells with shorter population doubling time possess a higher population doubling level, which is more susceptible to mitotic block and subsequent mitotic death induced by mitotic blockers. In this study, compounds selectively exhibit enhanced anti-proliferative activity in cancer cells with higher population doubling level, indicating their potential anti-mitotic effect.

A moderate anti-proliferative activity (GI_{50} ~ 5-7 μM) was observed with compound **15** (R = NO_2) against these cell lines. Replacement of the nitro with an amino at 3C-position of the pyridinyl ring resulting in **16** (R = NH_2) significantly enhanced activity, with GI_{50}s in a range of 0.005-0.006 μM against all tested tumour cell lines, being ~10-fold more potent than ON01910.Na. Substitution of the 3C-amino with a methanesulfonamide as in

18a (R = $NHSO_2Me$) reduced the potency, giving GI_{50} values around 0.5-0.8μM against three cell lines. Moderate cyctoxic activity was seen with **18b** (R = NHCOMe) and **18f** (R = $NHCH_2CONH_2$). However its ethyl 2-aminoacetate derivative **18d** (R = $NHCH_2CO_2Et$) and 2-aminoacetic acid analogue **18e** (R = $NHCH_2CO_2H$) significantly enhanced cytotoxic with GI_{50} in a range 0.38−0.94 μM against the tumor cell lines. To validate the critical requirement of secondary amine at the 3C-position of pyridine, the acetamide **18b** (R = NHCOMe) was replaced by an ethylacetamide (**18c**, R = N(Et)COMe). The substitution was not tolerated, resulting in significantly loss of activity. Compound **17** was also tested, but it showed low cytotoxicity. Overall, ON01910.Na has potent cytotoxicity with GI_{50}s in a range of 0.031-0.062 μM.

In similar experiments, a compound synthesised by my group colleague Mr. Anran Hu and coded as **AH-123**, was also included. As a representative of Class II of (E)-styrylsulfonyl methylpyridines, **AH-123** (R = NH_2, X_1 = C, X_2 = N) exhibited potent anti-proliferative activity, resulting in nanomolar GI_{50} values (6−8 nM) against all cancer cell lines.

Table 4.1 Summary of structure and biological activity

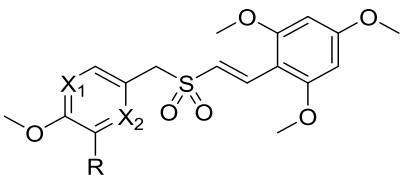

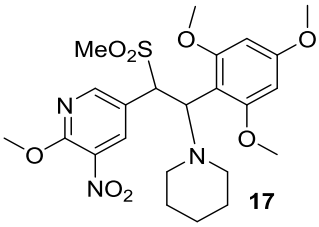

17

Code		Structure			72h-MTT cytotoxicity,* GI_{50} (μmol/L)		
		X_1	X_2	R	A2780 (PDT= 13.5 ± 3 h[152])	MCF-7 (PDT= 30.2 ± 0.7 h[153])	HCT-116 (PDT= 18.0 ± 3 h[154])
ON01910.Na		C	C	$NHCH_2CO_2H$	0.062 ± 0.040	0.050 ± 0.010	0.031 ± 0.003
15	**TL-66**	N	C	NO_2	7.21± 0.950	5.22 ± 0.160	7.43 ± 0.280
16	**TL-68**	N	C	NH_2	0.005 ± 0.001	0.006 ± 0.001	0.006 ± 0.001
18a	**TL-77**	N	C	$NHSO_2Me$	0.464 ± 0.029	0.78 ± 0.041	0.77 ±0.070
18b	**TL-81**	N	C	NHCOMe	7.095 ± 0.962	7.50 ± 1.060	8.219 ± 0.473
18d	**TL-94**	N	C	$NHCH_2CO_2Et$	0.409± 0.133	0.94 ± 0.010	0.517 ± 0.078
18e	**TL-110**	N	C	$NHCH_2CO_2H$	0.376 ± 0.093	–	0.410 ± 0.099
18f	**TL-116**	N	C	$NHCH_2CONH_2$	4.66 ± 0.263	>10	6.59 ± 0.710
18c	**TL-105**	N	C	N(Et)COMe	6.28 ± 0.600	>10	>10
–	**AH-123**	C	N	NH_2	0.007 ± 0.002	0.006 ± 0.001	0.008 ± 0.001
17	**TL-107**	–	–	–	4.85 ± 0.326	6.41 ± 1.120	4.40 ± 0.220

* Data expressed as the mean ± standard deviation of three independent experiments. PDT, Population doubling time.

4.2.2 Structure-activity relationship (SAR)

The established structure activity relationships (SAR) are shown schematically in Figure 4.1. SAR analysis suggested that the benzylstyrylsulfones moiety is essential for anti-proliferative activity. Substitutions on the benzyl ring system

were generally found to be tolerated, but the 2,4,6-trimethoxystyryl moiety is important for an optimum potency.[68, 131] A recent study also demonstrated that the (E)-isomers of styrylbenzylsulfonyl derivatives have higher antiproliferative activity compared to the respective (Z)-isomers.[136]

By introduction of a pyridinyl ring at different positions (nitrogen in X_1 or X_2 in Table 4.1), two novel chemical classes of (E)-styrylsulfonyl methylpyridines were generated and showed equivalent activities on cytotoxicity. SAR anylysis of styrylbenzylsulfones analogues generated by Reddy et al. indicated that amino group at the third position of aromatic ring is critical for compounds' activity.[61] Therefore, replacements of hydrogen atom in aromatic amine by various substituents are expected to be amenable to optimisation. As expected, the reported SAR for styrylbenzylsulfones is in harmony with the SAR of the (E)-3-(((2,4,6-trimethoxystyryl)sulfonyl)methyl)pyridines generated in house. So far as the compounds have been tested, substitutions on the 3C-position of pyridinyl ring with electron donating groups, such as amines and hydroxyl, afforded analogues with potent cytotoxicity. At the same time, substitutions on amino group were compared. Primary amine (**16**) possesses the best activity, while secondary amine with acetates (**18d** and **18e**) exhibited superior potency compared with acyl and sulfonyl groups. Furthermore, tertiary amine such as ethylacetamide (compound **18c)** resulted in significantly loss of activity. These observations indicate that repulsive interaction with the potential targets exists at this position, and smaller functional group in preferred at the substitution on amino group in the future structure optimization.

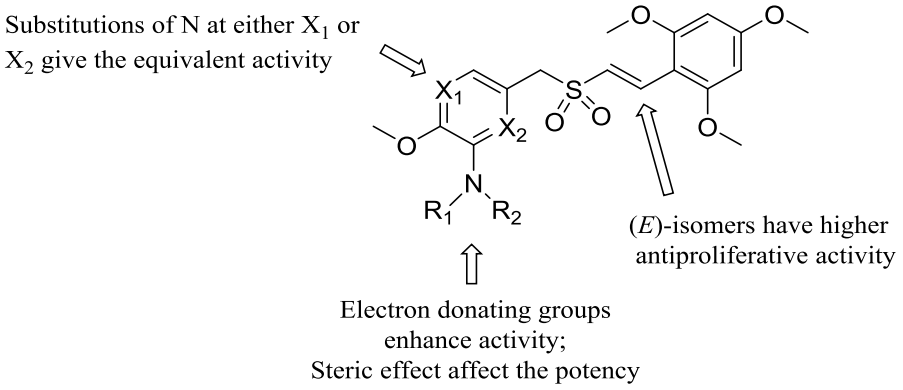

Figure 4.1 Summary of structure activity relationships of (*E*)-styrylsulfonyl methylpyridines

In our study, the molecule with methanesulfonamide group at 3C position (**18a**, TL-77) exhibited desire molecular potency. Methanesulfonamide group, due to its low lipophilicity nature, is widely introduced to the target molecules to confer physical properties (i.e. logD) and improve binding affinity to the enzymes.[155, 156] TL-77 should possess improved efficacy and oral bioavailability when compared to the benzylstyrylsulfonyl series.

As the leads of the two chemical series of (E)-styrylsulfonyl methylpyridines, TL-68 (**16**) and AH-123 exhibit similar cytotoxic profiles. Therefore, TL-68, TL-77 and AH-123 were selected for detailed primary cellular mode of action studies in comparison with ON01910.Na.

4.2.2.1 Discussion

In attempt to direct recognizing precise kinase inhibition, a kinase screening assay performed by Merck Millipore's KinaseProfiler™ was carried out for both TL-77 and ON01910.Na (ON01910.Na as the positive control) on six potential target proteins, including Aurora-A, Aurora-B, CDK1/cyclinB, PI3 Kinase (p110α/p85α), PI3 Kinase (p110β/p85α) and Plk1. (Appendix I) However, to our surprise, in this cell-free assay, neither compound inhibited the activity of Plk1 or PI3K, with no inhibitory effect on tested proteins.

The assay format used in KinaseProfiler test in this study is very similar to that used in the reported kinases study by Gumireddy et al [53], which proved ON01910.Na is a Plk1 inhibitor with the IC50 value of 9 - 10 nM. (Appendix I)

However, there are a couple of differences that may influence the result. Firstly, Gumireddy et al uses a much higher concentration of ATP (1 mM) than used in this study (70 uM). Although both compounds are not an ATP competitor, the ATP concentration may still make a difference, such as by inducing conformational change at the compound binding site. Secondly, Gumireddy et al uses a 30-minute pre-incubation of kinases with the compound, a step that is not included in our study. Vinyl sulfones (α,β-unsaturated sulfones), as good electrophiles, are able to readily form covalent adducts with many nucleophiles via Michael-type additions. It has been widely reported that vinyl sulfones are selective react quicker with thiol groups than with amines or other nucleophiles at comparable pKa values and steric environments.[157] The preference of vinyl sulfones for thiol groups could be utilized to selective targeting the cysteine residues in protein structures. Plk1 possesses three cysteines located in the active site (Cys 67, Cys 133, and Cys 212).[158] $Plk1^{Cys67}$ involves in molecular recognition by Plk1 inhibitors and improvement of the selectivity.[159] Moreover, other protein kinases are more commonly contain valine at this position, [159, 160] Therefore, benzylstyrylsulfonyl series (N01910.Na) as well as styrylsulfonyl methylpyridines (TL-77) with vinyl sulfones may have interactions with unpaired cysteine residues in Plk1. Pre-incubation of kinase with compounds may have a considerable effect on the apparent potency if the compound binds relatively slowly to the kinase. Therefore, further tests are required to determine the effect of compounds on kinases activity.

4.2.3 Primary cellular mode of action

4.2.3.1 Time-dependent anti-proliferation activity

Anti-proliferative activities of compounds TL-68, TL-77 and AH-123 were first assessed by the time-course MTT assays performed using HCT-116 and A2780 cells. As presented in

Table 4.2, all tested compounds increased potency with prolonged time and thus demonstrated a time dependent-manner.

Exposure of three compounds to HCT-116 and A2780 cells using the data from time-course MTT assays (Table 4.2) were further presented as plots in concentration × time vs time. As presented in Table 4.3 and Figure 4.2, ON01910.Na showed general consistent exposure from 24 h to 72 h in both cell lines, however, the product of concentration × time in A2780 (~2 μmol·h) is as twice as that in HCT-116 (4.1-5.8 μmol·h). These observations indicate that the anti- proliferative activity of ON01910.Na is cell line specific, and HCT-116 cells are more sensitive to this compound. The exposure of TL-77, on the other hand, reduced significantly from 91 μmol·h at 24 h to ~50 μmol·h (≥ 48 h) in HCT-116 cells. (Table 4.3) The same situation could be observed in A2780 cells, suggesting drug efficacy of TL-77 in cell culture is improved with prolonged time. At the same time, while relatively consistent drug exposure (1.49 - 2.6 μmol·h) ≤ 48 h of AH-123 were seen in both cell lines, its drug efficacies were largely improved (~0.5 μmol·h) when the treatment extended to 72h. (Table 4.3 and Figure 4.2)

Following 24 h exposure to HCT-116 cells, TL-68, AH-123 and ON01910.Na exhibited comparable cytotoxicity with GI_{50} values ~ 0.06 μM, while a GI_{50} value of 3.82 μM was observed after TL-77 treatment. Consequently, GI_{50}

values of 0.06 μM and 4 μM for respective compounds in HCT 116 cells were adopted as agent concentrations used in subsequent assays.

Table 4.2 MTT time-course experiments against human HCT-116 colon cancer cells and A2780 ovarian cancer cells

Cell line	Compound	Cytotoxicity, GI_{50} (μmol/L) ±SD*		
		24 h	48 h	72 h
HCT-116	ON01910.Na	0.068 ± 0.003	0.045 ±0.013	0.031 ± 0.003
	TL-68	0.051± 0.006	0.033 ±0.022	0.006 ±0.001
	TL-77	3.82± 0.683	1.02 ±0.022	0.77 ±0.070
	AH-123	0.062 ± 0.020	0.048 ±0.003	0.008±0.001
A2780	ON01910.Na	0.242 ±0.055	0.086 ±0.017	0.062 ± 0.040
	TL-68	–	–	0.005 ± 0.001
	TL-77	1.726 ±0.292	0.860 ± 0.493	0.464 ± 0.029
	AH-123	0.111 ±0.053	0.045 ±0.011	0.007 ± 0.002

The data given are mean values derived from at least three replicates (n = 3 per experiment) ± SD.

Table 4.3 Exposure of three compounds to HCT-116 and A2780 cells using the data from time-course MTT assays.

Cell line	Compounds	Exposure, Concentration × Time (μmol·h)		
		24h	48h	72h
HCT-116	ON01910.Na	1.632	2.16	2.232
	TL-77	91.68	48.96	55.44
	AH-123	1.488	2.304	0.576
A2780	ON01910.Na	5.808	4.128	4.464
	TL-77	41.424	41.28	33.408
	AH-123	2.664	2.16	0.504

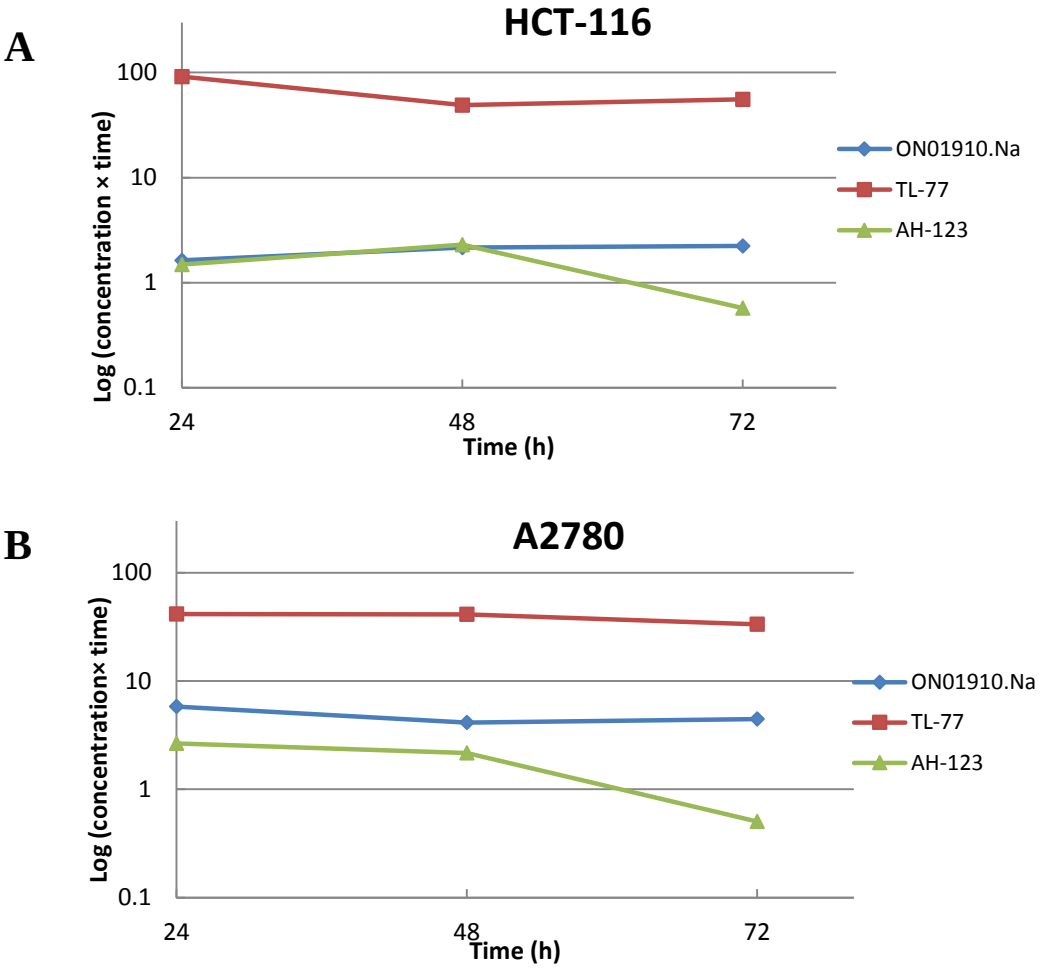

Figure 4.2 Plots in concentration × time vs time of three compounds in HCT-116 (A) and A2780 (B) cells using the data from time-course MTT assays.

To identify selectivity of compounds between cancer and normal cells, TL-68, TL-77, AH-123 and ON01910.Na were further tested against HCT-116 cancer cells and human microvascular endothelial HMEC-1 cells after 72h exposure.

As shown in Figure 4.3, despite their potent anti-proliferative activity against HCT-116 cancer cell lines (Figure 4.3 **A**), TL-68 and AH-123 showed little or no selectivity between cancer and normal cells, with high cytotoxicity on HMEC-1 cells (Figure 4.3 **B**). Overall, TL-77 demonstrated 4 fold greater potency against HCT-116 compared with normal cell line (HCT-116, GI_{50} = 770 nM; HMEC-1, GI_{50} = 2930 nM). Moreover, no significant selectivity of ON01910.Na between cancer cells (HCT-116, GI_{50} = 31 nM) and normal cells (HMEC-1, GI_{50} = 84 nM) was observed.

The positive values on Y axis represent cell growth. Approximate 5% cancer cells could still grow after 72 h treatment of TL-77 at the highest tested concentration, indicating the cell-kill reached a plateau. A possibility is that cells that not in G2/M phase escaped from mitotic block, and entered the next round of cell cycle without prior cytokinesis. This could be avoid by extend the treatment duration, as the plateau effect could not be observed after 96 h exposure (Figure 5.3). Additionally, combination therapy with other mitotic inhibitors could also avoid the plateau effect.

At the same time, the negative values on Y axis represent total cell death. In HMEC-1 cells (Figure 4.3 **B**), total cell death could be seen after all compounds treatment (from ≥ 0.04 μM of TL-68 and AH-123, and ≥ 0.2 μM of ON01910.Na), while this could not be observed until the concentration reached to 10 mM after TL-77 exposure.

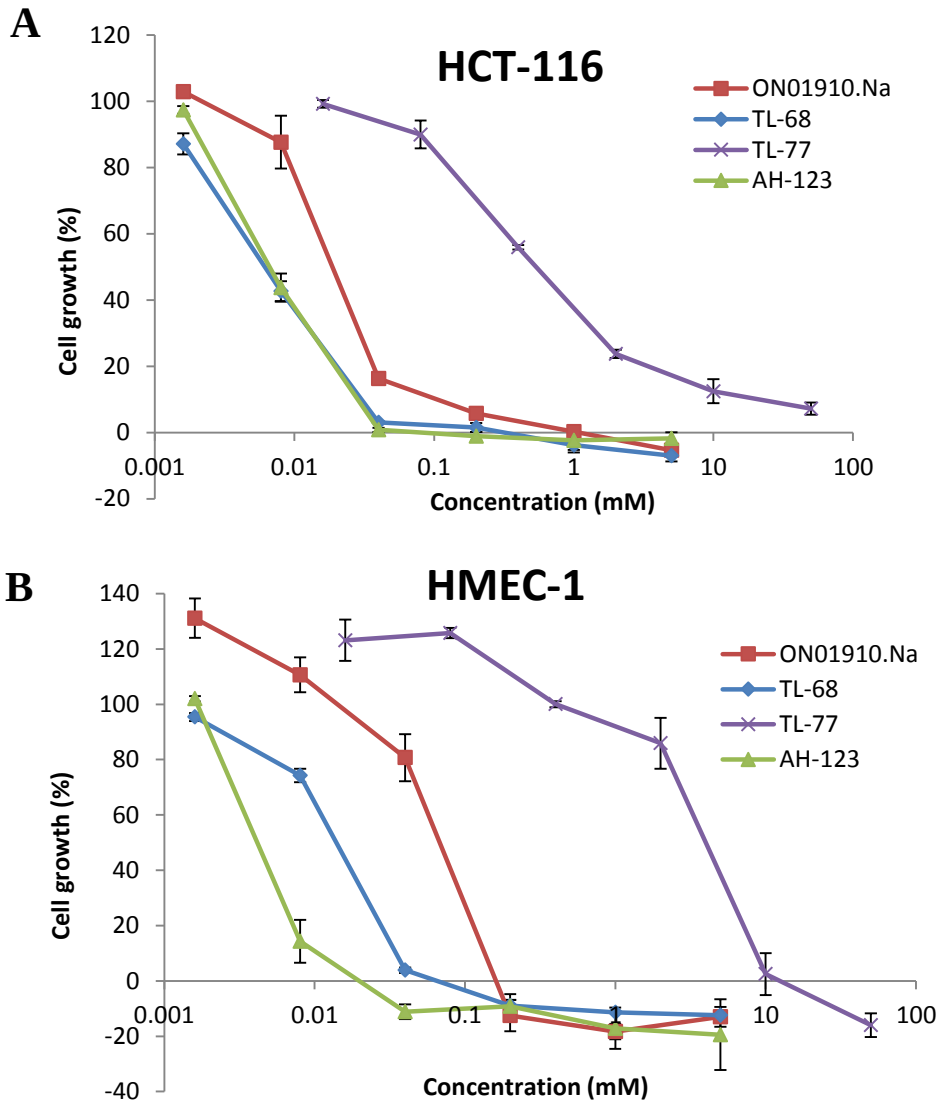

Figure 4.3 Anti-proliferative activity in human HCT-116 cancer cells (A) and HMEC-1 cells (B) by MTT 72 h assays.

The data given are mean values derived from at least three replicates (n = 3 per experiment) ± SD.

4.2.3.2 G2/M block on cell cycle effect

We next investigated whether the anti-proliferative effects of compounds were a consequence of cell cycle inhibition that caused activation of the cellular apoptosis program.

Analyses by flow cytometry in HCT-116 cells exposed severe perturbation of cell-cycle progression for all compounds (Figure 4.4). The results suggested that when treated with DMSO (0.2% v/v), most of the cells accumulated in the G1 phase (42.9%) without loss of viability. After treated with ON01910.Na for

24h at GI_{50} and $2\times GI_{50}$ (0.06 μM and 0.12 μM respectively), > 70% of cells were arrested in the G2/M phase (enhanced numbers of cells with 2N DNA content). Similar cell-cycle profiles were observed with TL-68, TL-77 and AH-123. Treatment with 0.06 μM TL-68 and AH-123 or 4 μM TL-77 resulted in accumulation of a respective 49.1%, 50.6% or 55.4% of G2/M cells, accompanied by substantial sub-G1 peaks indicating cell death. As the treatment concentrations increased to $2\times GI_{50}$, further G2/M phase arrests and increasing sub-G1 peaks were observed for TL-68, TL-77 and AH-123 in HCT-116 cells.

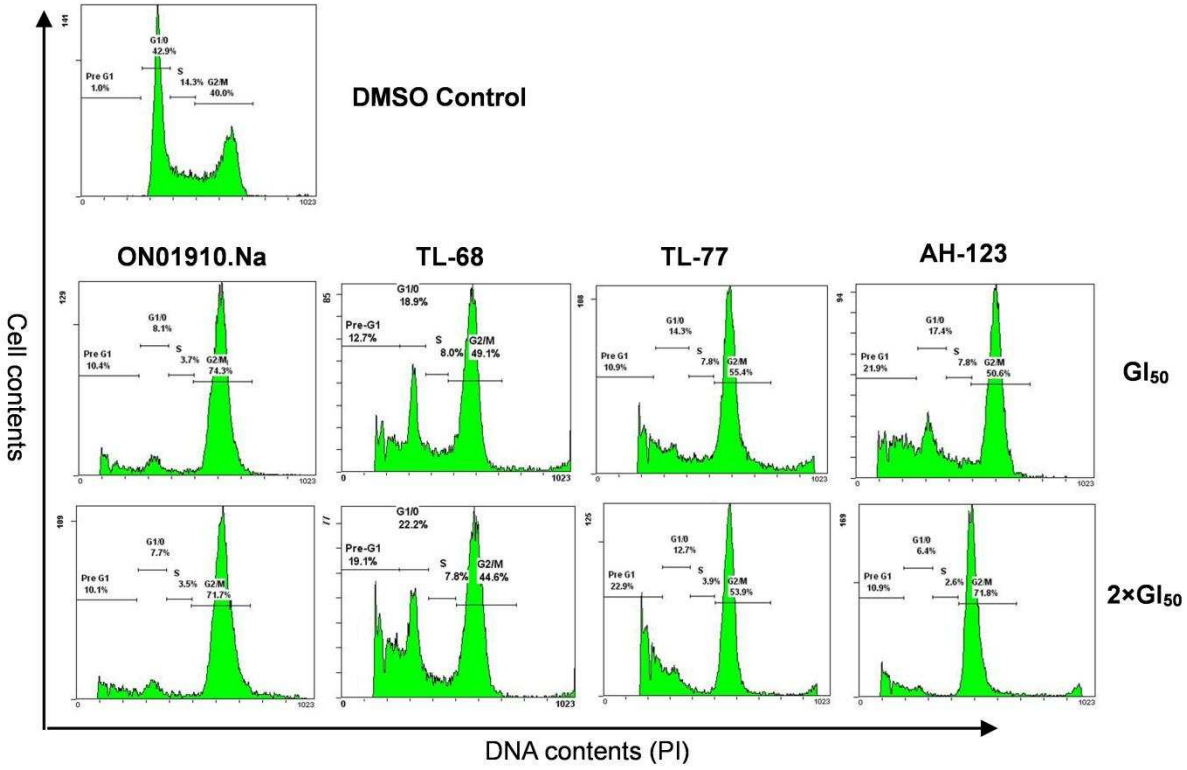

Figure 4.4 Cell-cycle effects of TL-68, TL-77, AH-123 and ON01910.Na on HCT-116 cells.

HCT-116 cells were treated with compounds for 24 h at the concentrations shown. Cells were fixed, stained with propidium iodide, and DNA content was analysed by flow cytometry.

4.2.3.3 Induction of apoptosis

Types of cell death include apoptosis, autophagy, mitotic catastrophe, necrosis and senescence. Cell morphology observation and annexinV/PI double staining were used to prove that compounds induced apoptosis in cancer cells.

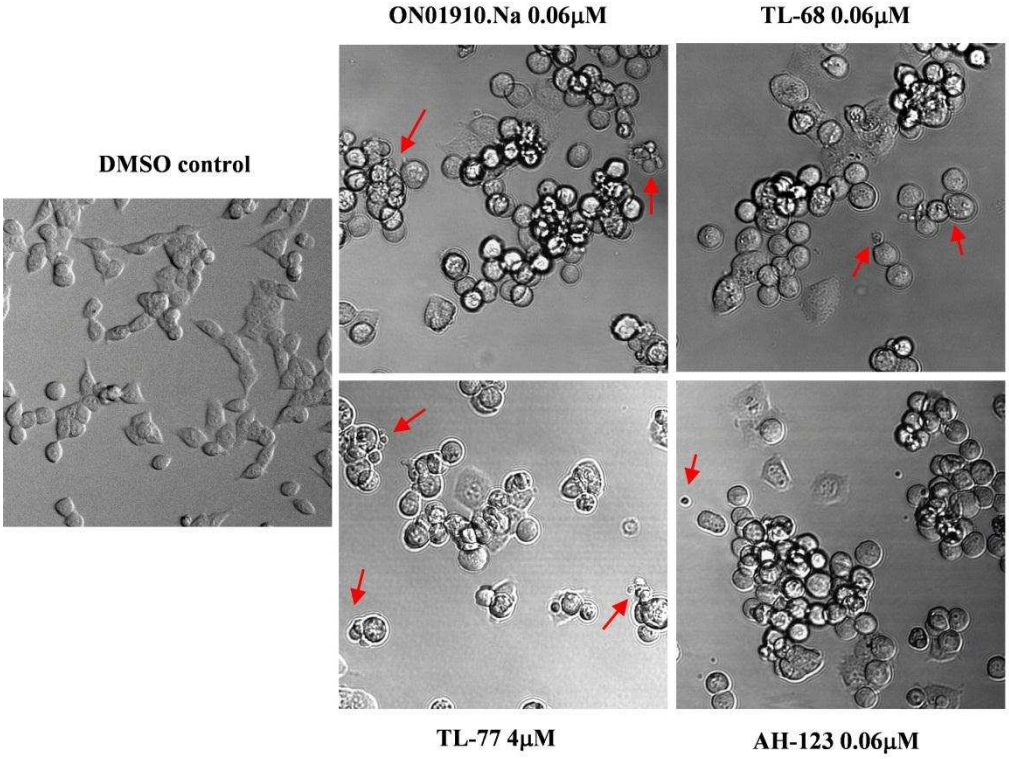

Figure 4.5 Images of cell death after treatment of TL-68, TL-77, AH-123 and ON01910.Na

HCT-116 cells were treated with compounds at GI_{50} concentrations for 24 h. DMSO vehicle treatment was used as negative control.

To investigate the morphological changes, HCT-116 cells were seeded into 6-well plates at 5000/well. Cell images were taken after 24 h treatment with TL-68, TL-77, AH-123, or ON01910.Na at GI_{50} concentrations. As illustrated in Figure 4.5**,** HCT-116 cells grew quickly after DMSO vehicle treatment (0.2% v/v), with nearly 60-80% confluency. However, after treatment of all compounds, the growth of cells was arrested with cell confluency less than 50%. For DMSO control, cells in the field of view appeared adherent. Cells were exhibited in spindle shape with clear, sharp boundaries between them. In

contrast, after treated with four compounds, cells display typical apoptotic morphology. Cell retraction, dynamic plasma membrane blebbing, cell fragments can be clearly detected microscopically (red arrows), suggesting cells were undergoing apoptosis.

To quantify the apoptosis caused by the exposure to compounds, HCT-116 cells exposed to TL-68, TL-77, AH-123, or ON01910.Na at GI_{50} and $2\times GI_{50}$ for a period of 48 h were analysed by Annexin V and propidium iodide staining. As shown in Figure 4.6, all four compounds induced significant apoptosis. ON01910.Na was most effective, inducing 45.9 - 48.6% apoptotic cells (annexin V-positive/PI negative cells) at concentrations of 0.06 μM and 0.12 μM. TL-77 induced apoptosis with 36.4% apoptotic cells at GI_{50} (4 μM), while a more obvious apoptotic effect were observed at $2\times GI_{50}$ value (42.2%). Generally, TL-68 and AH-123 exhibited equivalent apoptotic profiles; inducing ~ 37% apoptotic cells at GI_{50} concentrations. As the concentration increase to $2\times GI_{50}$, ~ 20% of necrotic population (annexin V negative/PI positive cells) were observed.

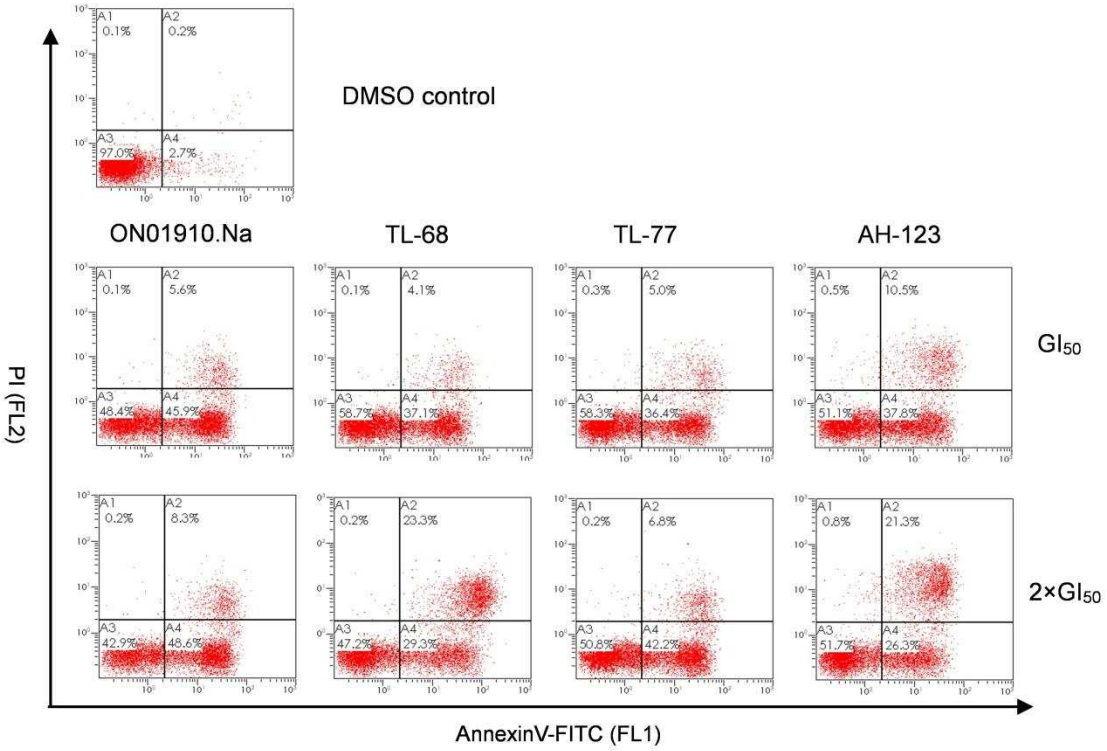

Figure 4.6 TL-68, TL-77, AH-123 and ON01910.Na induce apoptosis in HCT-116 cells.

HCT-116 cells were exposed to TL-68, TL-77, AH-123 or ON01910.Na for 48 h and stained using FITC-conjugated Annexin V and propidium iodide and subjected to flow cytometric analysis as described in the experimental procedures. A1, Annexin-negative and PI-positive dead cells; A2, double-positive late apoptotic cells; A3, double negative live cells; A4, Annexin V-positive, PI-negative early apoptotic cells. All of the above experiments were repeated three times, and a representative result is shown.

4.2.4 Pharmaceutical property assessment

Biopharmaceutical properties of lead compounds, including lipophilicity and metabolic stability, were evaluated by colleagues in Prof. Wang's research team in University of South Australia and are summarized in Table 4.4 (for more details please refer to the publication Lu T et. al. J Med Chem 2014).

Compounds TL-68. TL-77 and AH-123 possess favourable physicochemical properties. When compared with ON01910.Na, optimal lipophilicities were observed in three compounds with the $logD_{7.4}$ values ranging from 1.52 to 2.41. Metabolism was assessed using rat liver microsomal fractions. As shown in Table 4.4, while TL-77 exhibited excellent in vitro metabolic stability with a half-life of 70 min, TL-68 and AH-123 seemed more rapidly to be cleared in

microsomes ($t_{1/2}$ = 15-20 min). All tested compounds possess excellent aqueous solubility (>100 μM). The apparent permeability coefficients (P_{app}) were obtained from Caco-2 cell transport studies. This assay has been widely used to predict in vivo human intestinal absorption of the compounds across the gut wall by measuring the rate of transport of a compound across the Caco-2 cells. The cells have characteristics that resemble intestinal epithelial cells such as the formation of a polarized monolayer, well-defined brush border on the apical surface, and intercellular junctions. Assessing transport in both directions (apical to basolateral (A−B) and basolateral to apical (B−A)) across the cell monolayer enables an efflux ratio to be determined that provides an indicator as to whether a compound undergoes active efflux. The amino-containing analogues TL-68 and AH-123 were found to be highly permeable with apparent permeability coefficients (P_{app}) of 42.3 × 10^{-6} and 33.1 × 10^{-6} cm/s, respectively, suggesting the potential for high intestinal absorption. The efflux ratio (ER) of both compounds was less than 1, indicating that TL-68 and AH-123 were not subjected to active efflux that is normally indicated by an ER value greater than 2.[161] The permeability of TL-77 was lower (A−B P_{app} = 8.9 × 10^{-6} cm/s) and the efflux ratio was greater (ER = 5.29), compared to its respective amino-counterparts TL-68.

Table 4.4 Biopharmaceutical properties of TL-68, TL-77 and AH-123.

Parameter		TL-68	TL-77	AH-123
Dissociation constant	p*K*a [a]	2.39	7.66	4.67
Partition coefficient	$LogD_{7.4}$ (octanol) [b]	2.34	1.52	2.41
Microsomal stability	$t_{1/2}$ (min) [c]	20	70	15
Aqueous solubility	μM[d]	>100	>100	>100
Permeability	A−B P_{app} (10^{-6} cm/s) [e]	42.3	8.9	33.1
	B−A P_{app} (10^{-6} cm/s) [e]	21.5	47.1	26.2
	efflux ratio [e]	0.51	5.29	0.79

[a] Determined using a pH-metric method; [b] By shake flask; [c] Measured by disappearance of parent compound from a preparation of rat liver microsomes; [d] Measured by turbidimetric solubility assay; [e] Apparent permeability coefficient measured by Caco-2 assay. Efflux ratio = (mean B−A P_{app} / mean A−B P_{app}).

To assess potential oral bioavailability, TL-77 was next subjected to pharmacokinetic (PK) analysis in mice following a single intravenous (IV) dose of 2 mg/kg or an oral (PO) dose of 10 mg/kg. ON01910.Na was included in the study as a comparator. The PK analysis was carried out by Cyprotex Discovery Ltd. (Macclesfield, UK). Blood samples were collected at 0.030, 0.080, 0.25, 0.50, 1.0, 2.0, 4.0, 6.0, and 8.0 h. Pharmacokinetic parameters calculated included the total area under the plasma concentration-time curve (AUC_{0-t}), elimination half-life ($t_{1/2}$), volume of distribution (V_d), systemic clearance (Cl), and oral bioavailability (F). The peak plasma concentrations (C_{max}) were obtained by visual inspection of the plasma concentration-time curves. The PK parameters are shown in Table 4.5.

A plot of the compounds plasma concentrations versus time is provided in Figure 4.7. After PO dosing, plasma concentration-time profiles of TL-77 displayed a higher plasma concentration than ON01910.Na, which exhibited a rapid distribution phase ($t \leq 30$min) with a relatively slow terminal elimination phase. As shown in the figure, eliminations of both compounds included a prolonged terminal phase, where low plasma concentrations are sustained.

TL-77 was shown to have excellent oral bioavailability with F = 56%, good half-life ($t_{1/2}$ = 3.02 h) and AUC (7.2·h μM following PO administration). In contrast, ON01910.Na exhibited low oral bioavailability with an F = 9%; the half-life was shorter (~ 2.6 h) and low drug exposure in plasma (AUC = 1.0 μM·h following PO administration). Compared with the GI_{50}s achieved from MTT assays (Table 4.2 and Table 5.1), the plasma concentrations of TL-77 at

both IV and PO administration reached to high doses (C_{max} > 6.3 μM). Although the plasma concentration of ON01910.Na is high via IV administration (C_{max} = 11.7 μM), it only kept at 0.4 μM when being taken orally, indicating ON01910.Na was not utilized effectively in vivo. In short, TL-77 possesses superior oral bioavailability in single-dose pharmacokinetic studies in mice.

Table 4.5 Parameters in pharmacokinetic studies of TL-77 in mice .

Variables		TL-77		ON01910.Na	
Parameter (Unit)		2mg/kg IV	10mg/kg PO	2mg/kg IV	10mg/kg PO
Exposure	C_{max}(μM)	9.4	6.3	11.7	0.4
	AUC_{0-t}(μM·h)	2.6	7.2	2.06	1.0
Elimination	$t_{1/2}$(h)	3.22	3.02	2.53	2.66
Volume of Distribution	V_d(ml/kg)	7699	-	7482	-
Clearance	Cl(ml/min/kg)	27.6	-	33.9	-
Oral Bioavailability	F	56%		9%	

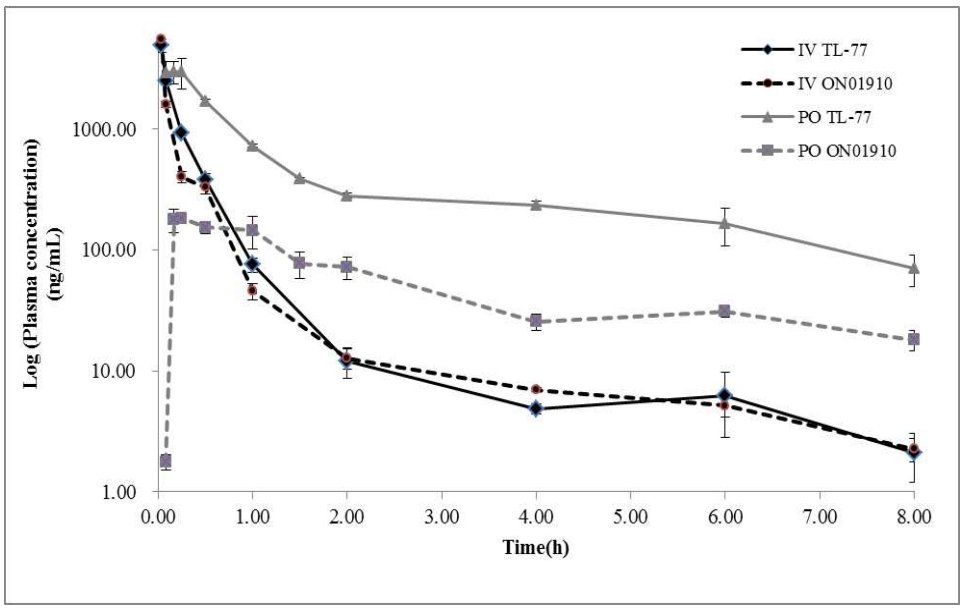

Figure 4.7 Plot of mean TL-77 and ON01910.Na plasma concentrations versus time following short term IV and PO infusions to mice

Time courses of mean plasma concentrations of compounds following continuous IV infusions of 2 mg/kg and PO infusions of 10 mg/kg TL-77 and ON01910.Na to healthy athymic mice (n=7–10).

4.3 Conclusion

In this chapter, SAR of novel series of (E)-3-((styrylsulfonyl)methyl)pyridine derivatives was discussed. Several compounds exhibited potent anti-proliferative activity in cancer cell lines. Lead compounds TL-68 and AH-123, containing an amino group at the respective 2C- and 3C-positions of styrylsulfonyl methylpyridine, were the most effective anti-proliferative agents in the series. Both of them were potent tumour suppressors (GI_{50} = 6-8 nM) and were >10-fold more potent than ON01910.Na.

In cellular mode of action studies, TL-68, TL-77 and AH-123 exhibited similar cell cycle effect to ON01910.Na in HCT-116 cancer cells, inducing cell cycle arrest at the G2/M phase. Cell morphology observation and annexinV/PI double staining proved that all the compounds cause the cell death by inducing apoptosis in cancer cells. Importantly, despite other three compounds have little selectivity between cancer and normal cells, TL-77 exhibited 4-fold greater potency against HCT-116 compared with untransformed HMEC-1 cell line. TL-68, AH-123, especially TL-77 possess desirable physicochemical properties, including favourable lipophilicity (pKa and $logD_{7.4}$) and metabolic stability. In the following pharmacokinetic studies performed in mice, TL-77 exhibited desirable pharmacokinetic properties (56% bioavailability, good half-life) in comparison with ON01910.Na, (9% bioavailability).

These data suggest that TL-77 and analogues represent promising orally bioavailable anticancer agents worthy of further evaluation.

5 Cellular mechanisms of action of TL-77 as mitotic kinase inhibitor

5.1 Introduction

Identification of the primary target(s) of designed anti-cancer kinase inhibitors in cancer cells plays a key role in kinase drug development. In a programme to identify a novel chemical series of molecules possessing similar modes of action, but improved pharmaceutical properties compared to ON01910.Na, I designed and synthesized a novel class of (E)-styrylsulfonyl methylpyridines. TL-77, as one of the lead compounds, has shown potent in vitro anti-tumour activities and improved oral bioavailability (Figure 5.1). I wished to investigated its cellular mechanism of action, as well as determine similarities and/or differences in mechanisms of action between TL-77 and ON01910.Na.

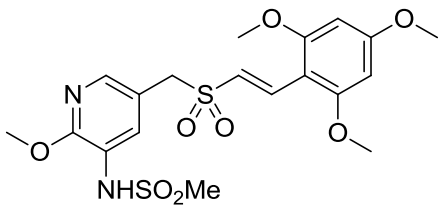

Figure 5.1 Chemical structure of TL-77, (*E*)-*N*-(2-methoxy-5-((2,4,6-trimethoxystyrylsulfonyl)methyl)pyridin-3-yl)methanesulfonamide.

5.2 TL-77 is a potent, time-dependent anti-proliferative agent

Anti-proliferative activities of TL-77 were first assessed against a panel of 10 tumour cell lines and 3 untransformed cell lines using a 96 h MTT cytotoxicity assay in comparison with ON01910.Na. Tumour cell lines from different organ origins were utillized, such as colon, breast, melanoma, ovary, cervix and

pancreas. To investigate tumour suppressor expression status sensitivity to the compounds, HCT-116 colon carcinoma (HCT-116 p53 (+/+) and HCT-116 p53 (-/-)), MDA-MB 468 breast (mutant p53, Rb negative) and MDA-MB 435 melanoma (mutant p53, Rb positive) were included. To test the toxicity of both compounds on normal cell lines, microvascular endothelial cells HMEC-1 and HUVEC as well as diploid MRC-5 fibroblasts were included. These three cell lines are well characterized and commonly used as non-cancerous cell lines for in vitro cytotoxicity testing.[162-164] The results are presented in Table 5.1. In addition, to further identify the sensitivity and selectivity of compounds towards cancer cells and non-transformed cells, a mean graph plots of GI_{50} values for both compounds are displayed as Figure 5.2.

As shown in Table 5.1, in general, similar sensitivity was observed for cells with different p53 and Rb status for both compounds, indicating their p53 and Rb independent anti-proliferative activity. TL-77 displayed potent anti-proliferative activity against a wide variety of tumour cell lines irrespective of tissue origin. It suppressed cancer cell proliferation with GI_{50} values ranging between 317 and 860 nM, but was less potent than ON01910.Na in the same cell lines. TL-77 exhibited modest selectivity: as illustrated in Table 5.1 and Figure 5.2, TL-77 demonstrated 2-fold greater potency in cancer cell line over normal cells. Optimally, 10-fold greater selectivity was observed. (A2780 GI_{50} = 317 nM; MRC-5 GI_{50} =3144 nM) Overall, ON01910.Na was a more potent suppressor of tumour cell proliferation in the same cell lines (GI_{50} = 7-62 nM). A safety profile of ON01910.Na on several normal human cell lines (HUVEC GI_{50} > 100 μM) has been reported.[61] However, in this study, ON01910.Na showed little to no selectivity against non-transformed human cells (GI_{50} = 30-51 nM).

Table 5.1 Anti-proliferative activity of TL-77 and ON01910.Na against a panel of cell lines.

Human cell lines			96h-MTT,* GI_{50} (nM) ± SD	
Origin	Destination	PDT	ON01910.Na	TL-77
Colon carcinoma	HCT-116 (p53+, Rb+)	18 ± 3 h[154]	21 ± 5	570 ± 23
	HCT-116 (p53-, Rb+)	20 h[165]	17 ± 2	860 ± 86
Breast carcinoma	MCF-7 (p53+,ER+)	30.2 ± 0.7 h[153]	50 ± 10	780 ± 25
	MDA-MB 231(p53-,ER-)	27.8 ± 5 h[166]	55 ± 15	671 ± 56
Melanoma	MDA-MB 468 (p53-,Rb–)	47 h[167]	39 ± 15	509 ± 130
	MDA-MB 435 (p53-,Rb+)	25.8 h[154]	12 ± 2	592 ± 128
Ovarian carcinoma	A2780	13.5 ± 3 h[152]	62 ± 4	317 ± 179
Cervical carcinoma	Hela	24 h	12 ± 1	682 ± 112
Pancreatic carcinoma	Mia-paca II	40 h[168, 169]	7 ± 2	463 ± 208
	PANC-1	52 h[168]	39 ± 6	875 ± 274
Microvascular endothelial	HMEC-1	55 h[170]	51 ± 2	1681 ± 270
Umbilical vein endothelial	HUVEC	48 h[171]	30 ± 1	1110 ± 270
Lung Fibroblast	MRC-5	32.7 ± 6 h[172]	49 ± 25	3144 ± 832

* Data expressed as the mean ± standard deviation of three independent experiments. ER, estrogen receptor; Rb, retinoblastoma protein; PDT, population doubling time.

Among 10 tested cancer cell lines (Figure 5.2), both compounds showed superior toxic effect towards HCT-116 (Colon), MDA-MB-435 (Melanoma) and Miapaca-II (Pancreatic) cells, while MCF-7 (Breast), MDA-MB-231 (Breast) and PANC-1 (Pancreatic) cells were less sensitive to both compounds.

In general, the anti-proliferative activity responses of most cancer cell lines are related to their population doubling time. (Table 5.1) In contrast, although possessing the equivalent population doubling levels to some of cancer cells (MDA-MB-468 and PANC-1, PDT~ 50 h), non-transformed cells (HMEC-1 and HUVEC, PDT~ 50 h) showed apparent less sensitive to the compounds.

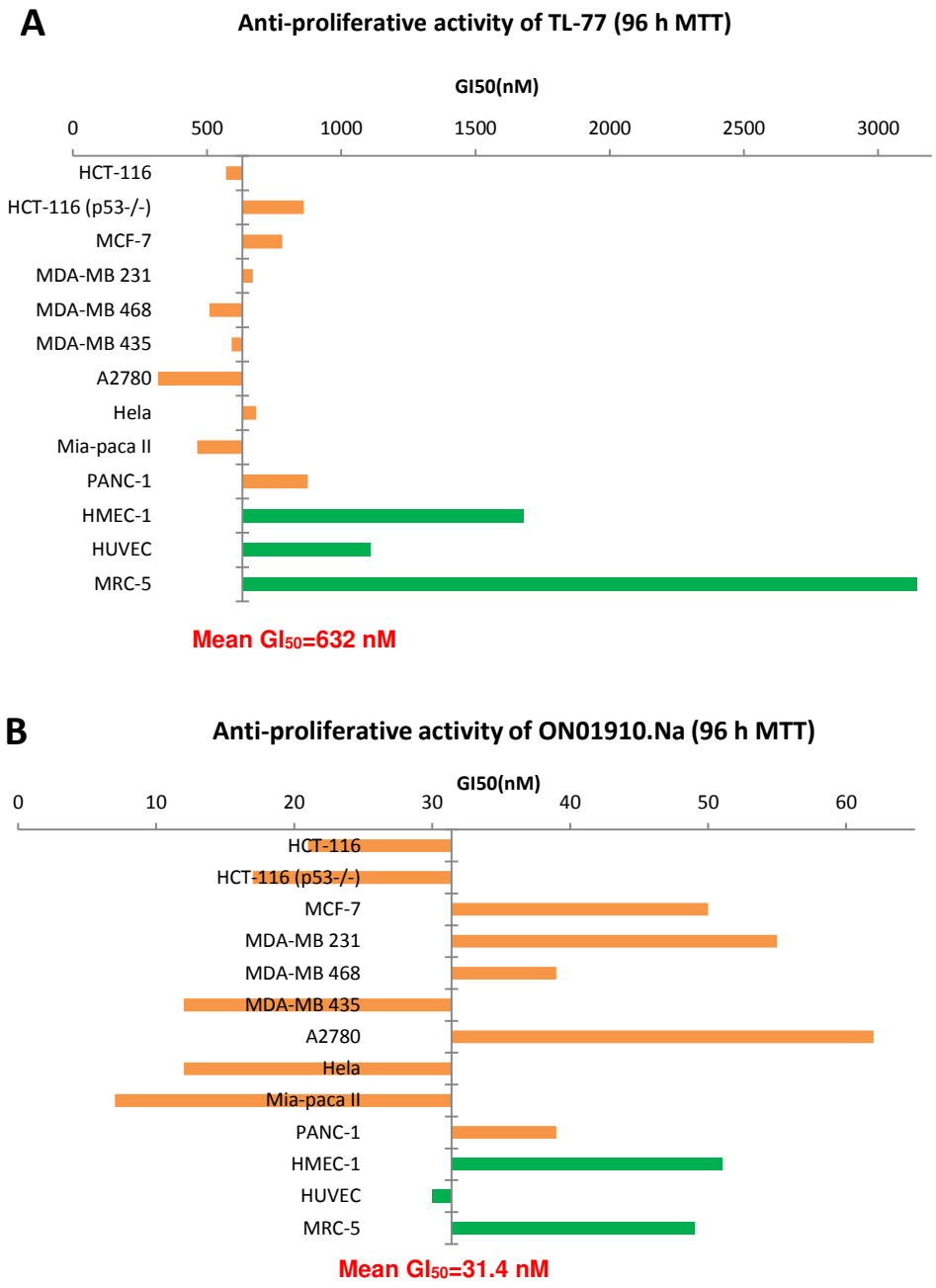

Figure 5.2 Mean graph plots of GI_{50} values for TL-77 (A) and ON01910.Na (B) against a panel of cell lines in 96 h MTT assay.

The mean GI_{50} for TL-77 and ON01910.Na across cancer cell lines was calculated. Cell lines that were more sensitive are displayed as bars to the right of the mean. Cell lines that were less sensitive are displayed with bars to the left. Cancer cell lines are represented in orange; non-transformed cell lines are shown in green.

Time-dependent anti-proliferative effects were further observed for both compounds as exemplified in two well-characterized cancer cell lines, HCT-116 and A2780 (Figure 5.3). In previous results (Table 5.1), ON01910.Na showed ~30-fold more potent anti-proliferative activity than TL-77. To improve the accuracy of screening data, 6 testing concentrations ranging from

0.0016 μM to 5 μM were used for ON01910.Na, which are one tenth of those for TL-77 (0.016-50 μM) in time-course MTT assays.

As displayed in Figure 5.3, after 24 h treatment, TL-77 started to suppress tumour cell proliferation from 0.4 μM in both HCT 116 and A2780 cells. At 48, 72 and 96 h time points in both cell lines, TL-77-treated cell numbers decreased sharply between 0.08 μM and 2 μM treatments. Meanwhile, remarkable time-dependent growth inhibitions induced by ON01910.Na were observed from 0.008 μM in both cell lines at tested time points, excepted that a moderate cytotoxicity in A2780 cells was observed as early as 24 h ON01910.Na exposure.

Following 24 h exposure to TL-77 or ON01910.Na, GI_{50} values of 4 μM and 0.06 μM respectively in HCT 116 cells, and 2 μM and 0.25 μM respectively in A2780 cells were observed and adopted as agent concentrations used in subsequent assays.

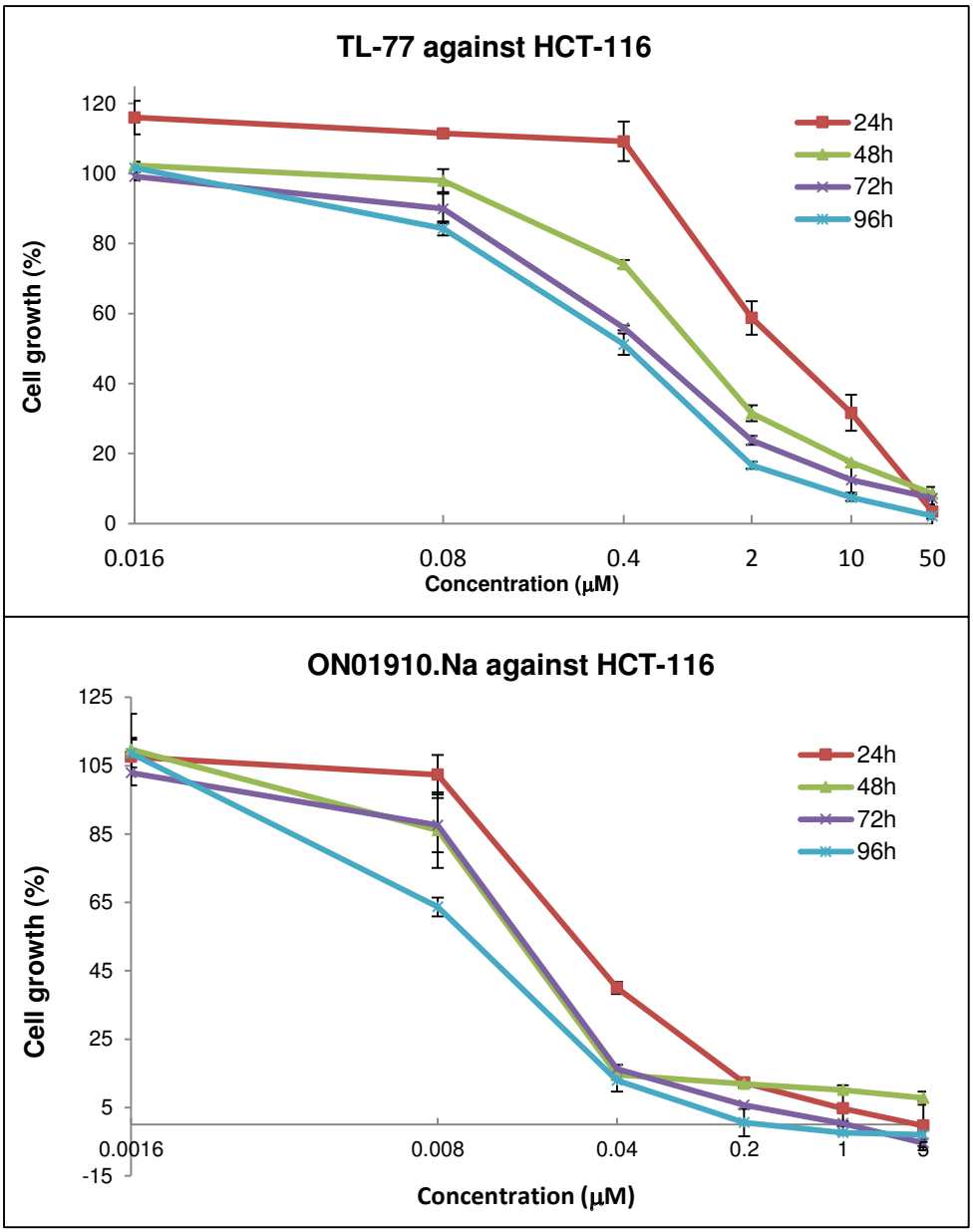
TL-77 against HCT-116
Cell growth (%)
120
100
80
60
40
20
0
0.016
0.08
0.4
2
10
50
Concentration (µM)
24h
48h
72h
96h
ON01910.Na against HCT-116
Cell growth (%)
125
105
85
65
45
25
5
-15
0.0016
0.008
0.04
0.2
1
5
Concentration (µM)
24h
48h
72h
96h

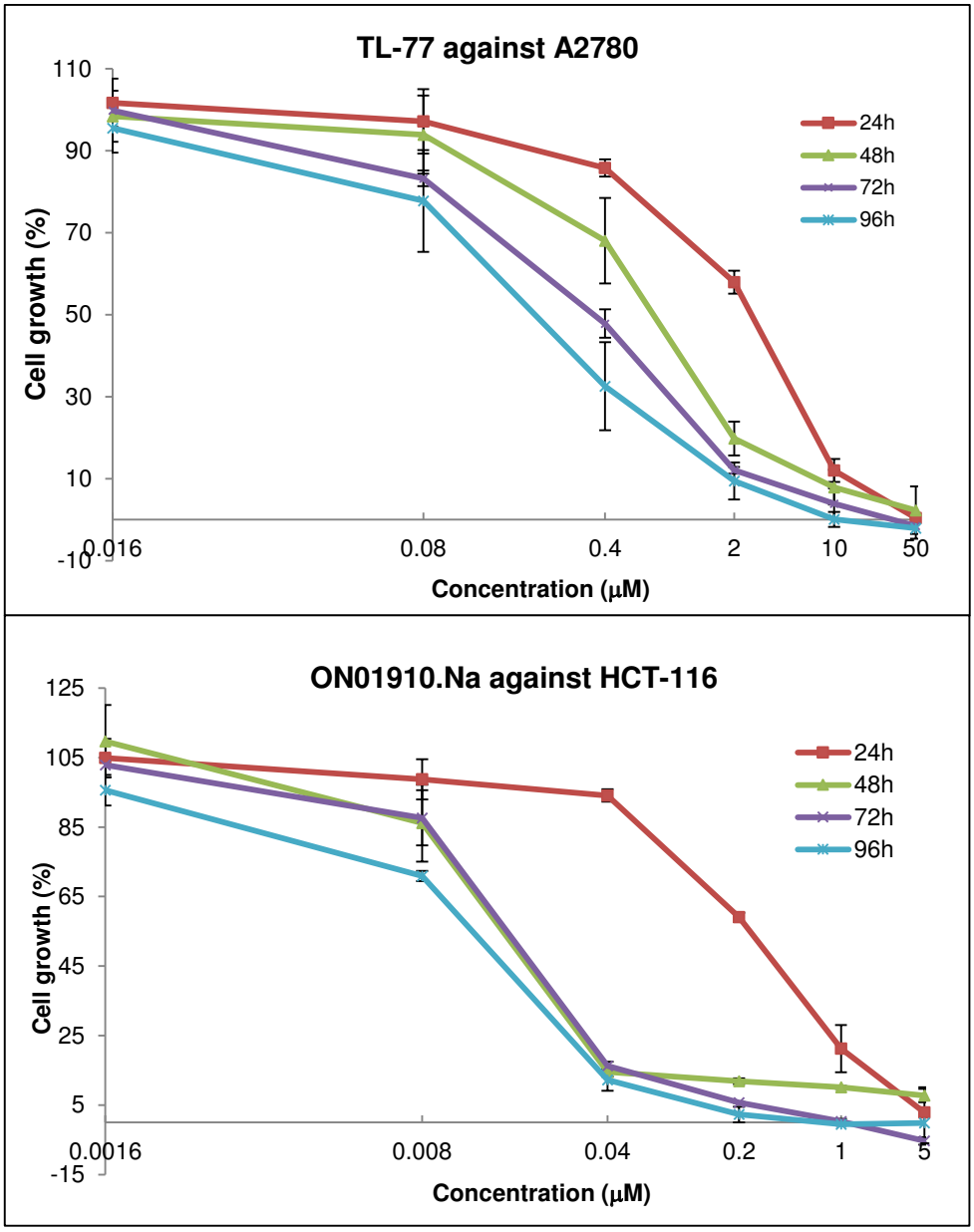

Figure 5.3 Time-course growth inhibition curves of TL-77 and ON01910.Na.

HCT-116 and A2780 cells were treated with compounds for a range of concentrations at 24h, 48h, 72h or 96h respectively. The range of concentrations: TL-77 (0.016, 0.08, 0.4, 2, 10, 50 μM); ON01910.Na (0.0016, 0.008, 0.04, 0.2, 1, 5 μM). The data given are mean values derived from at least three replicates ± SD.

5.3 TL-77 inhibits cell cycle progression

One of the major abnormalities caused by ON01910.Na is the mitotic arrest in many tumour cell lines.[53] TL-77 has displayed potent anti-proliferative activities. Thus, whether this effect was a consequence of inhibition of cell

cycle progression that caused activation of the cellular apoptosis programme was investigated.

5.3.1 Cell cycle analysis of TL-77 and ON01910.Na

The effects of the two compounds on tumour cell cycle progression were firstly assessed by flow cytometry in HCT-116 and A2780 cells. The cells were treated with compounds for 6, 12, 18 and 24 h at the concentrations shown in Figure 5.4. Analyses by flow cytometry exposed stark time-dependent G2/M cell cycle block and enhanced numbers of cells with 4N DNA content after treatment of cells with both compounds at GI_{50} values.

Particularly in HCT-116 cells (Figure 5.4 A), TL-77 caused accumulation of a significant G2/M cells population (>50%) as early as 6 h, while ON01910.Na caused the same effect (~50% G2/M arrest) after a longer exposure period (≥ 12 h). Following treatment of 4 μM TL-77 or 0.06 μM ON01910.Na for 24 h, 55.4% or 70.3% cells respectively arrested in the G2/M phase. Similar cell cycle profiles with TL-77 and ON01910.Na were observed in A2780 cells (Figure 5.4 B). Treatment with 2 μM TL-77 or 0.25 μM ON01910.Na resulted in accumulation of 56% or 29.7% G2/M cells respectively. No such mitotic abnormalities were observed in untreated cells.

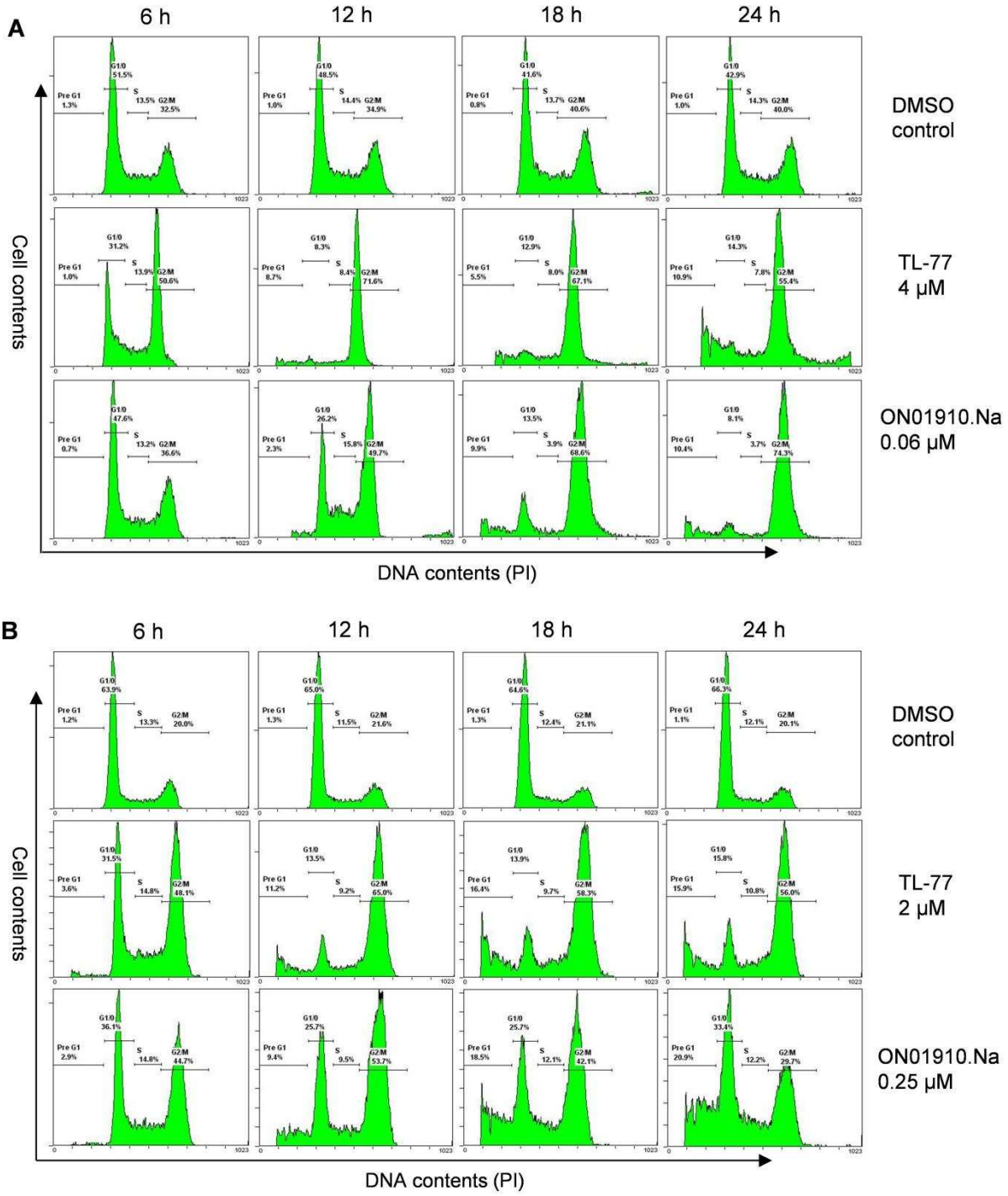

Figure 5.4 Cell cycle analysis of TL-77 and ON01910.Na on cancer cells.

HCT-116 (A) and A2780 (B) cells were treated with GI_{50} concentrations of TL-77 or ON01910.Na ≤ 24 h. Cells were fixed, stained with propidium iodide, and DNA content was analysed by flow cytometry.

Treatment of both cell lines for > 18 h caused accumulation of events containing substantial subG1 DNA content, which is an indication of cell death, suggesting that the induction of apoptosis might be a consequence of cell cycle

arrest. Cell cycle arrest was induced more rapidly when concentrations increased to 2xGI_{50} for both compounds (data not shown).

As TL-77 was significantly less active in proliferation assays carried out on untransformed cells, its cell-cycle effects on HMEC-1 cells was also investigated. The cells were treated with TL-77 or ON01910.Na for 6, 12, 18 and 24 h at the concentrations shown in Figure 5.5. Little or no disturbance of cell cycle distribution was observed with TL-77 (in contrast – 24 h ON01910.Na – substantial preG1).

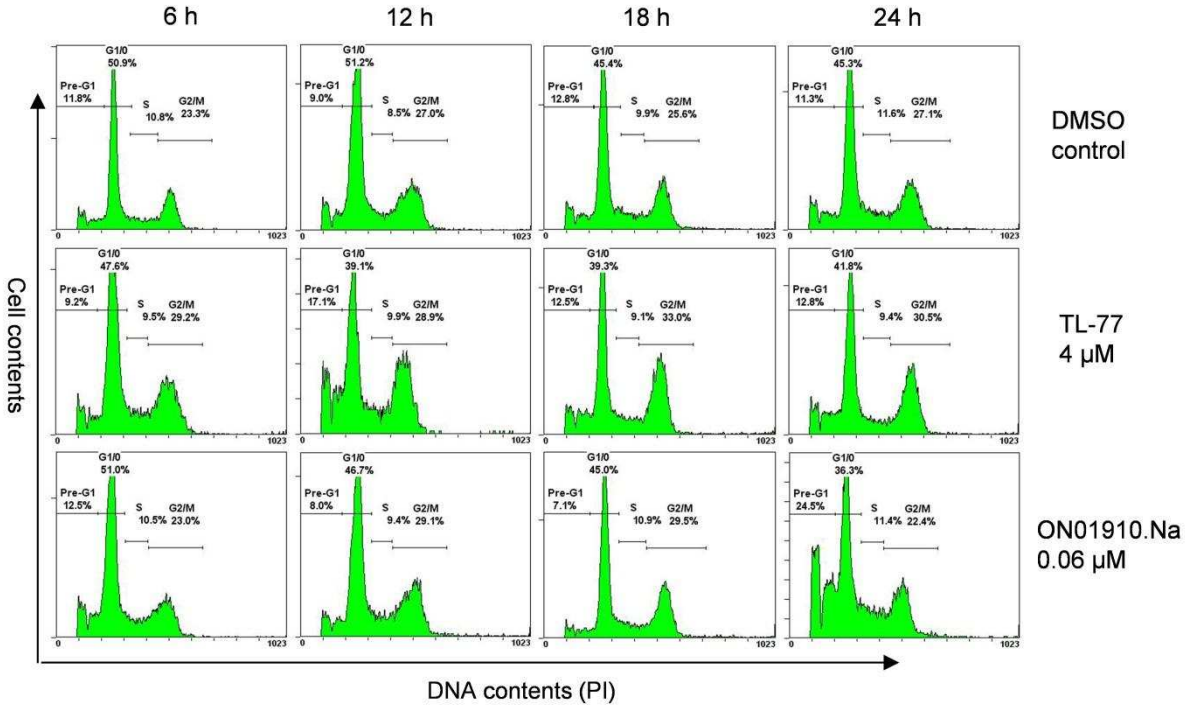

Figure 5.5 Cell cycle analysis of TL-77 and ON01910.Na on untransformed cells.

HMEC-1 cells were treated with GI_{50} concentrations of TL-77 or ON01910.Na ≤ 24 h. Cells were fixed, stained with propidium iodide, and DNA content was analysed by flow cytometry.

5.3.2 TL-77 evoked a notable mitotic block

DNA content analysis alone cannot resolve whether cells are delayed in G2 phase, entry into mitosis, and/or progression through mitosis. Phosphorylation of histone H3 is generally accepted as mitotic marker.[173] Therefore, the extent of histone H3 phosphorylation and the percentage of cells with condensed

mitotic chromosomes was analysed by fluorescence staining (mitotic index assay).

Effects of TL-77 on phospho-histone H3 in HCT-116 cells was analysed by Western blot analysis (Figure 5.6). As expected, treatment of ON01910.Na after 8 h led to a significant dose-dependent increase in the phospho-histone H3 content in HCT-116 cells peaking at 0.24 μM. Meanwhile, intense bands of phospho-histone H3 were observed in HCT-116 cells exposed to TL-77 at all tested concentrations (4-16 μM). This result revealed that TL-77 as well as ON01910.Na induced mitotic accumulation as an early event (≤ 8 h) in cancer cells.

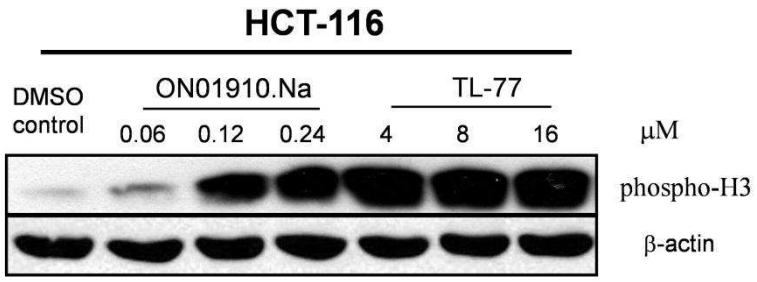

Figure 5.6 Effect of TL-77 on phosphorylated histone H3.

HCT-116 cells were incubated with indicated concentrations of TL-77or ON01910.Na for 8 h. β-Actin was used as an internal control for protein loading.

The mitotic accumulation induced by both compounds was then quantitatively analysed by mitotic index assay. Mitotic index indicates the ratio between the number of cells in mitosis and the total number of cells. It is calculated by measuring cell nuclei stained with the positive mitosis-specific antibody (anti-phospho-histone H3) versus total cell nuclei stained with Hoechst.

HCT-116 cells were treated with TL-77 or ON01910.Na for a period of 6 h or 12 h and the mitotic index was measured. As displayed in Figure 5.7 A, TL-77 increased mitotic index in a time- and dose-dependent manner. Following 6 h exposure to TL-77 (0.5-2xGI_{50}), ~ 15% of cells resided in mitosis compared

with 2% in control samples. An increased mitotic index (25%) was further observed in cells exposed to 4xGI_{50} TL-77 of (16 µM). After 12 h treatment with TL-77, a dramatic dose-dependent increase in mitotic index was observed (> 35%; 4 µM-16 µM TL-77). ON01910.Na caused less dramatic mitotic arrest. At concentrations > 0.06 µM, a gentle dose-dependent increase in mitotic index was observed at both 6 h and 12 h (Figure 5.7 B). Only at 4xGI_{50} value (0.24 µM ON01910.Na) was a time-dependent divergence observed (mitotic index 17% and 27% after 6 h and 12 h respectively).

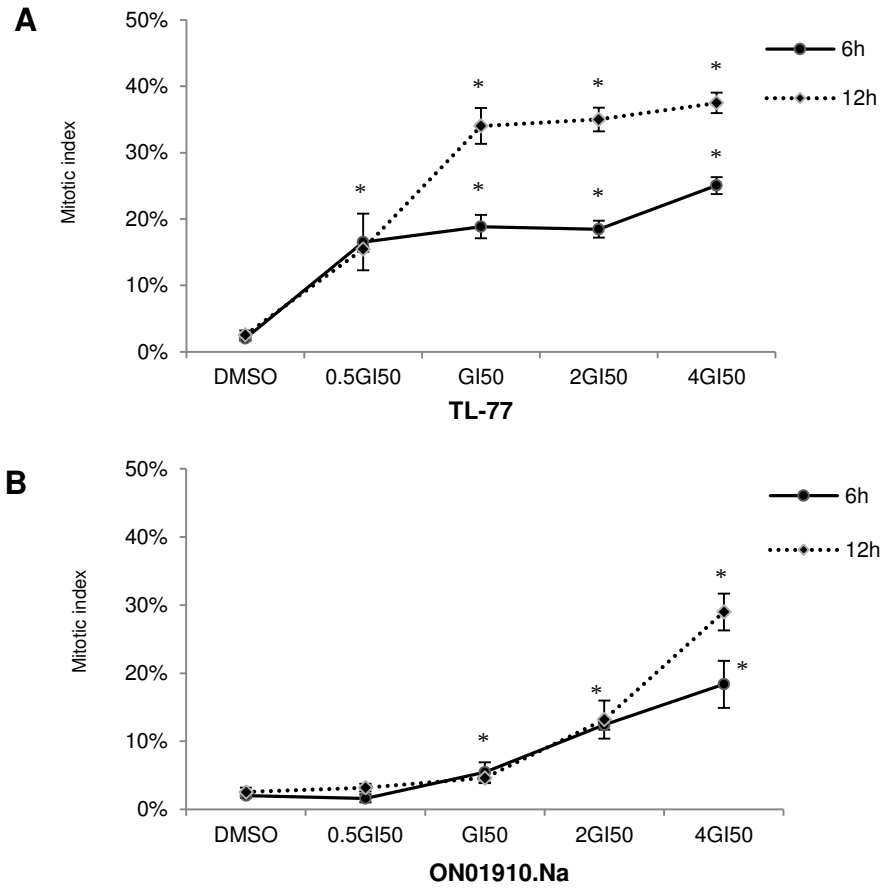

Figure 5.7 Cell cycle status of TL-77 and ON01910.Na detected by mitotic index in HCT-116 cells

HCT-116 cells were treated with concentrations of TL-77 (A) or ON01910.Na (B) and incubated for 6 h and 12 h. After fixation in 4% paraformaldehyde, cells were treated with P-histone H3 antibody and Hoechst. The cells were analysed by confocal laser microscopy. Vertical bars represent the means ± SD of at least 2 independent experiments (n = 3 per experiment). Values significantly ($p \leq 0.05$) different from DMSO vehicle control were marked with an asterisk (*).

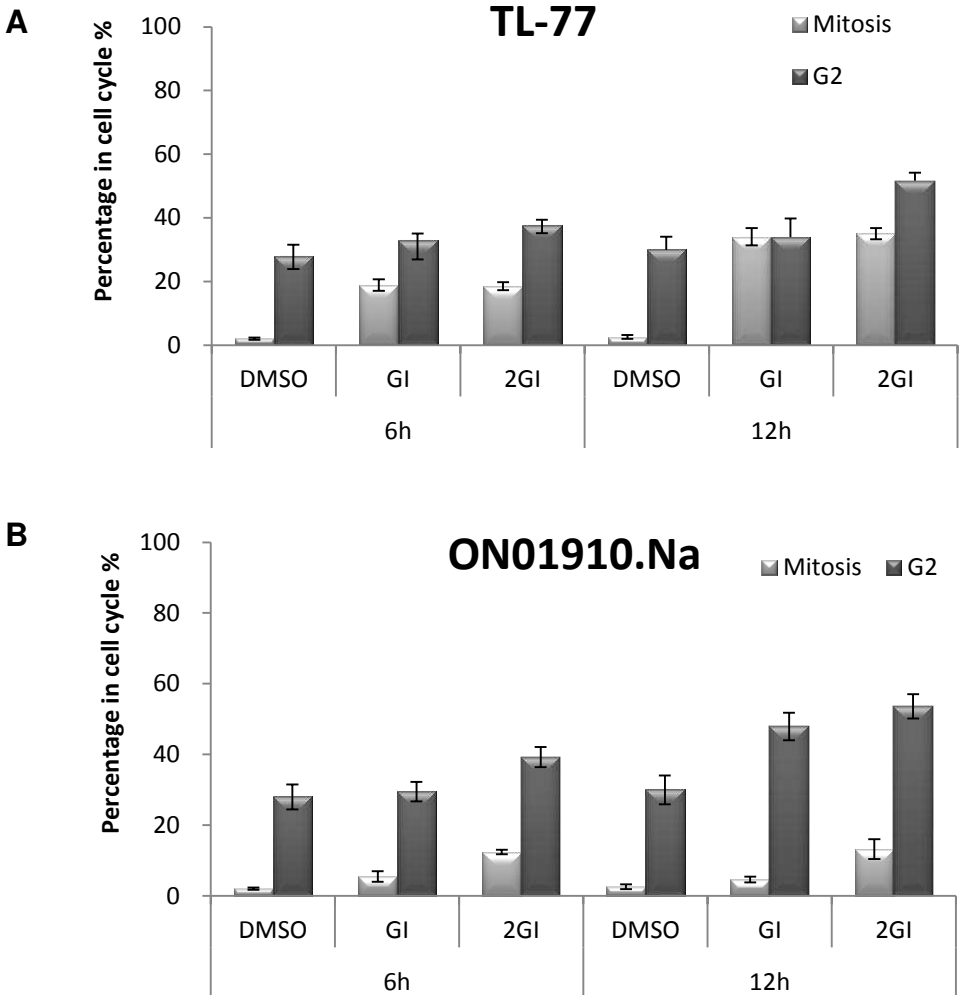

Figure 5.8 Cell cycle status of TL-77 and ON01910.Na plotted based on mitotic index and cell cycle in HCT-116 cells

A plot of mitotic index compared with the data from cell cycle analysis TL-77 (A) or ON01910.Na (B). The population mean of cells in G2 phase was obtained by subtracting mean of mitotic indices from mean of G2/M values at corresponding concentrations, $\mu_{G2} = \mu_{G2/M} - \mu_{Mitosis}$. The population of cells in G2/M phase and mitosis were considered as two random variables. The standard deviation is adopted as $SD_{12} = \sqrt{\sigma_1^2/n_1 + \sigma_2^2/n_2}$.[174] σ_1^2 and σ_2^2 are the population variances for the population of cells in G_2/M and mitotic, respectively. μ: population of cells.

Plots of mitotic index (detailing % mitotic cells in a given population) compared with data from cell cycle analyses (detailing G2/M events) are provided in Figure 5.8. By subtracting mitotic indices from G2/M values, the population of cells in G2 phase could be obtained. Data in Figure 5.8 **A** demonstrate that TL-77 evoked a notable mitotic block (6 h-12 h exposure). Whereas, numbers of TL-77 (1-2 GI_{50}) -treated cells in G2 phase remained stable at 6 h. In addition, ~20% increased G2 events was noticed when TL-77

exposure extended to 12 h at 2xGI_{50} (8 μM). In contrast, ON01910.Na-treated cells revealed a less significant but dose-dependent mitotic block (Figure 5.8 **B**). At 6 h, ON01910-treated cells started to arrest in G2 phase (~10%) at 2xGI_{50}. Furthermore, after 12 h treatment ON01910.Na sharply increased the numbers of cells in G2 phase (~20%-25%) at both GI_{50} and 2xGI_{50}. These results are consistent with cell cycle observations (Figure 5.4 **A**), where more rapid cell cycle arrest was observed in cells exposed to TL-77.

5.4 TL-77 induces spindle abnormalities

5.4.1 TL-77 inhibits microtubule polymerization

In view of the remarkable effects of the compounds on cell cycle progression, a biochemical assay was adopted to then examine whether either compound affected tubulin polymerization. Two known compounds, paclitaxel and nocodazole were set as the positive and negative controls, respectively. Paclitaxel binds to tubulin to suppress dissociation of microtubules[175], and promotes polymerization of purified tubulin. In contrast, nocodazole inhibits microtubule polymerization by binding to β-tubulin and preventing formation of one of the two interchain disulfide linkages between tubulins.[176, 177]

The two compounds' effects on microtubule polymerization were compared at 0.5xGI_{50}, GI_{50} and 1.5xGI_{50} for TL-77, GI_{50} and 2xGI_{50} for ON01910.Na. During preparation of the tubulin polymerization assay, slight precipitation of TL-77 at 8 μM (2xGI_{50} value) in H_2O solution was observed. Consequently, a concentration of 6 μM (1.5xGI_{50}) was applied instead. The results are shown in representative traces in Figure 5.9. TL-77 displayed a dose-dependent effect on microtubule formation (Figure 5.9 **A**). Similar to DMSO control (0.2% v/v), no influence on microtubule polymerization was observed after incubation of 2

μM TL-77. As the concentrations increased to 4 μM and 6 μM, TL-77 acted as a microtubule suppressor in a similar manner to nocodazole. Similar results were obtained with ON01910.Na at 0.06 μM and 0.12 μM (Figure 5.9 **B**). These data indicate that both compounds potently suppress microtubule polymerization in a manner similar to nocodazole at tested concentrations.

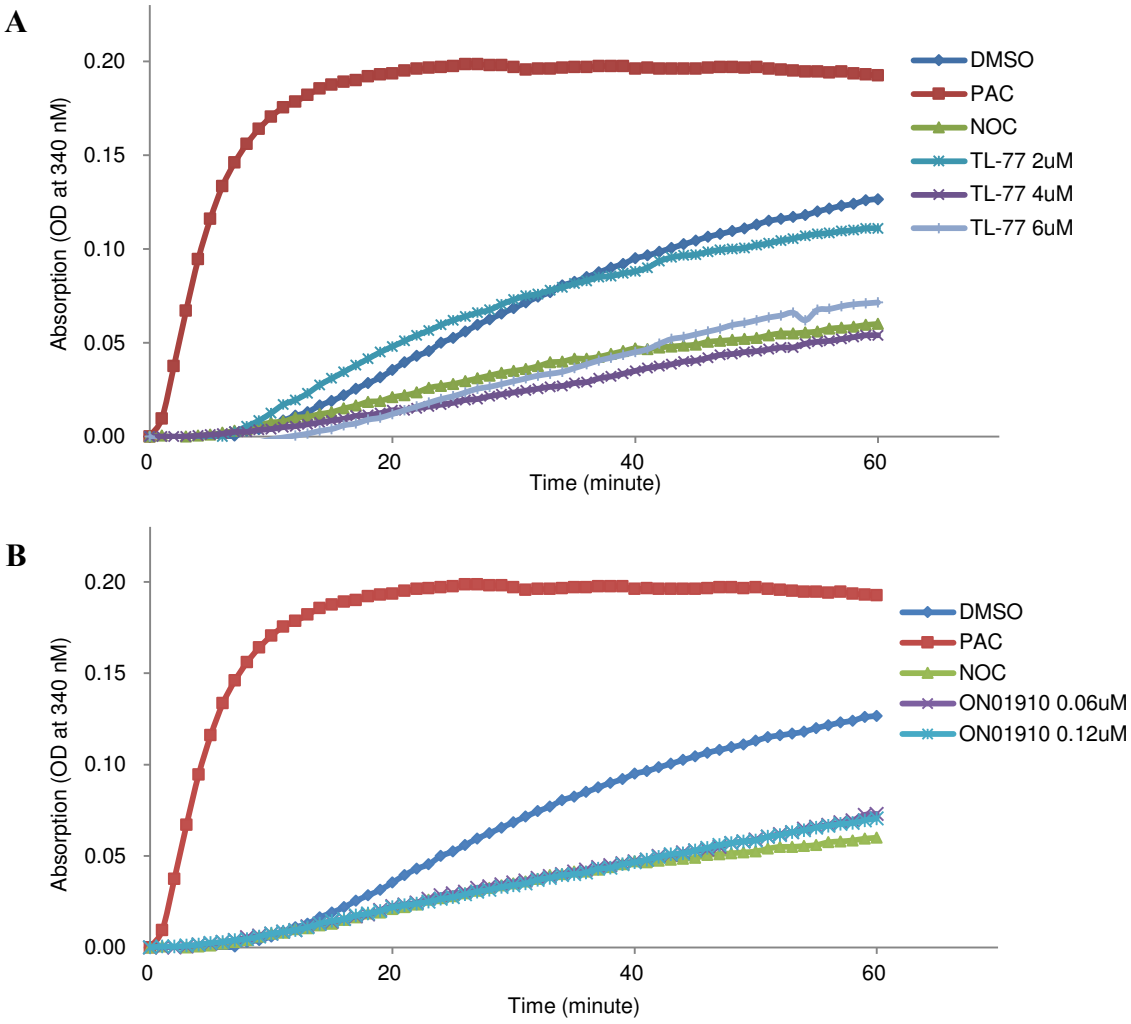

Figure 5.9 TL-77 and ON01910.Na inhibited tubulin polymerization.

Tubulin polymerization was measured according to the assay conditions described in Experimental Procedures. Paclitaxel and nocodazole were used as additional controls known to enhance or prevent tubulin polymerization, respectively. (A) TL-77 and (B) ON01910.Na are compared with control.

5.4.2 TL-77 perturbs spindle assembly in HCT-116 cells

To examine whether TL-77 could induce abnormal mitotic spindles in cancer cells, the spindle architecture was next examined using confocal microscopy. Immunofluorescent staining using anti-α-tubulin antibody was performed.

After 12 h DMSO treatment (0.2% v/v), interphase cells were observed with bipolar mitotic spindles (Figure 5.10 **A**). As depicted in Figure 5.10 **B**, both 4 μM and 8 μM TL-77 caused remarkable inhibition of microtubule assembly in treated cells. The phenotypes caused by TL-77 included abnormal mitotic spindle formation with tri- or multipolar spindles, chromosome misalignment, and complete loss of coordination in mitotic spindle assembly (red arrows). Monopolar spindles with circular chromosome arrangements, which are indicative of a centrosome separation failure, were also observed (white arrows). Meanwhile, abnormal mitotic spindle formation was also observed in cells after ON01910.Na treatment (Figure 5.10 **C**). Instead of generating multipolar spindles, cells exhibited fragmented microtubules following exposure to ON01910.Na, resulting in prevention of cell division. Paclitaxel and nocodazole were used in this study as positive and negative controls. Cells treated with paclitaxel displayed stabilized microtubules, accompanied by misaligned chromosomes (Figure 5.10 **D**). Microscopy of nocodazole-treated cells shows that they enter mitosis but cannot form metaphase spindles because microtubules cannot polymerize (Figure 5.10 **E**).

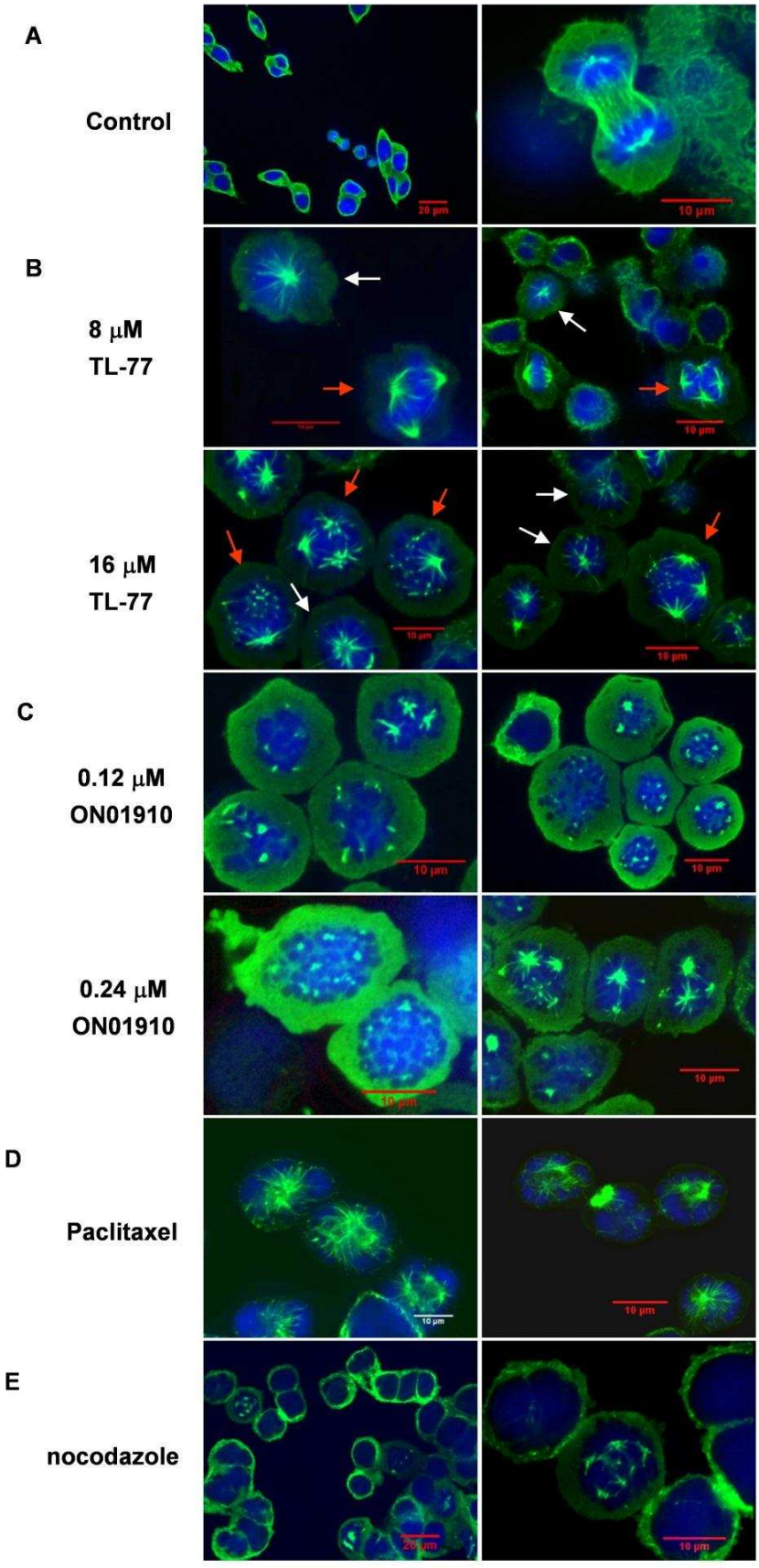

Figure 5.10 TL-77 induced spindle assembly and chromosome alignment in HCT-116 cells

HCT-116 cells were treated with DMSO (0.2% v/v), TL-77, ON01910.Na, paclitaxel or nocodazole for 12 h, fixed with 4% paraformaldehyde, and treated with anti-α-tubulin antibody (green, FITC conjugated) and Hoechst (blue). The cells were analysed by confocal laser microscopy. Arrows indicate mitotic spindle abnormalities and chromosomal misalignment.

5.4.3 Discussion

In cell-free conditions, ON01910.Na (0.06 μM and 0.12 μM) as well as TL-77 (4 μM and 6 μM) suppressed microtubule formation, acting in a similar manner to nocodazole.

However, minor inhibition or no effects of ON01910.Na on tubulin polymerization at 1 μM and 5 μM respectively has been reported.[53, 178] The apparent inconsistencies could be due to the differences in the experimental setup, such as testing buffer and compound concentrations. As mentioned by the manufacturer (refer to Material and Methods), glycerol (e.g. 10%) will result in enhanced polymerization. To sensitize the reaction, assay optimization of using G-PEM buffer minus glycerol is suggested. Therefore, I took this advice and glycerol was not included in this tubulin polymerization assay. According to published work, effect of ON01910.Na on tubulin polymerization were examined using G-PEM buffer in three glycerol concentrations (10%, 15% and 20%).[119] No results of tests performed in glycerol-free buffer were reported and the quantitative influence of glycerol concentrations on this assay is not clear so far.

But the consistency between the data sets in this study illustrated the reproducibility of tubulin polymerization results, Moreover, several reported experimental evidence have suggested that ON01910.Na is an inhibitor of tubulin polymerisation; cells with depolymerized microtubules were observed after treated with higher doses (2.5 μM) of ON01910.Na.[97-99] Therefore, based on our observation, it is concluded that inhibition of tubulin polymerization is an important molecular mechanism of action of TL-77 as well as ON01910.Na.

The mitotic spindle is critical for segregation of chromosomes to two daughter cells during mitosis. Failure of sister chromatids to attach to microtubules results in prolonged cell cycle arrest and caspase-dependent apoptosis.[179] Several mitosis-specific protein kinases are required to organize the bipolar spindle assembly and chromosome bi-orientation, including Cdc2, Aurora B and Plk1.[99] Plk1 has been identified to be a key player for G2/M transition and mitotic progression in both normal and tumour cells.[24] In late G2 phase and mitosis, Plk1 is essential for centrosome maturation, separation and mitotic spindle assembly.[84] Mutation of Polo leads to mitotic accumulation of cells that contain monopolar spindles, spindles with broad poles, or multipolar spindles.[180] Immunofluorescence staining of α-tubulin revealed that TL-77 promoted disassociation of microtubules, and inhibited mitotic spindle assembly, leading to formation of multipolar spindles and misalignment of chromosomes in vitro. This outcome is very similar to the phenotype observed with Plk1-depleted cells, which arrested in prometaphase with lack of spindle pole focusing and unstable attached chromosomes.[180] Taken together with cell cycle data, these observations suggest TL-77 inhibits tubulin polymerization, induces spindle abnormalities and results mitotic block.

5.5 Effect of TL-77 on cell cycle regulators

To explore the molecular consequences of TL-77 exposure, we then sought to assess factors that may indicate the degree of Plk1 and G2/M checkpoint inhibition. The cell cycle inhibition after exposure to TL-77 is correlated with Cdc25c activity (measuring total and phospho-Cdc25c) and cyclin B1 expression levels.

In eukaryotic cells, initiation of mitosis is triggered by activation of the Cdc2/cyclin B1 complex, the 'mitosis-promoting factor'. Cdc25c regulates Cdc2/cyclin B1 activity and controls entry into mitosis.[181, 182] Cdc25c has been described to be phosphorylated by Plk1 at Ser198 and therefore represents a direct substrate of Plk1.[24] Previous work reported that ON01910.Na inhibits activation of the phosphatase Cdc25c as one of its primary intracellular effects.[53, 96] Cdc25c from interphase cells was found to migrate as a 54 to 57 kDa doublet in SDS gels and exhibited basal phosphatase activity. In cultures enriched for mitotic cells, Cdc25c migrated at 66 kDa and exhibited elevated phosphatase activity.[183]

HCT-116 and A2780 cells were treated with TL-77 and ON01910.Na for 8 h. Cell lysates were immune-blotted with antibodies against phospho-Cdc25c (Ser198), Cdc25c and cyclin B1. The results and quantification of western blot (presented as fold change compared to control) are displayed in Figure 5.11. Dramatically reduced phosphorylation of Cdc25c (Ser198) caused by both compounds were observed in both cell lines after 8 h treatment. 40-70% phosphorylation of Cdc25c (Ser198) compared to control were inhibited by TL-77 (1-4xGI_{50}) in HCT-116 cells, while 50- 90% phosphorylation of Cdc25c (Ser198) were inhibited by TL-77 (1-4xGI_{50}) in A2780 cells. Similarly, ON01910.Na treatment also caused equivalent reduced levels of phospho-Cdc25c.

Additionally, activity of Cdc25c was determined with total Cdc25c antibody (Figure 5.11 second lane). As expected, a significant electrophoretic shift of Cdc25c from 54- 57 kDa to 66 kDa was visualized in TL-77-treated cells compared with control, indicating the conversion of interphase to mitotic Cdc25c when cells enter mitosis. ON01910.Na treatment also resulted in

increase in the electrophoretic mobility of Cdc25c starting from 0.12 μM in HCT-116 cells and 1 μM in A2780 cells respectively. In addition, it is noticed that the differential electrophoretic mobility of Cdc25c closely correlated to the abrogation of phospho-Cdc25c at Ser198. Therefore, it is highly likely that the differential electrophoretic mobility of Cdc25c in cells treated with both TL-77 and ON01910.Na may be due to inhibition of phosphorylation at Ser198.

Immunoblot analyses revealed that cyclin B1 accumulated in lysates of cells treated with TL-77 or ON01910.Na (8 h), indicating cells accumulated in a mitotic state. Suppression of cyclin B1 was detected in TL-77-treated cells (16 μM) as well as ON01910-treated cells (0.24 μM) after 24 h treatment (Figure 5.11).

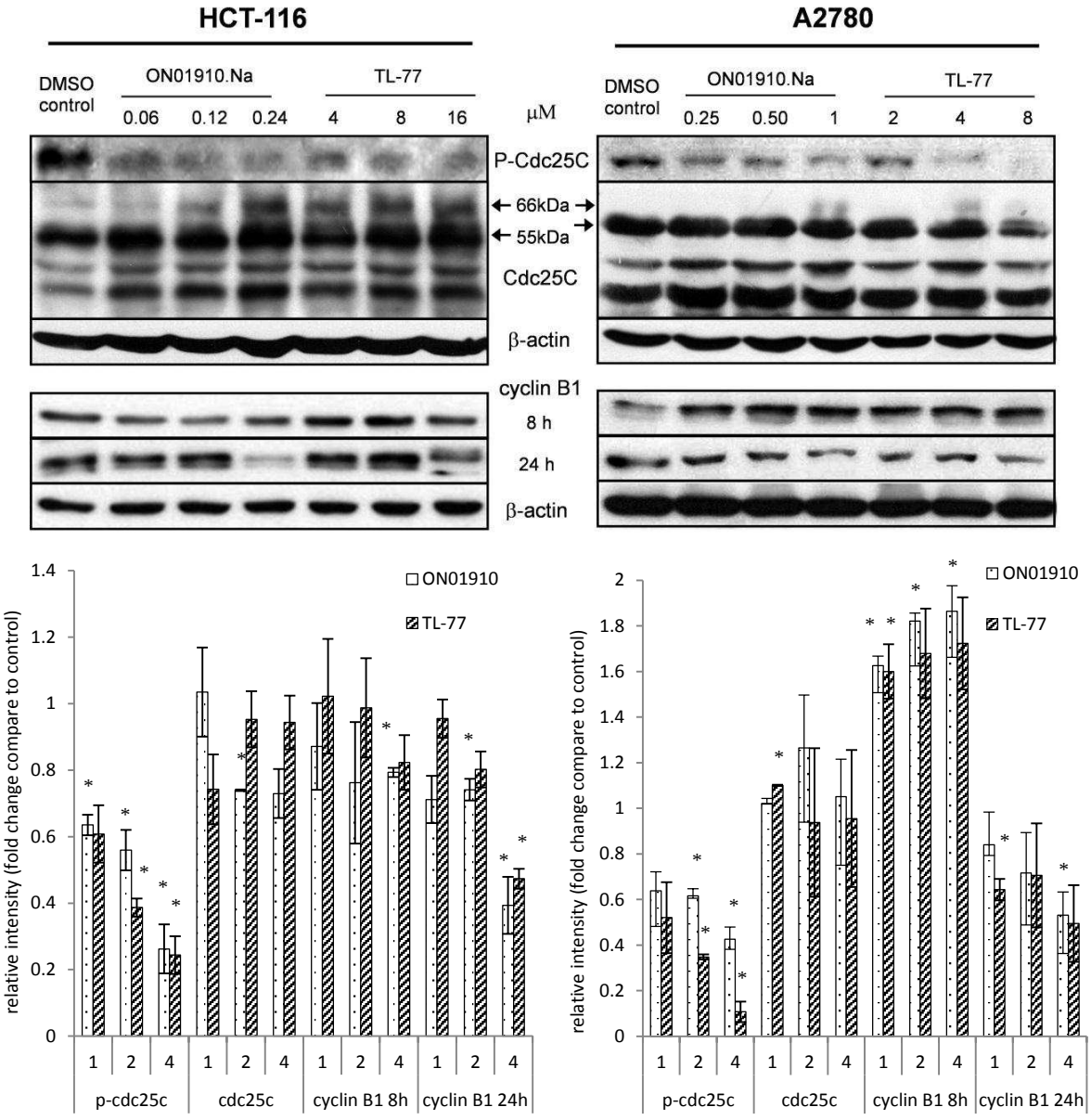

Figure 5.11 Effect of TL-77 on cell-cycle regulators.

HCT-116 and A2780 cells were incubated with indicated concentrations of TL-77 and ON01910.Na for 8 h or 24 h. Arrows, different electrophoretic mobilities of Cdc25c. Equal loading of lysates in each immunoblot was checked using an antibody against β-actin. The Western blot results were quantified and statistical analysis was performed (*P < 0.05). All of the aforementioned experiments were repeated three times, and a representative result is shown.

We next examined the effect of TL-77 on expression of the major cell cycle regulator cyclin D1. HCT-116 and A2780 cells were treated with TL-77 in parallel with ON01910.Na. As shown in Figure 5.12Error! Reference source not found., after 8 h treatment, expression of cyclin D1 was significantly inhibited in ON01910.Na-treated cells at 0.24 μM ($4xGI_{50}$) and TL-77-treated

cells from 8 μM ($2xGI_{50}$) in HCT-116 cells, while only minor inhibition of cyclin D1 expression was observed for both compounds at $4xGI_{50}$ in A2780 cells.

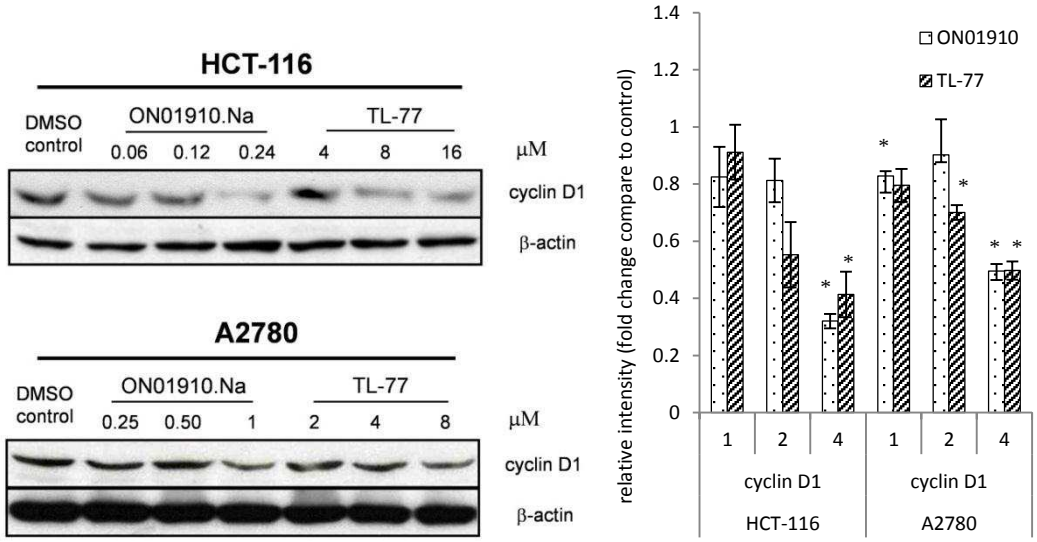

Figure 5.12 Effect of TL-77 and ON01910.Na on cyclin D1 expression.

HCT-116 and A2780 cells were incubated with indicated concentrations of TL-77, ON01910.Na for 8 h. β-Actin was used as an internal control for protein loading. The Western blot results were quantified and statistical analysis was performed (*$P < 0.05$). All of the aforementioned experiments were repeated three times, and a representative result is shown.

5.5.1 Discussion

Mitotic entry is triggered by a steep increase in cyclin B/Cdc2 activity.[184] Plk1 is suggested to regulate cyclin B/Cdc2 activity at several levels: it activates the phosphatase Cdc25c thereby triggering a dual positive amplification loop with cyclin B/Cdc2 - phosphorylating cyclin B1 and targeting it to the nucleus.[185, 186] The Xenopus Polo-like kinase Plx1 was shown to directly activate the phosphatase Cdc25c and depletion of Plx1 significantly delays both Cdc25c and cyclin B/Cdc2 activation.[187] In mammalian cells, Plk1 phosphorylates Cdc25c on Ser198 and regulates nuclear translocation of Cdc25c.[182] According to Schmidt et al., phosphorylation at Ser198 of Cdc25c has been suggested to serve as a reliable marker to track inhibition of Plk1 by small-molecule inhibitors in a cellular context.[24]

ON01910.Na is reported to inhibit Plk1 and decrease activity of Cdc25c.[53, 96] However, inconsistent effects of ON01910.Na on cyclin B/Cdc2 activity have been described.[78, 96, 188] In this study, TL-77 effectively inhibited phosphorylation of Cdc25c at Ser198. Additionally, lack of phospho-Cdc25c at Ser198 could be correlated with the differential electrophoretic mobility from 55-57 kDa to 66 kDa in total Cdc25c caused by TL-77 treatment.

Minor effects on cyclin B1 were observed after 8 h treatment for both compounds in both cell lines. Besides, data from mitotic index analysis indicated that TL-77 evoked a notable mitotic block (6 h-12 h exposure). TL-77 suppressed Cdc25c activity and the cyclin B1/Cdc2 complex still remained active. We therefore extrapolate that cells eventually entered mitosis during early stages of treatment (≤ 12 h). It is more likely that TL-77 inhibits the tubulin polymerization; cells consequently become blocked at the mitosis checkpoint with the outcome of multipolar spindles and misaligned chromosomes. Moreover, the dramatic influence caused by TL-77 on phosphorylation of mitotic regulators, such as Cdc25c and histone H3, indicate this compound also interact with the activity of kinase(s) which mediate mitotic checkpoint, such as Plk1.[29] Further investigations are still required. However, less efficiently G2/M arrests (≥ 6 h) with mild mitotic blocks were observed after exposure to ON01910.Na, suggesting a defect in mitotic entry. Meanwhile, instead of generating multipolar spindles, cells exposed to ON01910.Na exhibited fragmented microtubules. This may be due to the multi-targeted nature of ON01910.Na in cancer cells, which still requires further exploration.

After 24 h treatment, suppressed expression of cyclin B1 was observed in ON01910-treated cells (0.24 μM) as well as TL-77-treated cells (16 μM).

Moreover, mitotic index analyses have shown increasing G2 arrest in cells after treatment of both ON01910.Na and TL-77 ($2xGI_{50}$ only > 12 h). These data confirm the hypothesis that by inhibiting Cdc25c activity, both compounds maintain Cdc2 in its inactive state after longer exposure to compounds (12-24 h). Consequently, cells fail to traverse mitosis and become blocked in the G2/M phase of the cell cycle. These observations indicate a multi-faceted mechanism culminating in mitotic inhibition in cancer cells for both compounds.

5.6 Inhibition of PI3K/Akt/mTOR signal transduction caused by TL-77

ON01910.Na has been reported to inhibit PI3-K/Akt/mTOR signal transduction as the major target with suppression of cyclin D1, and activation of apoptosis.[78] Cyclin D1 down-regulation was observed in both HCT-116 (dramatically) and A2780 (mild) cell lines after TL-77 treatment. To determine whether TL-77 modulate PI3K/Akt/mTOR signalling, western blot expression of key effectors of the Akt/mTOR pathway was examined. Akt, a family of serine/threonine kinases, is the primary receptor of phosphoinositide 3-kinase (PI3K)-initiated signalling and controls essential cellular activities through phosphorylation of a number of downstream effectors.[102, 107] Through phosphoinositide-dependent protein kinases (PDKs), PI3K activates Akt, which in turn phosphorylates (thereby activating) mTOR protein at Ser 2448. Western blot analysis detecting phosphorylated Akt Ser 473 revealed that TL-77 ($\geq$ 4 μM) significantly inhibited Akt phosphorylation in HCT-116 cells, suggesting that TL-77 negatively regulates Akt in the same manner as ON01910.Na (Figure 5.13). To determine whether TL-77 inhibits effectors that

function upstream of Akt, we examined phosphorylation of PDK1, which is known to have a central function in Akt activation.[189] Western blot analysis revealed that phosphorylation of PDK1 was down-regulated in a dose-dependent manner by both compounds in HCT-116 cells. Complete inhibition of PDK1 phosphorylation was observed after 8 h exposure of cells to $4xGI_{50}$ TL-77 (16 μM) and ON01910.Na (0.24 μM) (Figure 5.13). But the treatment with both compounds for 8 h minimally affected the phosphorylated Akt and PDK1 in A2780 cells (Figure 5.13).

The impact of TL-77 on downstream effectors of Akt was further investigated. One known Akt substrate is a 40 kDa, proline-rich protein (PRAS40) that binds mTOR to transduce Akt signals to the mTOR complex. Phosphorylation of PRAS40 by Akt at Thr 246 helps to reduce PRAS40 inhibition of mTORC1.[190] Although ON01910.Na reduced phosphor-PRAS40 at 0.24 μM, which is first reported here, only minor inhibition of PRAS40 phosphorylation was observed in TL-77-treated HCT-116 cells. This observation was confirmed in A2780 cells. (Figure 5.13) Subsequently, ON01910.Na treatment significantly reduced phosphorylation of mTOR in both cell lines. Although treatment with TL-77 for 8 h did not induce changes in the phosphorylation status of mTOR in HCT-116 cells, a dramatic inhibition was shown at 8 μM in A2780 cells. (Figure 5.13) In addition, it was observed that neither compound affected expression of PTEN in HCT-116 cells, the 3' phosphatase major tumour suppressor protein and inhibitory regulator of PI3K/Akt signalling. (Figure 5.13)

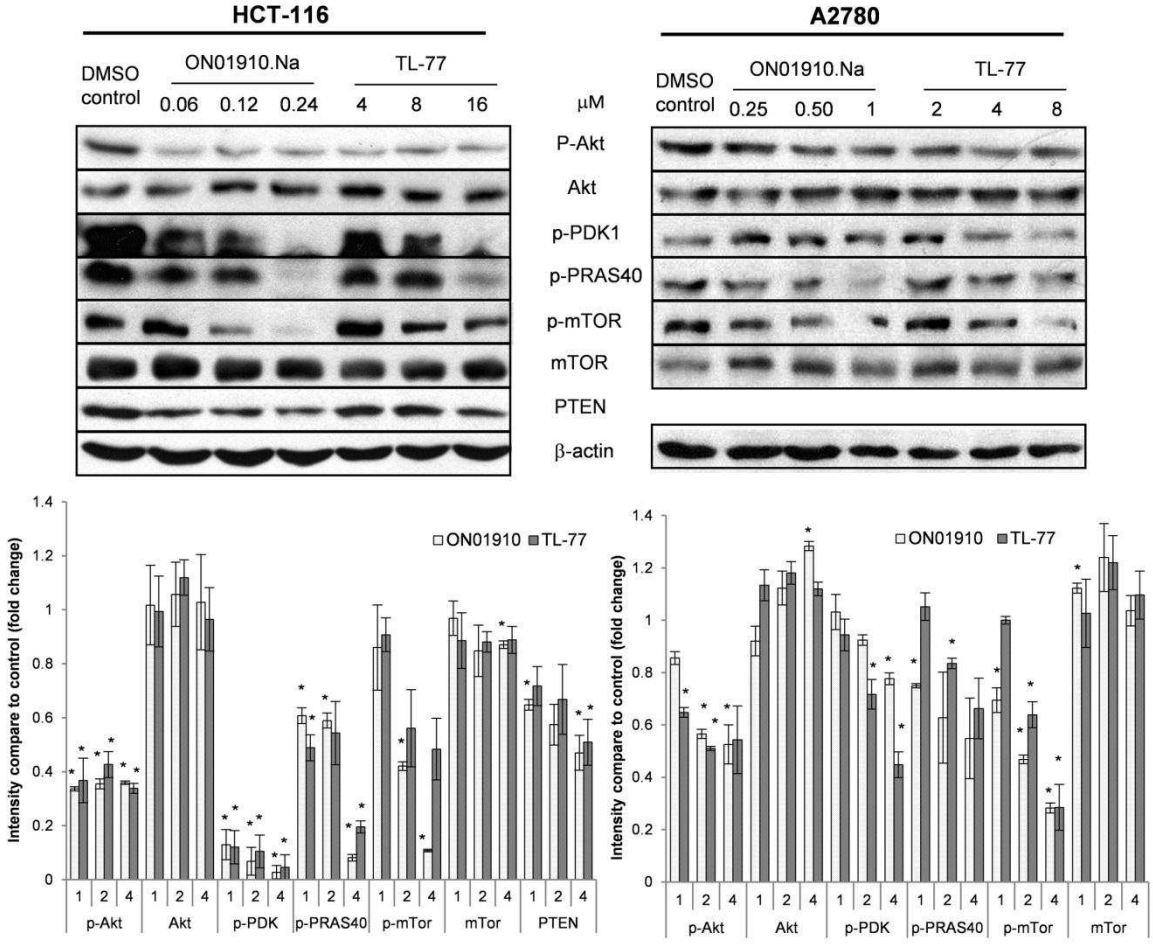

Figure 5.13 Effect of TL-77 on the Akt/mTOR signal transduction pathway.

HCT-116 and A2780 cells were incubated with indicated concentrations of TL-77, ON01910.Na for 8 h. The cells were lysed and subjected to Western blot analysis using indicated antibodies. Equal loading was confirmed in each lane by stripping and reprobing the blots with either anti-Akt antibody (second panel) or anti-mTOR antibody (sixth panel). β-Actin was used as an internal control for protein loading. The Western blot results were quantified and statistical analysis was performed (*$P < 0.05$). All of the aforementioned experiments were repeated three times, and a representative result is shown.

The PI3K/Akt pathway is a well-characterized cell survival signalling pathway that blocks apoptosis and promotes survival and growth in cancer cells.[191] TL-77, as well as ON01910.Na, inhibited the phosphorylation of Akt and PDK1. While ON01910.Na down regulated phosphor-mTOR in both cell lines, suppression of phosphor-mTOR is cell line specific following treatment with TL-77 (A2780 only). Also, the suppression of phosphor-PRAS40 were observed in ON01910.Na-treated cells at $4xGI_{50}$ for both cell lines, while only a moderate inhibition was detected at 16 μM ($4xGI_{50}$) in HCT-116 cells after

treated with TL-77. Taken together, these results indicate that TL-77 inhibits PI3K/Akt/mTOR signal transduction; however, compared with ON01910.Na, arrest of PI3K/Akt/mTOR signalling by TL-77 appears to be less significant and cell line-specific.

5.7 Molecular mechanism of TL-77-induced apoptosis

Apoptosis is a major form of cell death, characterized by a series of distinct morphological and biochemical alterations.[192] A series of typical apoptotic morphological changes in cell structure after exposures to TL-77 as well as ON01910.Na were clearly detected (refer to Chapter Three). The molecular mechanisms of TL-77-mediated apoptosis in HCT-116 and A2780 cell lines were further explored.

5.7.1 AnnexinV/PI double staining

One of the earlier events of apoptosis includes translocation of membrane phosphatidylserine (PS) from the inner to the outer leaflet of the plasma membrane. AnnexinV is a Ca^{2+} dependent phospholipid-binding protein that binds tightly to PS. Fluorochrome-labeled Annexin V binds to cells with exposed PS, therefore, serves as a sensitive probe for flow cytometric analysis of cells in the early stages of apoptosis.[193]

Propidium iodide (PI) is a fluorescent molecule that is used as a DNA stain to evaluate cell viability or DNA content in cells. Healthy cells with intact membranes exclude PI, whereas PI can penetrate the membranes of dead cells. Staining with FITC annexinV is usually used in conjunction with PI to differentiate necrotic, apoptotic and normal cells. Cells that are considered

viable are both Annexin V and PI negative; while early apoptotic cells are FITC annexin V positive and PI negative, and cells in late apoptosis or already dead are both Annexin V and PI positive. Progression through these three stages can be used to confirm cell apoptosis.

Induction of apoptosis by TL-77 or ON01910.Na was analysed by Annexin V/PI double staining in HCT-116 and A2780 cancer cells following treatments for 24 h and 48 h. As illustrated in Figure 5.14, both TL-77 and ON01910.Na induced apoptosis in dose- and time-dependent manners in both cancer cell lines. TL-77 induced HCT-116 apoptosis at GI_{50} and $2xGI_{50}$ values (4 μM and 8 μM respectively) ≥ 24 h exposure with maximal effect after 48 h treatment, whereas ON01910.Na triggered apoptosis more slowly than TL-77 (minor effect at 24 h, clear effect at 48 h) (Figure 5.14 **A**). A2780 cells appeared more sensitive to ON01910.Na and TL-77; both TL-77 and ON01910.Na at GI_{50} effectively induced apoptosis with > 30% (24 h) and > 60% (48 h) cells undergoing through early apoptosis (Figure 5.14 **B**). These time-dependent observations are consistent with cell cycle effects.

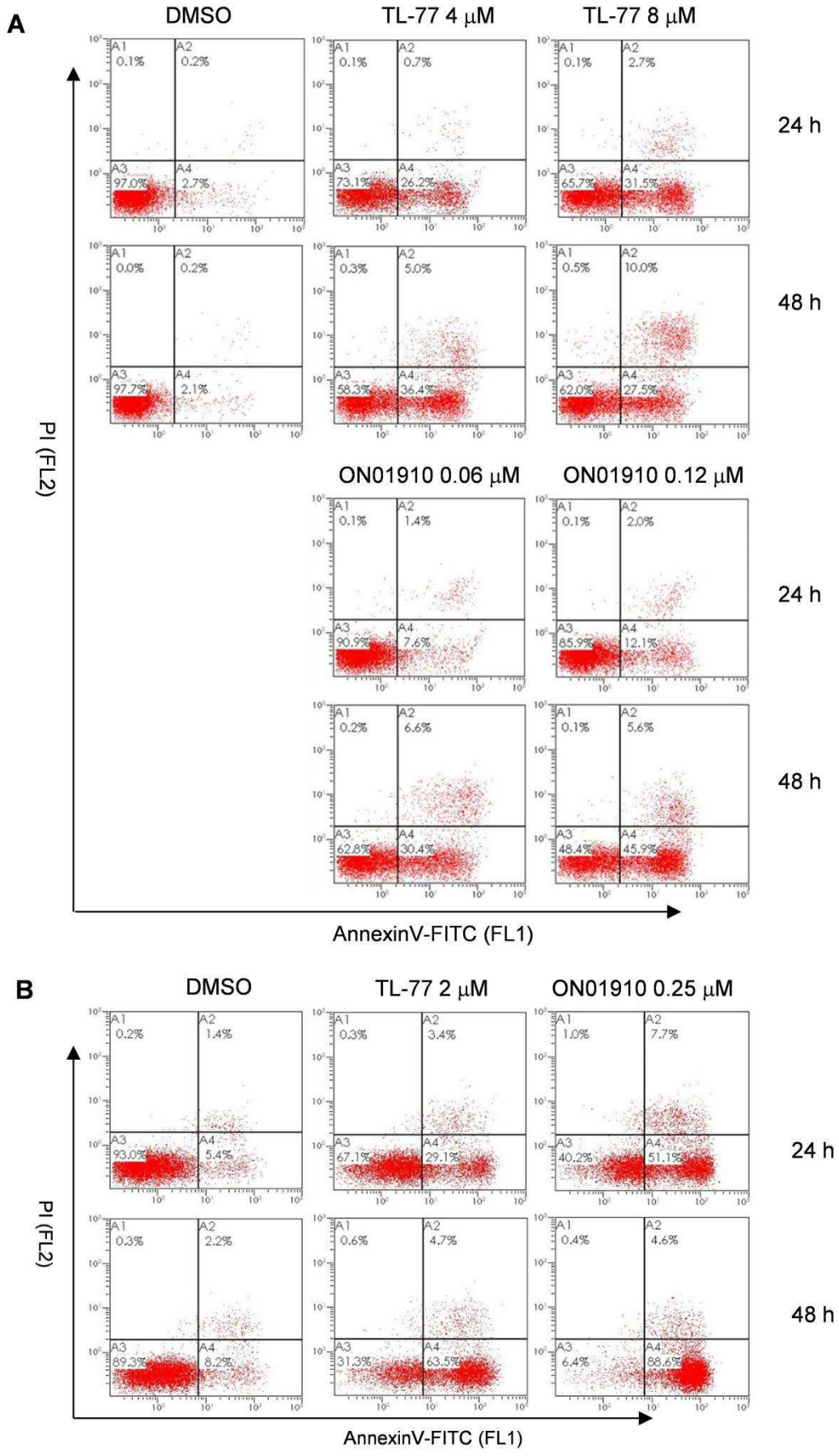

Figure 5.14 Induction of apoptosis by TL-77 and ON01910.Na in cancer cells.

(A) HCT-116 and (B) A2780 cells were exposed to different concentrations of TL-77 or ON01910.Na 24 h or 48 h and stained using FITC-conjugated Annexin V and propidium

iodide; 10000 cells per sample were subjected to flow cytometric analyses as described in the experimental procedures. A1, Annexin-negative and PI-positive dead cells; A2, double-positive late apoptotic cells; A3, double negative live cells; A4, Annexin V-positive, PI-negative early apoptotic cells. All of the above experiments were repeated three times, and a representative result is shown.

Induction of apoptosis was also tested in untransformed HMEC-1 cells after exposure to TL-77 or ON01910.Na for 24 h and 48 h (Figure 5.15). Importantly, HMEC-1 cells were less sensitive to TL-77 treatment compared to the cancer cell lines. Only ~ 13% - 18% apoptotic cells were detected following treatment with TL-77, which were 2 fold lower than apoptotic HCT-116 cells (~ 26% - 36%) at same concentration (4μM in Figure 5.14 **A**). In contrast, ON01910.Na induced detectable apoptosis (~ 21% - 36%) in HMEC-1 cells at 0.06 μM, showing minimal selectivity towards cancer over normal cells. These results are consistent with corresponding activities in the growth inhibition assays.

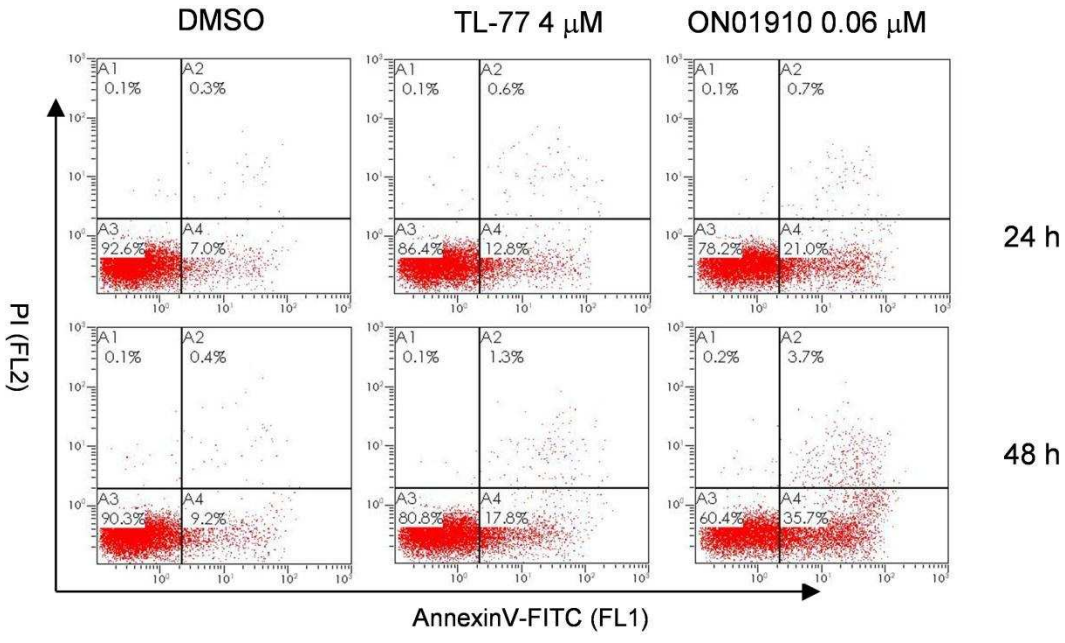

Figure 5.15 Induction of apoptosis by TL-77 and ON01910.Na in non-transformed cells.

HMEC-1 cells were exposed to different concentrations of TL-77 or ON01910.Na 24 h or 48 h and stained using FITC-conjugated Annexin V and PI; 10000 cells per sample were subjected to flow cytometric analyses as described in the experimental procedures. A1, Annexin-negative and PI-positive dead cells; A2, double-positive late apoptotic cells; A3, double negative live cells; A4, Annexin V-positive, PI-negative early apoptotic cells. All of the above experiments were repeated three times, and a representative result is shown.

5.7.2 TL-77 induces caspase-dependent apoptosis

Apoptotic signalling mainly converges in the activation of caspases, which propagate death signalling by cleaving key cellular proteins.[117] Induction of caspase 3/7 activity therefore was examined in HCT-116 and HMEC-1 cells after 24 h treatment either with TL-77 or ON01910.Na. Results in Figure 5.16 demonstrate that TL-77 dose-dependently enhanced caspase 3/7 activities in HCT-116 cells compared with DMSO control (0.2% v/v) at concentrations ≥ 2 µM (0.5xGI_{50}), confirming an active apoptotic process during this period. But no such activity was detected in HMEC-1 cells ≤ 16 µM (4xGI_{50}). On the contrary, ON01910.Na significantly activated caspase 3/7 > 0.06 µM (GI_{50}) in cancer cells and at 0.12 µM (2xGI_{50}) in normal cells. These results revealed that TL-77 as well as ON01910.Na induced caspase-dependent apoptosis in cancer cells, and further demonstrated the selective nature of TL-77-induced apoptosis.

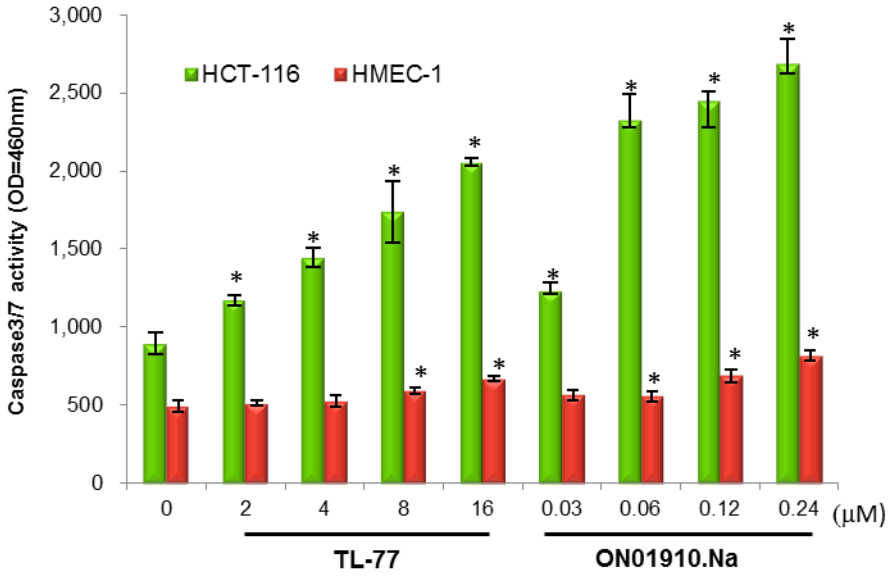

Figure 5.16 TL-77 and ON01910.Na induce caspase 3/7 activity in cancer and non-transformed cell lines.

HCT-116 and HMEC-1 were treated with indicated concentrations of TL-77 and ON01910.Na for 24 h. Caspase 3/7 activity was measured according to the assay conditions described in Experimental Procedures. Vertical bars represent the mean ± SD of three replicates; n = 2 per experiment. Values significantly ($p \leq 0.05$) different from DMSO vehicle control were marked

with an asterisk (*).

Effector caspases (Caspase-3, -6, -7) directly cleave a variety of substrates resulting in proteolysis of cellular proteins and apoptosis. The best characterized caspase substrate is poly-(ADP-ribose) polymerase (PARP), a family of proteins involved in DNA repair and is a key mediator of programmed cell death.[117] During apoptosis, PARP is inactivated by caspase-3 cleavage and converted from 116 kDa to fragments of 89 and 24 kDa.[194] Cleavage of PARP has been used extensively as a marker of cells undergoing apoptosis.[195] Western blot assays (Figure 5.17) revealed that both compounds inactivated PARP by causing caspase cleavage after 24 h treatments. TL-77 induced dose-dependent PARP cleavage in A2780 cells, while significant PARP cleavage was observed at all tested concentrations ($\geq$ 4 μM) in HCT-116 cells. Consistent with delayed apoptosis observed (in the Annexin V/PI dual staining assay; Figure 5.14 **A**), PARP cleavage in cells exposed to ON01910.Na was not detected below 0.24 μM (4xGI_{50}) treatments in HCT-116 cells.

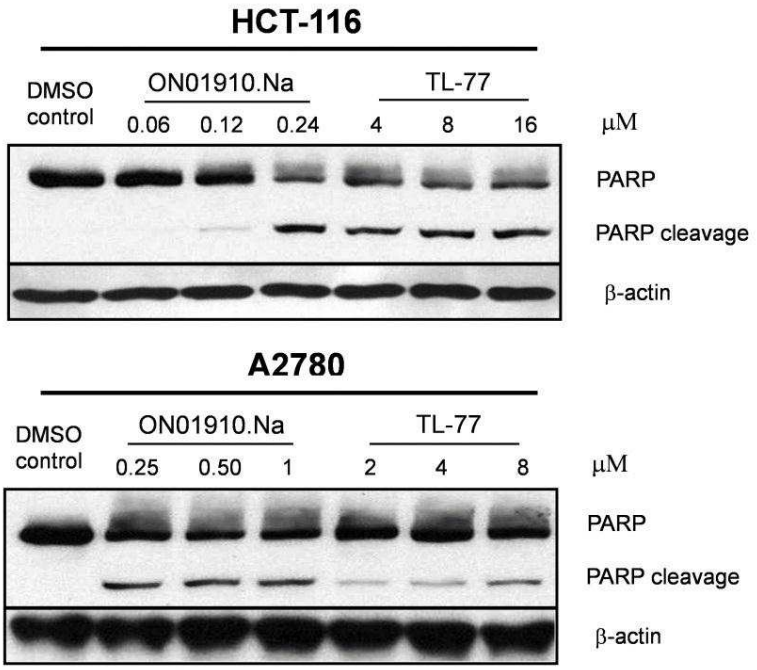

Figure 5.17 TL-77 inactivated PARP by causing caspase cleavage.

Western blot analyses in HCT-116 cells and A2780 cells. Cells were treated with indicated concentrations of TL-77 or ON01910.Na for 24 h. Cell lysates were subjected to Western blot analyses by using anti-PARP antibodies to assess the cleavage of PARP. β-Actin was used as an internal control for protein loading. All of the above experiments were repeated three times, and a representative result is shown.

5.7.3 TL-77 down-regulates expression of Bcl family proteins

Caspases and Bcl family proteins comprise the mediators of apoptosis. Apoptosis is affected by the stoichiometry between pro- (Bax, Bid) and anti-apoptotic (Bcl-xl, Mcl-1) molecules[196], the expression levels of Bcl-2 family members in HCT-116 cells after 24 h treatment was tested.

Bid plays the key role in releasing cytochrome c from mitochondria.[116] As an inactive precursor localized within the cytosol of cells, Bid is activated following cleavage by caspase-8; it subsequently translocates to the mitochondria and induces cytochrome c release, followed by mitochondrial damage.[117] As shown in Figure 5.18, expression levels of Bid were significantly reduced in TL-77-treated cells compared to controls, while ON01910.Na showed only a minor effect. Total protein levels of Bax in HCT-

116 cells following treatment with these compounds were then examined; we observed that the expression of these molecules was essentially unchanged. Expression of Bcl-xl and Mcl-1 however were significantly reduced in TL-77-treated cells compared to controls. Treatment with TL-77 at 16 μM for 24 h resulted in the complete inhibition of Bcl-xl protein expression. Mcl-1 is highly expressed in myeloid leukemia cell lines and its translation is regulated by the PI-3K/Akt pathway.

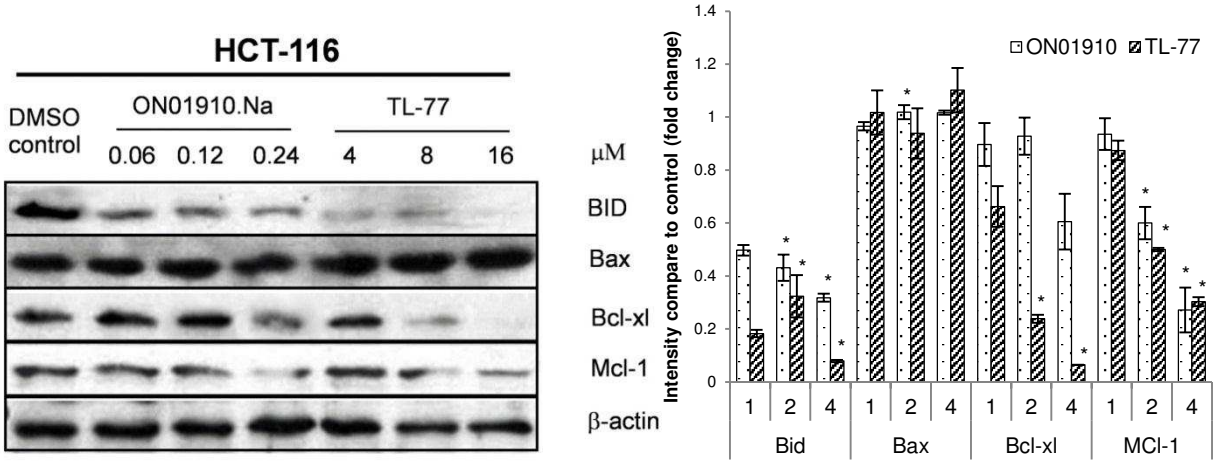

Figure 5.18 Effects of TL-77 on Bcl family proteins.

HCT-116 cells were treated with indicated concentrations of TL-77 or ON01910.Na for 24 h. Cell lysates were prepared and subjected to Western blot analyses by using anti-BID, anti-Bax, anti-Bcl-xl and Mcl-1 antibodies. β-Actin was used as an internal control for protein loading. All of the above experiments were repeated three times, and a representative result is shown.

5.7.4 Discussion

Anticancer drug-induced apoptosis is mainly controlled by two major pathways: the membrane death receptor (extrinsic) pathway and the mitochondrial (intrinsic) pathway.[117] The mitochondria-dependent pathway involves cleavage of a pro-apoptotic protein, Bid, resulting in the production of truncated Bid (tBid). Subsequent BID cleavage participates in cytochrome-c mediated apoptosis and activates caspase 3.[197] Bcl-xL prevents the release of cytochrome c by inhibiting the VDAC (Voltage-dependent anion channels)-mediated permeability transition pore.[197]

From our observations, dose- and time-dependent apoptosis induced by both compounds, detected by Annexin-V binding, is closely associated with induction of caspase 3/7 activity and PARP cleavage. In HCT-116 cells, TL-77 induced rapid apoptosis, whereas ON01910.Na only triggered apoptosis after a longer exposure period, an observation consistent with cell cycle effects, indicating that cell-cycle arrest may be the apoptotic trigger.

Analysis of Bcl-2 family proteins after treatment of cells with TL-77 and ON01910.Na revealed that neither compound altered expression levels of the pro-apoptotic molecule Bax. However, expression of Bid was significantly reduced in cells following TL-77 treatment. This may indicate that the precursor form of Bid translocates to mitochondria, where it induces cytochrome c release[116], suggesting the involvement of the mitochondrial pathway in TL-77-mediated apoptosis. Among the pro-survival molecules, expression of Bcl-xL and Mcl-1 was significantly inhibited by both compounds. Taken together, these data show that TL-77 and ON01910.Na selectively induce G2/M cell cycle block with ensuing induction of apoptosis through the mitochondrial pathway in tumour cells.

5.8 TL-77 induces DNA double-strand breaks

Cell cycle checkpoints are cellular responses to DNA damage by delaying progression of the cell cycle until DNA is repaired. Many anti-cancer drugs exert their effect through DNA damage and subsequent induction of apoptosis in cancer cells. H2AX is a variant of histone H2A required to maintain genomic stability.[198] Phosphorylation of Ser-139 of the histone variant H2AX, forming γ-H2AX, is an early cellular response to the induction of DNA double-strand breaks.[199] Detection of this phosphorylation event has emerged as a

highly specific and sensitive molecular marker for DNA double strand breaks induced by DNA-damaging agents.[200]

Cellular expression of γ-H2AX was detected following treatment of cells with TL-77 or ON01910.Na for 8 h and 24 h, indicative of DNA damage. Western blot analysis of HCT-116 cells after treatment with TL-77 and ON01910.Na for 8 h showed significant dose-dependent elevation of γ-H2AX (Figure 5.19). Following treatment of cells with either compound for 24 h, intense bands revealed high levels of γ-H2AX. These data reveal that early and prolonged phosphorylation of Histone H2AX has occurred after treatment with TL-77 or ON01910.Na. This observation illuminated that TL-77 induces rapid DNA-damage in cancer cells.

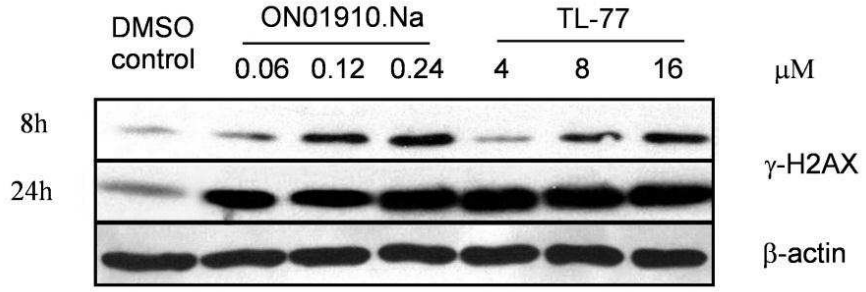

Figure 5.19 Induction of γ-H2AX by TL-77 and ON01910.Na.

Western blot analysis was performed in HCT-116 cell. Cells were treated with indicated concentrations of TL-77 or ON01910.Na for 8 or 24 h. β-Actin was used as an internal control for protein loading. All of the above experiments were repeated three times, and a representative result is shown.

5.9 Conclusion

In this section, preliminary cellular mechanisms of action of TL-77 have been investigated and compared with ON01910.Na. TL-77 exhibits excellent anti-proliferative activity against a wide range of human tumour cell lines. It demonstrates demonstrated > 2 fold greater potency in cancer cell lines over normal cells.. Cell cycle analyses reveal that TL-77 evokes profound G2/M cell

cycle arrest at ≥ 6 h in cancer cells, followed by the onset of apoptosis.

In cell-free conditions, TL-77 as well as ON01910.Na potently inhibits tubulin polymerization. Mitotically arrested cells display multipolar spindles and misalignment of chromosomes, indicating that TL-77 interferes with mitotic spindle assembly in cancer cells. The TL-77-treated cell phenotypic change is similar to that observed in Plk1-depleted cells. The underlying mechanism of G2/M arrest showed a strong inhibitory effect of Cdc25c phosphorylation and cyclin B1 protein expression: TL-77 inhibits phosphorylation of Cdc25c (Ser198), which is indicative Plk1 inhibition. Subsequent down-regulation of cyclin B induced by TL-77 block the mitotic entry. Thus, it is proposed that TL-77 arrests the DNA damage checkpoint, induces DNA damage, inhibits spindle assembly and induces mitotic block. Analysis of apoptotic signalling pathways reveals that TL-77 down-regulates expression of Bcl-2 family proteins (Bid, Bcl-xl and Mcl-1) and stimulates caspase activation (caspase 3,7), indicating TL-77 induces apoptosis through the mitochondrial pathway in tumour cells. These effects are comparable to those elicited by ON01910.Na.

Unlike ON01910.Na, however, TL-77 elicits lower toxicity in non-transformed cells and mediates rapid mitotic inhibitory effects. Moreover, non-significant effects on PI3K/AKT signal transduction are observed after TL-77 treatment. These observations indicate a multi-faceted mechanism of TL-77 culminating in mitotic inhibition in cancer cells. Therefore, further evaluation of this promising anti-tumour agent is justified.

6 Conclusion and future directions

6.1 General conclusion

The major goal of this project was to identify ON01910.Na mimetic compounds with superior drug properties, and to validate the mechanism of action. To achieve this goal, a novel series of (E)-3-((styrylsulfonyl)methyl)pyridines has been designed and synthesised. The lead compounds were identified through cellular and pharmacological screening. Preliminary cellular mechanisms of action of TL-77 have been investigated.

Our data suggest that lead compounds exhibit high potency and selectively cytotoxicity (2-10 folds) to cancer cells over untransformed cells. These compounds arrested cancer cells in the G2/M phase of cell cycle and induced apoptosis effectively. Importantly TL-77 possesses significantly improved pharmacological properties, with high oral bioavailability when compared to ON01910.Na. Therefore, the objectives of this study have been met. This work validates the novel (E)-styrylsulfonyl methylpyridines as anti-cancer agents and presents a strong rationale for further optimizing derivatives iteratively through chemical synthesis and biological evaluation. As a mitotic inhibitor, TL-77 represents a promising anti-cancer agent worthy of further evaluation.

6.2 Future directions

The hit-to-lead and optimization processes are iterative cycles of chemical synthesis and biological evaluation. Based on the study of TL-77 and other lead compounds, primary understandings of this analogue have been developed and structure modification is still required. Although TL-77 exhibited some

favourable physicochemical properties, the pharmaceutical assessment revealed a relatively high efflux ratio of TL-77 (ER= 5.29) indicating this compound may undergo active efflux. Therefore, the structural modification to improve permeability should be considered.

Cell cycle is a dynamics process. Among the protein complexes that vary during the cell cycle, almost all of complexes contain both periodically expressed (dynamic) and constitutively expressed (static) components. In Chapter four, TL-77 alters the expression of several checkpoint proteins, including Cdc25c, cyclin B1 and phospho-histone H3 have been discussed. In view of the dynamic expression of these markers during cell cycle, the activities of mitotic proteins are suggested to be correlated with the proportional changes, rather than absolute baseline levels. This could be achieved in the future evaluation by cell synchronization and addition of testing time points (reducing testing time interval). In this way, it is easier to monitor the expression changes of cell cycle proteins after in vitro and in vivo drug exposure.

In our study, multistep recognition was investigated for the molecular mechanism of TL-77 effecting cell cycle protein kinases. In attempt to direct recognizing precise kinase inhibition, a kinase screen assay (Merck Millipore's KinaseProfiler™) was conducted for both TL-77 and ON01910.Na (ON01910.Na as the positive control) on six potential target proteins. (Appendix I) However, neither compounds showed inhibitory effect on tested proteins. According to reported work, kinase inhibitory effects of ON01910.Na were identified by kinase assays using recombinant protein kinases, such as PI3 Kinases and Plk1, isolated from insect cells or Sf9 cells and incubating with compounds, [γ-^{32}P] ATP and substates.[53, 78] Therefore, the poor reproducibility

is a big concern. Yet, in cell-based assays in this study, clear down-regulation of phosphorylated Cdc25c protein was observed, indicating inhibition of Plk1 activity. Detailed possible explanations have been discussed in Chapter four (4.2.2.1).Therefore, developing reliable biochemical assays to validate the target(s) of this analogue is urgent and essential, and this will become a challenge and main goal for the future understanding of mechanisms of action.

7 Experimental section

7.1 General chemical procedure

Chemicals and solvents were purchased from commercial standard suppliers and used as received. Reactions were monitored by analytical thin-layer chromatography (TLC) using Merck silica gel 60 GF254 pre-coated (0.2 mm). TLC plates were visualised under UV light (254 nm). Purification by column chromatography and flash chromatography was performed using Merck silica gel 60 (0.040-0.063 mm). Flash chromatography was performed using Biotage® FlashMaster Personal Plus flash chromatography.

^{1}H and ^{13}C Nuclear magnetic resonance (NMR) spectra were recorded on a Bruker-AV 400 spectrometer (^{1}H at 400 MHz and ^{13}C NMR at 100 MHz). NMR spectra were processed using the Bruker Topspin 3.2 software. Deuterated solvents used were $CDCl_3$ (Cambridge Isotope Laboratories Inc.) and CD_3OD (Sigma-Aldrich). ^{1}H NMR signals are reported with chemical shift values δ (ppm), multiplicity (s = singlet, d = doublet, t = triplet, q = quartet, m = multiplet and br = broad), relative integral, coupling constants J (Hz) and assignments. Mass spectra were recorded on a High Resolution Time of Flight (TOF) electrospray ionisation (ES) system comprising of a Waters 2795 Separations module and Micromass LCT Platform, data was processed using MassLynx™ software. Melting points were recorded on an Electrothermal IA 9100 digital melting point apparatus.

The purity of compounds used for biological tests was determined by analytic high performance liquid chromatography (HPLC), and is greater than 95%. Analytical HPLC was carried out on Waters automated LC system (Waters

2525 binary gradient pump coupled to Waters 2767 sample manager and to Waters 2487 dual λ absorbance detector), with phenomenex Gemini-NX 5u C18 110A 250 × 4.60 mm column, UV detector at λ=254 nm. The systems used were:

- Method A: 10% MeOH containing 0.1% TFA for 4 min, followed by linear gradient 10% to 100% MeOH over 12 min at a flow rate of 1 ml/min;
- Method B: 10% MeCN containing 0.1% TFA for 4 min, followed by linear gradient 10% to 100% MeCN over 12 min at a flow rate of 1 ml/min.

2-Methoxy-5-methyl-3-nitropyridine (2).

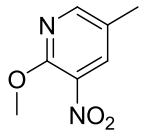

To anhydrous MeOH (100 ml) was added Na (2.31 g, 100 mmol), and the resulting solution went clear over the course of 30 min. Compound **1** (17.2 g, 99.7 mmol) was added at room temperature. The reaction mixture was heated at reflux for 4 h under N_2, cooled down to room temperature and concentrated under reduced pressure. The residue was diluted with H_2O (100 ml) and extracted with CH_2Cl_2 (2 × 50 ml). The organic extracts were combined, washed with brine (30 ml), dried over $MgSO_4$ and concentrated under reduced pressure. The residue was crystallized (EtOH:H_2O = 1:15, 320 ml) to give **2** as a pale orange solid (15.4 g, 92%). m.p. 76-78 °C. ^{1}H NMR (400 MHz, DMSO-d_6) δ 2.31 (s, 3H, pyridine-CH_3), 3.98 (s, 3H, OCH_3), 8.30 (d, 1H, J 2.0, pyridine-H), 8.35 (d, 1H, J 2.0, pyridine-H). ^{13}C NMR (100 MHz, DMSO-d_6) δ 16.8, 54.9, 127.4, 133.7, 135.9, 152.0, 154.3. HRMS (ESI) m/z 169.0570 $[M+H]^+$; calcd. for $C_7H_9N_2O_3$ $[M+H]^+$ 169.0608.

5-(Bromomethyl)-2-methoxy-3-nitropyridine (3).

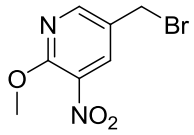

To a solution of compound **2** (8.40 g, 50.0 mmol) in carbon tetrachloride (100 ml) were added benzoyl peroxide (3.50 g, 14.4 mmol) and N-bromosuccinimide (17.8 g, 100 mmol). The reaction mixture was heated at reflux for 48 h under N_2, cooled down to room temperature and concentrated under reduced pressure. The residue was diluted with saturated Na_2CO_3 (200 ml) and extracted with CH_2Cl_2 (3 × 50 ml). The organic extracts were combined, washed with brine (50 ml), dried over $MgSO_4$ and concentrated under reduced pressure. The residue was purified by flash column chromatography (silica gel, petroleum ether ramping to EtOAc:petroleum ether = 1:99) to give **3** as a pale yellow solid (4.10 g, 33%). m.p. 92-94 °C. ^{1}H NMR (400 MHz, $CDCl_3$) δ 4.15 (s, 3H, OCH_3), 4.51 (s, 2H, CH_2), 8.34 (d, 1H, J 2.4, pyridine-H), 8.43 (d, 1H, J 2.0, pyridine-H). ^{13}C NMR (100 MHz, $CDCl_3$) δ 27.7, 55.2, 127.2, 133.7, 135.7, 151.4, 156.3. HRMS (ESI) m/z 246.9654 [M(^{79}Br)+H]$^+$, 248.9631 [M(^{81}Br)+H]$^+$; calcd. for $C_7H_8BrN_2O_3$ [M(^{79}Br)+H]$^+$ 246.9713, [M(^{81}Br)+H]$^+$ 248.9693.

Methyl 2-(((6-methoxy-5-nitropyridin-3-yl)methyl)thio)acetate (4).

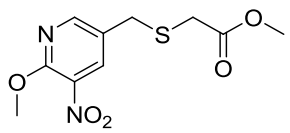

To a solution of compound **3** (4.92 g, 19.9 mmol) in MeOH (50 ml) were added methyl thioglycolate (2.70 ml, 30.2 mmol) and Na_2CO_3 (2.12 g, 20.0 mmol). The reaction mixture was stirred at room temperature for 1 h and concentrated under reduced pressure. The residue was dissolved in EtOAc (200

ml), and the solids were filtered and washed with EtOAc (2 × 25 ml). The filtrate and EtOAc washings were combined and concentrated under reduced pressure. The residue was crystallized with EtOH (50 ml) to give **4** as a pale green solid (3.99 g, 74%). m.p. 57-60 °C. ^{1}H NMR (400 MHz, DMSO-d_6) δ 3.32 (s, 2H, SCH_2COOCH_3), 3.59 (s, 3H, $COOCH_3$), 3.90 (s, 2H, pyridine-CH_2S), 4.03 (s, 3H, pyridine-OCH_3), 8.42 (d, 1H, J 2.0, pyridine-H), 8.44 (d, 1H, J 2.0, pyridine-H). ^{13}C NMR (100 MHz, DMSO-d_6) δ 31.6, 32.6, 52.5, 55.2, 128.4, 133.8, 136.1, 152.1, 155.2, 170.7. HRMS (ESI) m/z 273.0573 $[M+H]^+$; calcd. for $C_{10}H_{13}N_2O_5S$ $[M+H]^+$ 273.0540.

Methyl 2-(((6-methoxy-5-nitropyridin-3-yl)methyl)sulfonyl)acetate (5).

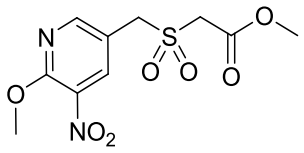

To a solution of compound **4** (1.64 g, 6.02 mmol) in CH_3COOH (40 ml) was added 30% H_2O_2 (2.60 ml, 22.9 mmol). The reaction mixture was stirred at 60 °C for 6 h and concentrated under reduced pressure. The residue was crystallized with EtOH (50 ml), and the solid was filtered to give **5** as a pale yellow solid (1.80 g, 98%). m.p. 137-140 °C. ^{1}H NMR (400 MHz, DMSO-d_6) δ 3.73 (s, 3H, $COOCH_3$), 4.07 (s, 3H, pyridine-OCH_3), 4.47 (s, 2H), 4.80 (s, 2H) (total 4H, CH_2SCH_2), 8.48 (s, 1H, pyridine-H), 8.51 (s, 1H, pyridine-H). ^{13}C NMR (100 MHz, DMSO-d_6) δ 53.4, 55.2, 55.4, 56.7, 118.3, 133.7, 138.0, 154.3, 156.3, 163.9. HRMS (ESI) m/z 305.0519 $[M+H]^+$; calcd. for $C_{10}H_{13}N_2O_7S$ $[M+H]^+$ 305.0438.

2-(((6-Methoxy-5-nitropyridin-3-yl)methyl)sulfonyl)acetic acid (6).

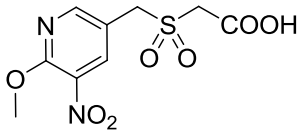

To a solution of compound **5** (1.83 g, 6.01 mmol) in MeOH/H_2O (1:1, 20 ml) was added Na_2CO_3 (1.80 g, 17.0 mmol). The reaction mixture was stirred at room temperature for 4 h and concentrated under reduced pressure. The residue was acidified to pH 2 with 1 M HCl, and the precipitate was filtered to give **6** as a white solid (1.72 g, 99%). m.p. 183-186 °C. ^{1}H NMR (500 MHz, DMSO-d_6) δ 4.06 (s, 3H, OCH_3), 4.29 (s, 2H), 4.77 (s, 2H) (total 4H, CH_2SCH_2), 8.47 (d, 1H, J 2.5, pyridine-H), 8.50 (d, 1H, J 2.0, pyridine-H), 13.57 (br s, 1H, COOH). ^{13}C NMR (125 MHz, DMSO-d_6) δ 55.1, 55.4, 57.2, 118.5, 133.7, 138.0, 154.3, 156.2, 164.9. HRMS (ESI) m/z 289.0064 $[M-H]^-$; calcd. for $C_9H_9N_2O_7S$ $[M-H]^-$ 289.0136.

(E)-2-Methoxy-3-nitro-5-(((2,4,6-trimethoxystyryl)sulfonyl)methyl)pyridine (7).

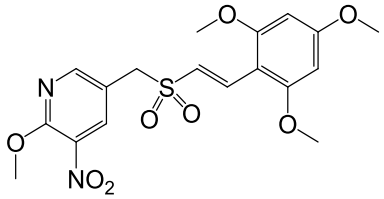

To a solution of compound **6** (14.5 g, 50.0 mmol) in toluene (750 ml) were added 2,4,6-trimethoxybenzaldehyde (10.8 g, 55.0 mmol), benzoic acid (0.915 g, 7.49 mmol) and piperidine (642 µl, 6.50 mmol). The reaction mixture was heated at reflux for 3 h under N_2, and the water generated was removed using a Dean-Stark apparatus. The reaction mixture was cooled down to room temperature and concentrated under reduced pressure. The residue was washed with MeOH (100 ml) and CH_3CO_2H (200 ml) to give **7** as a pale brown solid

(8.70 g, 41%). m.p. 187-189 °C. ^{1}H NMR (400 MHz, $CDCl_3$) δ 3.87 (s, 6H), 3.88 (s, 3H), 4.12 (s, 3H), (total 12H, 4 × OCH_3), 4.26 (s, 2H, CH_2), 6.11 (s, 2H, benzene-H), 7.06 (d, 1H, J 15.6, SO_2CH=CH), 7.80 (d, 1H, J 15.6, SO_2CH=CH), 8.34 (d, 1H, J 2.4, pyridine-H), 8.40 (d, 1H, J 2.0, pyridine-H). ^{13}C NMR (100 MHz, DMSO-d_6) δ 55.3, 56.1, 56.5, 91.2, 91.4, 102.8, 120.0, 122.7, 133.3, 135.3, 137.0, 154.1, 156.0, 161.5, 164.5 (three carbon signals overlapping or obscured). HRMS (ESI) m/z 425.1146 $[M+H]^+$; calcd. for $C_{18}H_{21}N_2O_8S$ $[M+H]^+$ 425.1013. Anal. RP-HPLC: t_R 13.24 min, purity > 97% (method A); t_R 11.18 min, purity > 98% (method B).

(E)-2-Methoxy-5-(((2,4,6-trimethoxystyryl)sulfonyl)methyl)pyridin-3-amine (8).

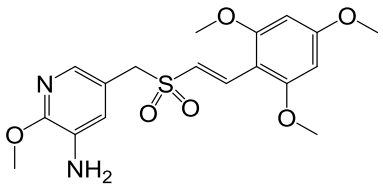

To a solution of compound **7** (5.00 g, 11.8 mmol) in MeOH/CH_3COOH (3:4, 350 ml) was added iron powder (5.24 g, 93.8 mmol). The reaction mixture was heated at 50 °C for 3 h under N_2 and concentrated under reduced pressure. The residue was dissolved in CH_2Cl_2 (200 ml), and 1 M NaOH (100 ml) was added. The precipitate was removed by centrifugation. The aqueous layer was separated and extracted with CH_2Cl_2 (2 × 100 ml). The organic layer and extracts were combined, dried over $MgSO_4$ and concentrated under reduced pressure. The residue was washed with EtOAc (200 ml) to give **8** as a white solid (3.15 g, 68%). m.p. 170-172 °C. ^{1}H NMR (500 MHz, DMSO-d_6) δ 3.84 (s, 3H), 3.85 (s, 3H), 3.86 (s, 6H) (total 12H, 4 × OCH_3), 4.27 (s, 2H, CH_2), 5.04 (s, 2H, NH_2) 6.30 (s, 2H, benzene-H), 6.88 (s, 1H, pyridine-H), 7.09 (d, 1H, J 15.5, SO_2CH=CH), 7.28 (s, 1H, pyridine-H), 7.57 (d, 1H, J 15.5,

$SO_2CH=CH$). ^{13}C NMR (125 MHz, DMSO-d_6) δ 53.4, 56.1, 56.6, 57.8, 91.4, 103.0, 119.0, 121.2, 123.9, 132.5, 133.5, 134.8, 152.3, 161.4, 164.1 (three carbon signals overlapping or obscured). HRMS (ESI) m/z 395.1250 $[M+H]^+$; calcd. for $C_{18}H_{23}N_2O_6S$ $[M+H]^+$ 395.1271. Anal. RP-HPLC: t_R 12.69 min, purity > 98% (method A); t_R 10.35 min, purity > 98% (method B).

(E)-N-(2-Methoxy-5-(((2,4,6-trimethoxystyryl)sulfonyl)methyl)pyridin-3-yl)methanesulfonamide (9a).

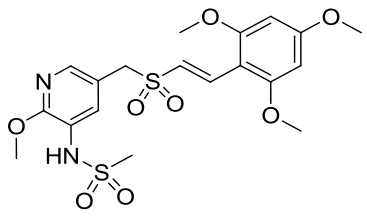

To a solution of compound **8** (1.00 g, 2.54 mmol) in anhydrous pyridine (25 ml) at 0 °C was added dropwise methanesulfonyl chloride (400 µl, 5.17 mmol). The reaction mixture was stirred at room temperature for 13 h and concentrated under reduced pressure. The residue was dissolved in CH_2Cl_2 (150 ml) and washed with H_2O (3 × 30 ml). The organic phase was concentrated under reduced pressure, and the residue was purified by an Isolera Four automated flash chromatography system using a 50 g KP-SIL SNAP flash cartridge (silica gel, EtOAc:hexane = 0:100 ramping to 100:0) to give **9a** as a white solid (0.914 g, 76%). m.p. 211-212 °C. ^1H NMR (500 MHz, DMSO-d_6) δ 2.96 (s, 3H, SO_2CH_3), 3.85 (s, 3H), 3.86 (s, 6H), 3.90 (s, 3H) (total 12H, 4 × OCH_3), 4.47 (s, 2H, CH_2), 6.29 (s, 2H, benzene-H), 7.12 (d, 1H, J 15.5, $SO_2CH=CH$), 7.54 (d, 1H, J 15.5, $SO_2CH=CH$), 7.65 (d, 1H, J 2.5, pyridine-H), 7.91 (d, 1H, J 2.0, pyridine-H), 9.25 (s, 1H, $NHSO_2$). ^{13}C NMR (100 MHz, acetone-d_6) δ 38.8, 53.3, 55.1, 55.5, 57.4, 90.7, 103.2, 119.4, 121.7, 123.2, 130.2, 134.7, 143.7, 154.1, 161.5, 164.3 (three carbon signals overlapping or obscured).

HRMS (ESI) m/z 473.1115 $[M+H]^+$; calcd. for $C_{19}H_{25}N_2O_8S_2$ $[M+H]^+$ 473.1047. Anal. RP-HPLC: t_R 12.74 min, purity > 98% (method A); t_R 10.16 min, purity > 97% (method B).

(E)-N-(2-Methoxy-5-(((2,4,6-trimethoxystyryl)sulfonyl)methyl)pyridin-3-yl)acetamide (9b).

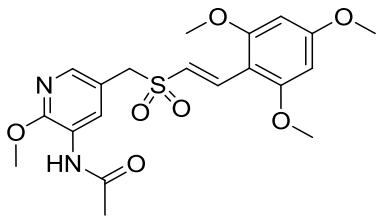

To a solution of compound **8** (240 mg, 0.608 mmol) in anhydrous pyridine (10 ml) at 0 ºC was added dropwise acetyl chloride (110 µl, 1.55 mmol). The reaction mixture was stirred at room temperature for 12 h and concentrated under reduced pressure. The residue was acidified to pH ~ 6-7 with 2 M HCl and extracted with CH_2Cl_2 (2 × 10 ml). The organic extracts were combined, washed with saturated Na_2CO_3 (10 ml) and brine (10 ml), dried over $MgSO_4$ and concnetrated under reduced pressure. The residue was purified by flash column chromatography (silica gel, EtOAc:petroleum ether = 3:1) to give **9b** as a white solid (114 mg, 43%). m.p. 190-192 °C. ^{1}H NMR (400 MHz, $CDCl_3$) δ 2.21 (s, 3H, $NHCOCH_3$), 3.86 (s, 6H), 3.87 (s, 3H), 4.03 (s, 3H) (total 12H, 4 × OCH_3), 4.21 (s, 2H, CH_2), 6.11 (s, 2H, benzene-H), 7.13 (d, 1H, J 15.6, SO_2CH=CH), 7.61 (s, 1H, NHCO), 7.88 (d, 1H, J 15.6, SO_2CH=CH), 7.89 (d, 1H, J 2.0, pyridine-H), 8.65 (d, 1H, J 2.0, pyridine-H). ^{13}C NMR (100 MHz, $CDCl_3$) δ 24.8, 54.0, 55.5, 55.8, 58.8, 90.3, 103.8, 118.3, 122.3, 122.5, 128.8, 136.1, 142.0, 152.9, 161.6, 163.9, 168.6 (three carbon signals overlapping or obscured). HRMS (ESI) m/z 437.1460 $[M+H]^+$; calcd. for $C_{20}H_{25}N_2O_7S$

$[M+H]^+$ 437.1377. Anal. RP-HPLC: t_R 12.53 min, purity > 99% (method C); t_R 13.52 min, purity > 96% (method D).

(E)-N-Ethyl-N-(2-methoxy-5-(((2,4,6-trimethoxystyryl)sulfonyl)methyl)pyridin-3-yl)acetamide (9c).

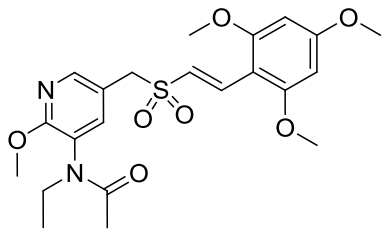

To a solution of compound **9b** (50 mg, 0.11 mmol) in anhydrous DMF (10 ml) was added NaH (0.60 mg, 0.025 mmol). The reaction mixture was stirred at room temperature for 45 min. Iodoethane (60 µL, 0.75 mmol) was added dropwise. The reaction mixture was stirred at room temperature for 3.5 h, dilute with H_2O (10 ml) and extracted with CH_2Cl_2 (2 × 20 ml). The organic extracts was combined, washed with brine (10 ml), dried over $MgSO_4$ and concentrated under reduced pressure. The residue was purified by flash column chromatography (silica gel, EtOAc:petroleum ether = 1:1) to give **9c** as a white solid (37 mg, 70 %). m.p. 168-171 °C. ^{1}H NMR (400 MHz, $CDCl_3$) δ 0.99 (t, 3H, J 7.2, CH_2CH_3), 1.71 (s, 3H, $COCH_3$), 3.39 (m,1H, CH_2CH_3), 3.80 (m,1H, CH_2CH_3), 3.81 (s, 6H), 3.84 (s, 3H), 3.96 (s, 3H) (total 12H, 4 × OCH_3), 4.20 (s, 2H, pyridine-CH_2SO_2), 6.07 (s, 2H, benzene-H), 7.04 (d, 1H, J 15.6, SO_2CH=CH), 7.48 (d, 1H, J 2.0, pyridine-H), 7.74 (d, 1H, J 15.6, SO_2CH=CH), 8.13 (d, 1H, J 2.0, pyridine-H). ^{13}C NMR (100 MHz, $CDCl_3$) δ 12.9, 22.2, 42.5, 54.1, 55.5, 55.8, 57.9, 90.4, 103.6, 118.6, 121.4, 125.6, 136.9, 140.4, 148.2, 160.2, 161.6, 164.2, 170.4 (three carbon signals overlapping). HRMS (ESI) m/z 465.1393 $[M+H]^+$; calcd. for $C_{22}H_{29}N_2O_7S$ $[M+H]^+$

465.1690. Anal. RP-HPLC: t_R 12.80 min, purity > 99% (method C); t_R 15.47 min, purity > 97% (method D).

(E)-Ethyl 2-((2-methoxy-5-(((2,4,6-trimethoxystyryl)sulfonyl)methyl)pyridin-3-yl)amino)acetate (9d).

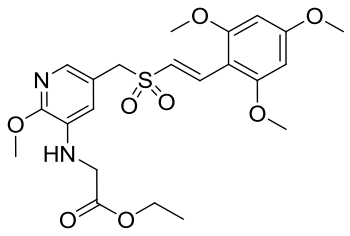

To a solution of compound **8** (140 mg, 0.355 mmol) in DMF (10 ml) were added ethyl bromoacetate (110 μl, 0.995 mmol) and K_2CO_3 (138 mg, 0.999 mmol). The reaction mixture was heated at 60 °C overnight, diluted with H_2O (20 ml) and extracted with EtOAc (2 × 20 ml). The organic extracts were combined, washed with brine (10 ml), dried over $MgSO_4$ and concentrated under reduced pressure. The residue was purified by flash column chromatography (silica gel, EtOAc:petroleum ether = 3:2) to give **9d** as a white solid (124 mg, 73%). m.p. 151-153 °C. ^{1}H NMR (400 MHz, $CDCl_3$) δ 1.33 (t, 3H, J 7.0, CH_2CH_3), 3.85 (s, 6H), 3.87 (s, 3H) (total 9H, 3 × OCH_3), 3.90 (d, 2H, J 2.8, $NHCH_2$), 4.00 (s, 3H, OCH_3), 4.15 (s, 2H, pyridine-CH_2SO_2), 4.27 (q, 2H, J 7.2, CH_2CH_3), 4.83 (d, 1H, J 5.8, $NHCH_2$), 6.10 (s, 2H, benzene-H), 6.74 (d, 1H, J 2.0, pyridine-H), 7.04 (d, 1H, J 15.6, SO_2CH=CH), 7.44 (d, 1H, J 2.0, pyridine-H), 7.81 (d, 1H, J 15.6, SO_2CH=CH). ^{13}C NMR (100 MHz, $CDCl_3$) δ 14.2, 44.9, 55.4, 55.7, 59.2, 61.5, 90.4, 103.8, 116.8, 118.5, 122.3, 131.8, 135.1, 136.0, 152.7, 161.5, 163.9, 170.4 (four carbon signals overlapping or obscured). HRMS (ESI) m/z 481.1364 $[M+H]^+$; calcd. for $C_{22}H_{29}N_2O_8S$ $[M+H]^+$ 481.1639. Anal. RP-HPLC: t_R 13.09 min, purity > 95% (method C); t_R 14.80 min, purity > 95% (method D).

(E)-2-((2-Methoxy-5-(((2,4,6-trimethoxystyryl)sulfonyl)methyl)pyridin-3-yl)amino)acetic acid (9e).

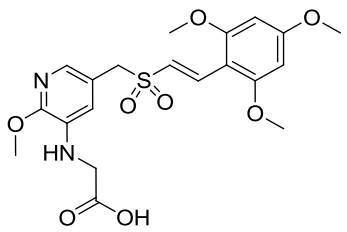

To a solution of compound **9d** (114 mg, 0.237 mmol) in THF (10 ml) was added a solution of NaOH (10.0 mg, 0.250 mmol) in H_2O (10 ml). The reaction mixture was stirred at room temperature for 1 h, acidified to pH = 1 - 2 with 2 M HCl and extracted with EtOAc (3 × 10 ml). The organic extracts were combined, washed with brine (10 ml), dried over $MgSO_4$ and concentrated under reduced pressure. The residue was purified by flash column chromatography (silica gel, EtOAc:petroleum ether = 3:2 to EtOAc:MeOH = 5:1) . The resulting solid was further washed with Acetone and dried to give **9e** as a white solid (74.5 mg, 69.5%). m.p. 79-81 °C. ^{1}H NMR (400 MHz, DMSO-d_6) δ 3.72 (s, 2H, $NHCH_2$), 3.84 (s, 3H), 3.85 (s, 6H), 3.88 (s, 3H) (total 12H, 4 × OCH_3), 4.31 (s, 2H, pyridine-CH_2SO_2), 5.33 (br s, 1H, $NHCH_2$), 6.29 (s, 2H, benzene-H), 6.65 (d, 1H, J 1.6, pyridine-H), 7.11 (d, 1H, J 15.6, SO_2CH=CH), 7.34 (d, 1H, J 1.6, pyridine-H), 7.54 (d, 1H, J 15.6, SO_2CH=CH). ^{13}C NMR (100 MHz, DMSO-d_6) δ 44.4, 53.6, 55.4, 56.1, 56.5, 91.4, 103.0, 117.2, 119.2, 123.8, 132.2, 133.8, 134.6, 152.1, 161.4, 164.2, 172.2 (three carbon signals overlapping or obscured). HRMS (ESI) m/z 451.1245 $[M-H]^-$; calcd. for $C_{20}H_{23}N_2O_8S$ $[M-H]^-$ 451.1181. Anal. RP-HPLC: t_R 12.52 min, purity > 98% (method C); t_R 13.30 min, purity > 98% (method D).

(E)-2-((2-Methoxy-5-(((2,4,6-trimethoxystyryl)sulfonyl)methyl)pyridin-3-yl)amino)acetamide (9f).

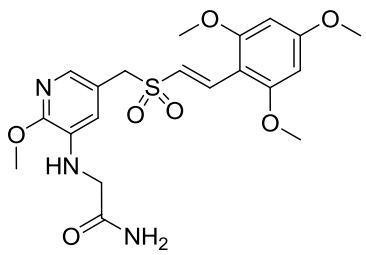

To a solution of compound **9d** (118 mg, 0.246 mmol) in H_2O (5 ml) was added ammonia (7 M in MeOH, 8.00 ml, 56.0 mmol). The reaction mixture was heated at 60 °C overnight and concentrated under reduced pressure. The residue was purified by flash column chromatography (silica gel, EtOAc:petroleum ether = 1:1) to give **9f** as a brown solid (115 mg, 97%). m.p. 211-213 °C. ^{1}H NMR (400 MHz, DMSO-d_6) δ 3.56 (d, 2H, J 5.6, $NHCH_2$), 3.84 (s, 3H), 3.85 (s, 6H), 3.87 (s, 3H) (total 12H, 4 × OCH_3), 4.32 (s, 2H, pyridine-CH_2SO_2), 5.38 (t, 1H, J 5.4, $NHCH_2$), 6.29 (s, 2H, benzene-H), 6.61 (d, 1H, J 2.0, pyridne-H), 7.10 (d, 1H, J 15.6, SO_2CH=CH), 7.31 (m, 2H, NH_2), 7.34 (d, 1H, J 2.0, pyridine-H), 7.55 (d, 1H, J 15.6, SO_2CH=CH). ^{13}C NMR (100 MHz, DMSO-d_6) δ 45.8, 53.6, 56.1, 56.5, 57.9, 91.4, 103.0, 117.1, 119.2, 123.7, 132.4, 133.8, 134.6, 152.3, 161.4, 164.2, 171.5 (three carbon signals overlapping or obscured). HRMS (ESI) m/z 452.1560 $[M+H]^+$; calcd. for $C_{20}H_{26}N_3O_7S$ $[M+H]^+$ 452.1486. Anal. RP-HPLC: t_R 12.19 min, purity > 98%(method C); t_R 12.67 min, purity > 97% (method D).

2-Methoxy-5-(1-(methylsulfonyl)-2-(piperidin-1-yl)-2-(2,4,6-trimethoxyphenyl)ethyl)-3-nitropyridine (10).

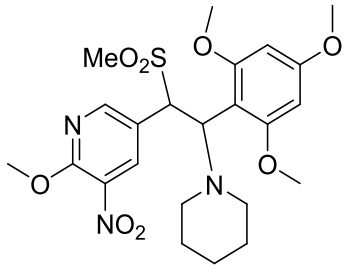

To a solution of compound **6** (2.03 g, 6.99 mmol) in anhydrous pyridine (20 ml) were added 2,4,6-trimethoxybenzaldehyde (1.37 g, 6.98 mmol) and piperidine (500 µl, 5.06 mmol). The reaction mixture was heated at reflux for 3 h under N_2, cooled to room temperature and concentrated under reduced pressure. The residue was acidified to pH ~ 7 with 2 M HCl and extracted with CH_2Cl_2 (2 × 50 ml). The organic extracts were combined, washed with saturated Na_2CO_3 (30 ml) and brine (30 ml), dried over $MgSO_4$ and concentrated under reduced pressure. The residue was purified by flash column chromatography (silica gel, EtOAc:CH_2Cl_2:petroleum ether = 1:2:8) to give **10** as a white solid (1.02 g, 29%). m.p. 198-200 °C. ^{1}H NMR (400 MHz, $CDCl_3$) δ 1.30 (s, 2H, piperidine-H), 1.48-1.57 (m, 5H, piperidine-H), 2.55 (br d, 3H, J 96.0, piperidine-H), 3.45 (s, 3H, SO_2CH_3), 3.61 (s, 3H), 3.70 (s, 3H), 3.83 (s, 3H), 3.98 (s, 3H) (total 12H, 4 × OCH_3), 5.10 (d, 1H, J 12.0) , 5.37 (d, 1H, J 12.0) (total 2H, pyridine-CHCH-benzene), 5.78 (d, 1H, J 2.0, benzene-H), 6.03 (d, 1H, J 2.0, benzene-H), 8.11 (d, 1H, J 2.4, pyridine-H), 8.15 (d, 1H, J 2.4, pyridine-H). ^{13}C NMR (100 MHz, DMSO-d_6) δ 24.3, 26.5, 44.6, 55.0, 55.1, 55.2, 56.0, 59.4, 102.7, 120.9, 156.4, 159.2, 159.8, 161.0 (nine carbon signals overlapping or obscured). HRMS (ESI) m/z 510.1417 $[M+H]^+$; calcd. for $C_{23}H_{32}N_3O_8S$ $[M+H]^+$ 510.1905. Anal. RP-HPLC: t_R 11.62 min, purity > 95% (method C); t_R 12.22 min, purity > 99% (method D).

7.2 General biology procedures

7.2.1 Materials

MTT assay

MTT Sigma-aldrich (cat: M2128-1G); DMSO Sigma-aldrich (cat: D5879-1L).

Cell cycle analysis

Buffers and Solutions: Hypotonic Fluorochrome solution (0.1% sodium citrate; 0.1% Triton X-100; 50 μg/ml propidium iodide; 100ug/ml RNAseA in dH_2O)

Annexin V/PI staining assay

Reagents: FITC Annexin V (BD Biosciences, cat: 556420); propidium iodide (Sigma, cat: P4170)

Buffers and Solutions: 10 × binding buffer (0.1 M HEPES, Ph 7.4; 1.3 M NaCl; 25 mM $CaCl_2$); propidium iodide solution (50 μg/ml in PBS).

Western blot analysis

Reagents: PageRuler Plus Prestained Protein Ladder (Thermo, cat: #26619); Immun-Blot PVDF Membrane (Bio-Rad, cat: #162-0177); Empty Gel Cassettes, mini, 1.5 mm (Invitrogen, cat: NC2015); Albumin from bovine serum (BSA) (Sigma, cat: A4503); DC™ Protein Assay Reagent A/B/S (Bio-Rad, cat: 500-0113/0114/0115); Acrylamide/Bis-acrylamide, 30% solution (Sigma, cat: A3699); Triton-X 100 (Sigma, cat: X100); Ammonium persulfate (AMPS); N,N,N',N'-Tetramethylethylenediamine (TEMED); Complete Mini protease inhibitor cocktail tablet (Roche, cat: 04693159001); PhosSTOP Phosphatase Inhibitor Cocktail Tablets (Roche, cat: 04906845001); Amersham ECL Western Blotting Detection Reagents (GE Healthcare, cat: RPN2106); Amersham Hyperfilm ECL (GE Healthcare, cat: 28906837).

Table 7.1 Buffers and Solutions

Gel	For a 10 ml separating gel					For a 5 ml stacking gel
Acrylamide percentage	6%	8%	10%	12%	15%	-
dH_2O	5.2 ml	4.6 ml	3.8 ml	3.2 ml	2.2 ml	3.4 ml
30% Acrylamide/Bis-acrylamide	2 ml	2.6 ml	3.4 ml	4 ml	5 ml	0.83 ml
1.5 M Tris-HCl (pH 8.8)	2.6 ml	2.6 ml	2.6 ml	2.6 ml	2.6 ml	
0.5 M Tris-HCl (pH 6.8)						0.63 ml
10% sodium dodecyl sulfate (SDS)	100 µl	100 µl	100 µl	100 µl	100 µl	50 µl
10% ammonium persulfate (APS)	100 µl	100 µl	100 µl	100 µl	100 µl	50 µl
TEMED	8 µl	6 µl	4 µl	4 µl	4 µl	5 µl

Running buffer 1L (3.03g Trizma Base, 14.4 g glycine, 1 g SDS); Transfer buffer 1L (3.03 g Trizma Base, 14.4 g glycine, 0.375 g SDS, 200 ml methanol, pH 7.6); TBST 1L (8 g NaCl, 2.42 g Trizma Base pH 7.6, 0.05% Tween 20); 4 × Loading buffer 10 ml (4 ml 100% glycerol, 2.4 ml 1 M Tris-HCl pH 6.8, 0.8 g SDS, 4 mg bromophenol blue, 0.5 ml ß-mercaptoethanol, 3.1 ml water); NP40 Cell Lysis Buffer (150 mM NaCl, 1.0% Triton X-100, 0.1% SDS, 50 mM Tris-HCl pH 8.0, a tablet of Protease Inhibitor and Phosphatase Inhibitor);

Stripping buffer 100 ml (0.76 g Trizma base, 2 g SDS, 0.7 ml β-mercaptoethanol).

Table 7.2 Antibodies

Antibody	Dilution	Storage	Company	Cat.
Phospho-Akt Pathway Antibody Sampler Kit	1:1000	-20 °C	Cell signaling	#9916
mTOR Substrates Antibody Sampler Kit	1:1000	-20 °C	Cell signaling	#9862
Bcl-xl	1:1000	-20 °C	Sigma	B9429
Bax	1:1000	-20 °C	Cell signaling	#2772
Bid	1:1000	-20 °C	Cell signaling	#2002
Cdc25c	1:1000	-20 °C	Cell signaling	#4688
Phospho-Cdc25c (S198)	1:1000	-20 °C	Cell signaling	#9529
cyclin B1	1:1000	-20 °C	Cell signaling	#4135
cyclin D1	1:1000	-20 °C	Cell signaling	#2922
Mcl-1	1:1000	-20 °C	Cell signaling	#4572
γ-H2AX	1:2000	4 °C	Millipore	#05-636
PARP	1:1000	-20 °C	Cell signaling	#9542
β-actin	1:4000	-20 °C	Cell signaling	#4970
goat anti-mouse IgG	1:4000	4 °C	Dako	P0447
goat anti-rabbit IgG	1:4000	4 °C	Dako	P0448

Tubulin polymerization assay

Tubulin Polymerization HTS Assay Kit (Cytoskeleton, cat: BK004P)

Immunofluorescence microscopy

Reagents: phosphate buffered saline (PBS) (Sigma, cat: P4417); Formaldehyde solution, 37% in H_2O (Sigma, cat: F8775); Monoclonal Anti-α-Tubulin−FITC antibody produced in mouse (Sigma, cat: F2168); Alexa Fluor® 488 Goat Anti-Mouse IgG (H+L) Antibody (Invitrogen, cat: #A-11029).

Buffers and Solutions: 1 × Wash Buffer 100 ml (10 ml 10 × Wash Buffer, 90 ml dH_2O); Fixation Solution 12 ml (1.2 ml 37% formaldehyde, 10.8 ml 1 × Wash Buffer); 1 × Blocking Buffer 100 ml (10 ml 10 × Blocking Buffer, 90 ml dH_2O); 1 × Permeabilization Buffer 20 ml (2 ml 10 × Permeabilization buffer, 18 ml dH_2O); Primary Antibody Solution 6 ml (15 µl Mitotic Index Primary Antibody, 6 ml 1 × Blocking Buffer); Staining Solution 6 ml (12 µl Secondary Antibody, 0.3 µl Hoechst Dye, 6 ml 1 × Blocking Buffer).

Caspase 3/7 assay

Apo-ONE® Homogeneous Caspase-3/7 Assay (Promega G7790)

7.2.2 Methods

7.2.2.1 General cell culture

All cell lines were obtained from the American Type Tissue Culture Collection (ATCC), expanded and stored in the liquid nitrogen cell bank at the Centre for Biomolecular Sciences, University of Nottingham, UK. All cancer cell lines were maintained in RPMI-1640 medium with 10% foetal bovine serum (FBS). The FBS was inactivated by heating at 56 °C for 60 min to denature complement proteins which would evoke cellular immune responses. MRC-5 cell lines were cultured in minimum essential medium with 10% FBS, 1% of 7.5% sodium bicarbonate, 1% 0.1 mM non-essential amino acids, 1% 1 M HEPES, 1% 200 mM L-glutamine and 1% penicillin. Human dermal microvascular endothelial cells (HMEC-1) were maintained in EBM-2 medium with 10% FBS. Human umbilical cord vein endothelial cells (HUVECs) were maintained in EBM-2 medium with 10% FBS and EGM-2. Cells were incubated in a humidified incubator at 37 °C with 5% CO_2.

7.2.2.2 Preparation of compounds solution

The tested compounds were weighed using mini gram scales and were dissolved in DMSO to make up a 10 mM concentration stock solutions which were stored at -20 ^{o}C.

7.2.2.3 MTT cytotoxicity assay (96 h)

MTT assay is a quantitative colorimetric method to determine viable cell number in proliferation and cytotoxicity studies. 3-(4,5-Dimethylthiazol-2-yl)-2,5-diphenyltetrazolium bromide (MTT), a yellow tetrazole, is reduced by mitochondrial succinate dehydrogenase in living cells to its insoluble purple formazan, which could be dissolve by DMSO to produce a colored solution. The absorbance which reflects the amount of living cells can be measured spectrophotometrically.

Day 1: Cells were seeded at 3 x 10^3 per well in a 96 well plates in a volume of 180 µl cell culture medium. 2 additional columns of cells were plated in the T_0 plate for each cell line. All plates were incubated at 37 ^{o}C with 5% CO_2 overnight.

Day 2: T_0 plate was treated with 50 µl MTT solution (2 mg/ml in PBS) per well and then incubated for a further 2-4 h at 37 ^{o}C with 5% CO_2. Following aspiration of media/MTT mixture and addition of 150 µL DMSO per well, the T_0 plate was shaken for 5 min. Absorbance of each well was quantified at 550 nm using a Perkin Elmer plate reader and data were transferred to Microsoft Excel. At the same time, test compounds in 10 mM DMSO stock solution were diluted to a concentration range between 1000 µM and 0.1 µM with medium. For each concentration, 20 µl dilution was added per well in triplicate for each cell line resulting in a dilution range from 100 µM to 0.01 µM.

Day 6: After 96 hours exposure to test agent, to all wells were added 50 µl MTT solution. Plates were analysed in the same manner as the T_0 plate. Each assay was performed at least 2 times for candidate screening and at least 3 times for mechanism studies of lead compounds. All data were transferred to Microsoft Excel. To determine GI_{50} values of test agents (concentration required to 50% growth inhibition), dose-response curves were constructed using nonlinear regression analysis. The mean value and standard deviation of each compound was calculated by Excel.

7.2.2.4 Cell cycle analysis

The analysis of cell cycle distribution was performed by flow cytometric measurement of cellular DNA contents. HCT-116, A2780 and HMEC-1 cells were seeded in 6-well plates at a density of 5×10^5 cells/well and incubated at 37 °C 5% CO_2 overnight. Following incubation with compounds at appropriate concentrations and time points, the cells were collected with the medium in a FACS tube and centrifuged at 1200 rpm for 5 min at 4 °C. The supernatants were discarded. Cells were washed twice with cold PBS and gently re-suspended in 400 µl of fluorochrome solution. Then, cells were protected from light and stored at 4 °C overnight. Prior to flow cytometric analysis, the cell suspension was syringed to obtain a single cell suspension. DNA content was measured by a Beckman Coulter EPICS-XL MCL™ flow cytometer, and data was analysed using the EXPO32™ software.

7.2.2.5 Annexin V/PI staining assay

AnnexinV/propidium iodide (PI) staining was a commonly used quantitatively method for studying apoptotic cells. HCT-116, A2780 and HMEC-1 cells were seeded in 6-well plates at a density of 4×10^5 per well and incubated at 37 °C 5%

CO_2 overnight. After the appropriate incubation time, cells were collected with the medium in a FACS tube and centrifuged at 1200 rpm for 5 min at 4 °C. The cells were gently re-suspended with 1 ml fresh medium. Then 1 x 10^5 of cells were transferred into a fresh FACS tube. After washing (1 ml PBS), cells were re-suspended in 100 µl binding buffer and 5 µl Annexin V-FITC. After 15 min incubation in the dark at room temperature, samples were added with 400 µl binding buffer, together with 5 µl PI. Samples were kept on ice and protected from light for a further 10 min and analysed using FACS after vortex within 1 h.

7.2.2.6 Mitotic index assay

Mitotic index is a measure of the proliferation status of a cell population. It is defined as the ratio between the number of cells in mitosis and the total number of cells. HCT-116 cells were seeded at the density of 1 × 10^4 cells/well in Packard ViewPlate black clear bottom 96-well microtitre plates. After the appropriate incubation time with compounds at 37 °C and 5% CO_2, the medium was removed. Followed by 10 min fixation in 100 µl of fixation solution at 37 °C, cells were washed once with 100 µl/well of 1 × blocking buffer and subsequently permeabilized in 100 µl of 1 × permeabilization buffer for 15 min. After washing, cells were incubated with 50 µl/well primary antibody solution for 1 h, and then with staining solution for another 1 h. Fluorescence was measured at 460 nm at room temperature using a Leica DMIRE2 fluorescence microscope to calculate the mitotic index which is the percentage of cell nuclei stained with the mitosis-specific antibody (anti-phospho-Histone H3) versus total cell nuclei stained with Hoechst. Vinblastine (0.5 µM) was used as a positive control and DMSO (0.2%) was used as a negative control. Assays were carried out using duplicate plates.

7.2.2.7 Caspase-3/7 assay

Caspase activity was determined using the Apo-ONE® Homogeneous Caspase-3/7 Assay (Promega G7790), following the manufacturer's instructions. Fluorescence was measured at 460 nm at room temperature using an EnVision multilabel plate reader (PerkinElmer).

7.2.2.8 Western blot analysis

Western Blot analyses were performed in a standard manner. Following separation by polyacrylamide gel electrophoresis, the proteins were electro transferred to membranes and detected with specific antibodies.

7.2.2.8.1 Cell lysate preparation

Cells were seeded at a density of 10^6 on a 10 cm tissue culture plate and incubated at 37 °C 5% CO_2 overnight. After treatment with compounds at appropriate concentrations and time points, the cells were collected with the medium and centrifuged at 1200 rpm for 5 min, 4 °C. The pellet was washed with ice-cold PBS and re-suspended in lysis buffer (containing Protease Inhibitor and Phosphatase Inhibitor) for 30 min at 4 °C. Cell lysates were centrifuged (13000 rpm, 4 °C, 10 min) to remove insoluble proteins and cell debris.

7.2.2.8.2 Protein determination

A Bradford assay was performed to determine the protein content in the lysates using the Bio-Rad DC protein assay. Firstly, the protein was diluted 1:10 in water and left on ice. Cell lysates were then stored at -20 °C temporarily for later use. BSA protein standards were prepared at a concentration range of 10, 5, 2.5, 2, 1.5, 1, 0.75, 0 mg/ml BSA with RIPA buffer. 5 µl of each of the BSA

standards or protein was pipetted in a 96-well plate with 3 replicates of each sample. Then 200 µl of Bradford reagent was added to each well and mixed gently to avoid any bubbles. After 15-20 min incubation at room temperature, absorbance of each well was quantified at 595 nm using a Perkin Elmer plate reader and data was transferred to Microsoft Excel. A standard curve was plotted to determine the protein concentrations.

7.2.2.8.3 Gel electrophoresis

Proteins were separated using gel electrophoresis. SDS denatures proteins by negatively charging the polypeptides in proportion to their length once they have been treated with strong reducing agents. In denaturing SDS-PAGE (SDS polyacrylamide gel electrophoresis), therefore, proteins are separated according to their molecular weight. Depending on the molecular weight of the protein of interest, different concentrations of acrylamide were used in the gels (6-15%). In a gel cassette, polymerization was initiated when AMPS and TEMED were added to the separating buffer. Once the separating gel had polymerized, stacking gel buffer with AMPS and TEMED was added. Simultaneously, a comb was placed on the top of the cassette to create sample wells.

Cell lysate samples were prepared containing 50-100 µg total protein depending on cell lines. Along with loading buffer, samples were denatured at 95 °C for 5-10 min and subsequently loaded into narrow wells using special gel loading tips. PageRuler Plus Prestained Protein Ladder (5 µl) was added to the first well for determination of the protein size and also to monitor the progress of the electrophoretic run. Protein samples were separated at a voltage between 60-180 V in running buffer until the migration front reaches the bottom of the gel. The gel was then removed from cassettes.

7.2.2.8.4 Transfer of proteins and staining (Western blotting)

Proteins separated by SDS-PAGE in gels were electro-transferred onto PVDF membranes using transfer buffer in semi-dry conditions (at 25 V for 1.5 h). The membranes were washed using 20 ml of 1x PBS and then blocked with either 5% BSA or 10% dried non-fat milk (dependant on primary antibodies) in TBST for 1 h at room temperature with gentle shaking. All primary and secondary antibodies used are shown in Table 7.2 with corresponding concentrations used for the Western blot. Membranes were incubated with primary antibody overnight at 4 °C with agitation. To remove residual primary antibody, the membranes were washed 3 times in TBST while shaking, 5-10 min per wash. Membranes were next incubated with appropriate HRP-conjugated secondary antibodies for 1 h at room temperature, and rinsed again with TBST.

7.2.2.8.5 Detection

All blots were visualized using enhanced chemiluminescence according to the manufacturer's instruction. Following the procedures in the manufacturer's instruction of Amersham™ ECL™ Western Blotting Detection Reagents, membranes were exposed to X-ray films in the dark for appropriate exposure times. Films were developed manually.

7.2.2.9 Tubulin polymerization assay

The Tubulin Polymerization HTS Assay Kit from Cytoskeleton was used according to the manufacturer's protocol. The kit-based assay is an adaptation of a method[202], where polymerization is monitored by optical density enhancement as it occurs. Briefly, test compounds and their corresponding vehicles were pipetted into a 96-well microtiter plate, then tubulin reaction mixture was quickly added to the wells, and tubulin polymerization was

initiated and monitored at 37 °C for 1 h by recording fluorescence absorbance at 340 nm. The tubulin reaction mixture was composed of 80 mM PIPES (pH 6.9), 1 mM $MgCl_2$, 1 mM EGTA, 1.0 mM GTP and 2 mg/ml of highly purified porcine brain tubulin heterodimer.

7.2.2.10 Immunofluorescence microscopy

HCT-116 cells were cultured at a density of 2×10^3 cells/well to the 6 cell-plates containing gelatin-coated coverslips. After appropriate concentrations and time points of treatments, the coverslips were washed twice with PBS and transferred into a petri dish with two sheets of moistened filter pater. Cells were fixed in 3.7% formaldehyde for 15 min and washed briefly in PBS. Excess PBS was removed by touching to dry filter paper. Then, cells were permeabilized with 0.3% Triton-X 100 in PBS for 5 min. To block non-specific binding sites, cells were incubated with blocking buffer for 45 min at room temperature. Fixed cells were incubated with anti-mouse α-tubulin antibody (1: 50 dilution) for 2 h at room temperature, and then exposed to the secondary antibody (FITC-conjugated goat anti-mouse IgG at 1:100 dilution) for 2 h at room temperature in the dark, followed by DNA staining with Hoechst. Photomicrographs were obtained using a Leica TCS SP2 Confocal Spectral Microscope.

7.2.2.11 Statistical analysis

All experiments were performed in triplicate and repeated at least twice. Similar results were obtained and representative experiments were selected for figures. Student's t-test for paired sample was used to determine statistical significance. $P \leq 0.05$ was considered to be statistically significant.

8 References

1. CRUK, Vol. 2014 (Cancer Research UK, 2014).
2. Harrington, K.J. Biology of cancer. Medicine **39**, 689-692 (2011).
3. Weston, A. & Harris, C.C. Chemical Carcinogenesis, in Holland-Frei Cancer Medicine, Edn. 6th edition. (eds. D.W. Kufe et al.) (Hamilton (ON): BC Decker, 2003).
4. Workman, P. Drugging the cancer kinome: progress and challenges in developing personalized molecular cancer therapeutics. Cold Spring Harb Symp Quant Biol **70**, 499-515 (2005).
5. Lazebnik, Y. What are the hallmarks of cancer? Nat Rev Cancer **10**, 232-233 (2010).
6. Hanahan, D. & Weinberg, R.A. The hallmarks of cancer. Cell **100**, 57-70 (2000).
7. Hanahan, D. & Weinberg, R.A. Hallmarks of cancer: the next generation. Cell **144**, 646-674 (2011).
8. Campisi, J. Cancer and ageing: rival demons? Nat Rev Cancer **3**, 339-349 (2003).
9. Sherr, C.J. & McCormick, F. The RB and p53 pathways in cancer. Cancer Cell **2**, 103-112 (2002).
10. Cory, S. & Adams, J.M. The Bcl2 family: regulators of the cellular life-or-death switch. Nat Rev Cancer **2**, 647-656 (2002).
11. Adams, J.M. & Cory, S. The Bcl-2 apoptotic switch in cancer development and therapy. Oncogene **26**, 1324-1337 (2007).
12. Lowe, S.W., Cepero, E. & Evan, G. Intrinsic tumour suppression. Nature **432**, 307-315 (2004).
13. Shay, J.W. & Wright, W.E. Hayflick, his limit, and cellular ageing. Nat Rev Mol Cell Biol **1**, 72-76 (2000).

14. Cong, Y.S., Wright, W.E. & Shay, J.W. Human telomerase and its regulation. Microbiol Mol Biol Rev **66**, 407-425, table of contents (2002).

15. Blasco, M.A. Telomeres and human disease: ageing, cancer and beyond. Nat Rev Genet **6**, 611-622 (2005).

16. Hahn, W.C. et al. Creation of human tumour cells with defined genetic elements. Nature **400**, 464-468 (1999).

17. Plank, M.J. & Sleeman, B.D. Tumour-induced Angiogenesis: A Review. Journal of Theoretical Medicine **5**, 137–153 (2003).

18. Joyce, J.A. & Pollard, J.W. Microenvironmental regulation of metastasis. Nat Rev Cancer **9**, 239-252 (2009).

19. Talmadge, J.E. & Fidler, I.J. AACR centennial series: the biology of cancer metastasis: historical perspective. Cancer Res **70**, 5649-5669 (2010).

20. WARBURG, O. On the origin of cancer cells. Science **123**, 309-314 (1956).

21. Deshpande, A., Sicinski, P. & Hinds, P.W. Cyclins and cdks in development and cancer: a perspective. Oncogene **24**, 2909-2915 (2005).

22. Fischer, M.P. Cell cycle inhibitors in cancer: current status and future directions, in Cancer drug design and discovery. (ed. N. Stephen) 253-283 (Academic Press Elsevier Inc., Oxford, UK; 2008).

23. Schwartz, G.K. & Shah, M.A. Targeting the cell cycle: a new approach to cancer therapy. J Clin Oncol **23**, 9408-9421 (2005).

24. Schmidt, M. et al. Molecular alterations after Polo-like kinase 1 mRNA suppression versus pharmacologic inhibition in cancer cells. Mol Cancer Ther **5**, 809-817 (2006).

25. Vermeulen, K., Van Bockstaele, D.R. & Berneman, Z.N. The cell cycle: a review of regulation, deregulation and therapeutic targets in cancer. Cell Prolif **36**, 131-149 (2003).

26. Sanchez, V., McElroy, A.K. & Spector, D.H. Mechanisms governing maintenance of Cdk1/cyclin B1 kinase activity in cells infected with human cytomegalovirus. J Virol **77**, 13214-13224 (2003).

27. Seki, A., Coppinger, J.A., Jang, C.Y., Yates, J.R. & Fang, G. Bora and the kinase Aurora a cooperatively activate the kinase Plk1 and control mitotic entry. Science **320**, 1655-1658 (2008).

28. Stark, G.R. & Taylor, W.R. Control of the G2/M transition. Mol Biotechnol **32**, 227-248 (2006).

29. Barr, F.A., Sillje, H.H. & Nigg, E.A. Polo-like kinases and the orchestration of cell division. Nat Rev Mol Cell Biol **5**, 429-440 (2004).

30. Niida, H. & Nakanishi, M. DNA damage checkpoints in mammals. Mutagenesis **21**, 3-9 (2006).

31. Musacchio, A. & Salmon, E.D. The spindle-assembly checkpoint in space and time. Nat Rev Mol Cell Biol **8**, 379-393 (2007).

32. Pitts, T.M., Davis, S.L., Eckhardt, S.G. & Bradshaw-Pierce, E.L. Targeting nuclear kinases in cancer: development of cell cycle kinase inhibitors. Pharmacol Ther **142**, 258-269 (2014).

33. Liu, P., Cheng, H., Roberts, T.M. & Zhao, J.J. Targeting the phosphoinositide 3-kinase pathway in cancer. Nat Rev Drug Discov **8**, 627-644 (2009).

34. Carnero, A. Targeting the cell cycle for cancer therapy. Br J Cancer **87**, 129-133 (2002).

35. DiPaola, R.S. To arrest or not to G(2)-M Cell-cycle arrest : commentary re: A. K. Tyagi et al., Silibinin strongly synergizes human prostate carcinoma DU145 cells to doxorubicin-induced growth inhibition, G(2)-M arrest, and apoptosis. Clin. cancer res., 8: 3512-3519, 2002. Clin Cancer Res **8**, 3311-3314 (2002).

36. Hirose, Y., Berger, M.S. & Pieper, R.O. Abrogation of the Chk1-mediated G(2) checkpoint pathway potentiates temozolomide-induced toxicity in a p53-independent manner in human glioblastoma cells. Cancer Res **61**, 5843-5849 (2001).

37. Jackson, J.R. et al. An indolocarbazole inhibitor of human checkpoint kinase (Chk1) abrogates cell cycle arrest caused by DNA damage. Cancer Res **60**, 566-572 (2000).

38. Tyagi, A.K., Singh, R.P., Agarwal, C., Chan, D.C. & Agarwal, R. Silibinin strongly synergizes human prostate carcinoma DU145 cells to doxorubicin-induced growth Inhibition, G2-M arrest, and apoptosis. Clin Cancer Res **8**, 3512-3519 (2002).

39. David J. Matthews, M.E.G. Targeting Protein Kinase for Cancer Therapy, Edn. 1 edition (12 Mar 2010). (Wiley-Blackwell, 2010).

40. Bogoyevitch, M.A. & Fairlie, D.P. A new paradigm for protein kinase inhibition: blocking phosphorylation without directly targeting ATP binding. Drug Discov Today **12**, 622-633 (2007).

41. Rongshi Li, J.A.S. Kinase Inhibitor drugs. (A. John Wiley & Sons, 2009).

42. Manning, G., Whyte, D.B., Martinez, R., Hunter, T. & Sudarsanam, S. The protein kinase complement of the human genome. Science **298**, 1912-1934 (2002).

43. Ubersax, J.A. & Ferrell, J.E. Mechanisms of specificity in protein phosphorylation. Nat Rev Mol Cell Biol **8**, 530-541 (2007).

44. Bossemeyer, D. Protein kinases--structure and function. FEBS Lett **369**, 57-61 (1995).

45. Pellicena, P. & Kuriyan, J. Protein-protein interactions in the allosteric regulation of protein kinases. Curr Opin Struct Biol **16**, 702-709 (2006).

46. Musgrave, I.F. Structure and function of protein kinases and protein phosphatases. IDrugs **1**, 617-619 (1998).

47. Nolen, B., Taylor, S. & Ghosh, G. Regulation of protein kinases; controlling activity through activation segment conformation. Mol Cell **15**, 661-675 (2004).

48. Liu, Y. & Gray, N.S. Rational design of inhibitors that bind to inactive kinase conformations. Nat Chem Biol **2**, 358-364 (2006).

49. Gavrin, L.K. & Saiah, E. Approaches to discover non-ATP site kinase inhibitors. MedChemComm **4**, 41-51 (2013).

50. Karaman, M.W. et al. A quantitative analysis of kinase inhibitor selectivity. Nat Biotechnol **26**, 127-132 (2008).

51. Kirkland, L.O. & McInnes, C. Non-ATP competitive protein kinase inhibitors as anti-tumor therapeutics. Biochem Pharmacol **77**, 1561-1571 (2009).

52. Blanc, J., Geney, R. & Menet, C. Type II kinase inhibitors: an opportunity in cancer for rational design. Anticancer Agents Med Chem **13**, 731-747 (2013).

53. Gumireddy, K. et al. ON01910, a non-ATP-competitive small molecule inhibitor of Plk1, is a potent anticancer agent. Cancer Cell **7**, 275-286 (2005).

54. Workman, P. & Collins, I. Modern cancer drug discovery: integrating targets, technologies and treatments, in Cancer drug design and discovery. (ed. S. Neidle) 3-38 (Academic Press Elsevier Inc., Oxford, UK; 2008).

55. Galluzzi, L., Senovilla, L., Zitvogel, L. & Kroemer, G. The secret ally: immunostimulation by anticancer drugs. Nat Rev Drug Discov **11**, 215-233 (2012).

56. Fischer, J. & Ganellin, C.R. Analogue-based Drug Discovery. (Wiley-VCH, 2006).

57. Hoelder, S., Clarke, P.A. & Workman, P. Discovery of small molecule cancer drugs: successes, challenges and opportunities. Mol Oncol **6**, 155-176 (2012).

58. Hughes, J.P., Rees, S., Kalindjian, S.B. & Philpott, K.L. Principles of early drug discovery. Br J Pharmacol **162**, 1239-1249 (2011).

59. Tobert, J.A. Lovastatin and beyond: the history of the HMG-CoA reductase inhibitors. Nat Rev Drug Discov **2**, 517-526 (2003).

60. Reddy, E.P., Reddy, M. V. Ramana, Bell, Stanley C. in US Patent Publication (Source: USPTO) Vol. US 7598232 B2. (ed. U.P. Publication) 187 (Temple University - Of the Commonwealth System of Higher Education, Onconova Therapeutics, Inc., US; 2009).

61. Reddy, M.V. et al. Discovery of a Clinical Stage Multi-Kinase Inhibitor Sodium (E)-2-{2-Methoxy-5-[(2',4',6'-trimethoxystyrylsulfonyl)methyl]phenylamino} acetate (ON 01910.Na):

Synthesis, Structure-Activity Relationship, and Biological Activity. J Med Chem (2011).

62. Chun, A.W., Cosenza, S.C., Taft, D.R. & Maniar, M. Preclinical pharmacokinetics and in vitro activity of ON 01910.Na, a novel anti-cancer agent. Cancer Chemother Pharmacol **65**, 177-186 (2009).

63. Nuthalapati, S. et al. Preclinical pharmacokinetic and pharmacodynamic evaluation of novel anticancer agents, ON01910.Na (Rigosertib, Estybon) and ON013105, for brain tumor chemotherapy. Pharm Res **29**, 2499-2511 (2012).

64. Jimeno, A. et al. Phase I study of ON 01910.Na, a novel modulator of the Polo-like kinase 1 pathway, in adult patients with solid tumors. J Clin Oncol **26**, 5504-5510 (2008).

65. Schoffski, P. Polo-like kinase (PLK) inhibitors in preclinical and early clinical development in oncology. Oncologist **14**, 559-570 (2009).

66. Olnes, M.J. et al. Directed therapy for patients with myelodysplastic syndromes (MDS) by suppression of cyclin D1 with ON 01910.Na. Leuk Res **36**, 982-989 (2012).

67. onconova Therapeutics, I., Vol. 2014 (2014).

68. Reddy, M.V. et al. Design, synthesis, and biological evaluation of (E)-styrylbenzylsulfones as novel anticancer agents. J Med Chem **51**, 86-100 (2008).

69. Park, I.W., Reddy, M.V., Reddy, E.P. & Groopman, J.E. Evaluation of novel cell cycle inhibitors in mantle cell lymphoma. Oncogene **26**, 5635-5642 (2007).

70. Elaine M Sloand, M.J.O., Naomi Galili, Aarthi Shenoy, Loretta Pfannes, Francois Wilhelm, Barbara Weinstein, Phillip Scheinberg,Jerome E. Groopman, and Azra Raza in 51st ASH Annual Meeting and Exposition (New Orleans, LA; 2009).

71. Silverman, L.R. et al. Clinical activity and safety of the dual pathway inhibitor rigosertib for higher risk myelodysplastic syndromes following DNA methyltransferase inhibitor therapy. Hematol Oncol (2014).

72. onconova Therapeutics, I. in Onconova Announces Results From Phase 3 ONTIME Trial of Rigosertib in Higher Risk Myelodysplastic Syndromes (MDS) (2014).

73. Komrokji, R.S. et al. Phase I clinical trial of oral rigosertib in patients with myelodysplastic syndromes. Br J Haematol **162**, 517-524 (2013).

74. Bowles, D.W. et al. Phase I study of oral rigosertib (ON 01910.Na), a dual inhibitor of the PI3K and Plk1 pathways, in adult patients with advanced solid malignancies. Clin Cancer Res **20**, 1656-1665 (2014).

75. White, M.P., Babayeva, M., Taft, D.R. & Maniar, M. Determination of intestinal permeability of rigosertib (ON 01910.Na, Estybon): correlation with systemic exposure. J Pharm Pharmacol **65**, 960-969 (2013).

76. Jimeno A, H.M., Vol. US20110201675 A1 (The Johns Hopkins University, USA; 2011).

77. Irina Oussenko, J.F.H., E. Premkumar Reddy, Takao Ohnuma in American Association for Cancer Research Annual Meeting (Washington, D.C.; 2010).

78. Prasad, A. et al. Styryl sulfonyl compounds inhibit translation of cyclin D1 in mantle cell lymphoma cells. Oncogene **28**, 1518-1528 (2009).

79. Lowery, D.M., Lim, D. & Yaffe, M.B. Structure and function of Polo-like kinases. Oncogene **24**, 248-259 (2005).

80. Sunkel, C.E. & Glover, D.M. polo, a mitotic mutant of Drosophila displaying abnormal spindle poles. J Cell Sci **89 (Pt 1)**, 25-38 (1988).

81. Strebhardt, K. Multifaceted polo-like kinases: drug targets and antitargets for cancer therapy. Nat Rev Drug Discov **9**, 643-660 (2010).

82. von Schubert, C. & Nigg, E.A. Polo-like kinases. Curr Biol **23**, R225-227 (2013).

83. Elia, A.E. et al. The molecular basis for phosphodependent substrate targeting and regulation of Plks by the Polo-box domain. Cell **115**, 83-95 (2003).

84. Eckerdt, F., Yuan, J. & Strebhardt, K. Polo-like kinases and oncogenesis. Oncogene **24**, 267-276 (2005).

85. Glover, D.M., Hagan, I.M. & Tavares, A.A. Polo-like kinases: a team that plays throughout mitosis. Genes Dev **12**, 3777-3787 (1998).

86. Stewart, H.J., Kishikova, L., Powell, F.L., Wheatley, S.P. & Chevassut, T.J. The polo-like kinase inhibitor BI 2536 exhibits potent activity against malignant plasma cells and represents a novel therapy in multiple myeloma. Exp Hematol **39**, 330-338 (2011).

87. Wang, S. & Fischer, P.M. Cyclin-dependent kinase 9: a key transcriptional regulator and potential drug target in oncology, virology and cardiology. Trends Pharmacol Sci **29**, 302-313 (2008).

88. Yamamoto, Y. et al. Overexpression of polo-like kinase 1 (PLK1) and chromosomal instability in bladder cancer. Oncology **70**, 231-237 (2006).

89. Smith, M.R. et al. Malignant transformation of mammalian cells initiated by constitutive expression of the polo-like kinase. Biochem Biophys Res Commun **234**, 397-405 (1997).

90. Olmos, D., Swanton, C. & de Bono, J. Targeting polo-like kinase: learning too little too late? J Clin Oncol **26**, 5497-5499 (2008).

91. Liu, X. & Erikson, R.L. Polo-like kinase (Plk)1 depletion induces apoptosis in cancer cells. Proc Natl Acad Sci U S A **100**, 5789-5794 (2003).

92. Spankuch, B., Kurunci-Csacsko, E., Kaufmann, M. & Strebhardt, K. Rational combinations of siRNAs targeting Plk1 with breast cancer drugs. Oncogene **26**, 5793-5807 (2007).

93. Liu, X., Lei, M. & Erikson, R.L. Normal cells, but not cancer cells, survive severe Plk1 depletion. Mol Cell Biol **26**, 2093-2108 (2006).

94. Reddy, P.E.R.V., Ramana M. , Vol. United States Patent 6541475 (ed. U. States) (Temple University - Of the Commonwealth System of Higher Education (Philadelphia, PA), United States; 2003).

95. Strebhardt, K. & Ullrich, A. Targeting polo-like kinase 1 for cancer therapy. Nat Rev Cancer **6**, 321-330 (2006).

96. Jimeno, A. et al. Evaluation of the novel mitotic modulator ON 01910.Na in pancreatic cancer and preclinical development of an ex vivo predictive assay. Oncogene **28**, 610-618 (2009).

97. Steegmaier, M. et al. BI 2536, a potent and selective inhibitor of polo-like kinase 1, inhibits tumor growth in vivo. Curr Biol **17**, 316-322 (2007).

98. Schmidt, M. & Bastians, H. Mitotic drug targets and the development of novel anti-mitotic anticancer drugs. Drug Resist Updat **10**, 162-181 (2007).

99. Peters, U., Cherian, J., Kim, J.H., Kwok, B.H. & Kapoor, T.M. Probing cell-division phenotype space and Polo-like kinase function using small molecules. Nat Chem Biol **2**, 618-626 (2006).

100. Workman, P., Clarke, P.A., Raynaud, F.I. & van Montfort, R.L. Drugging the PI3 kinome: from chemical tools to drugs in the clinic. Cancer Res **70**, 2146-2157 (2010).

101. Porta, C., Paglino, C. & Mosca, A. Targeting PI3K/Akt/mTOR Signaling in Cancer. Front Oncol **4**, 64 (2014).

102. Shaw, R.J. & Cantley, L.C. Ras, PI(3)K and mTOR signalling controls tumour cell growth. Nature **441**, 424-430 (2006).

103. Fruman, D.A. & Rommel, C. PI3K and cancer: lessons, challenges and opportunities. Nat Rev Drug Discov **13**, 140-156 (2014).

104. Stein, R.C. Prospects for phosphoinositide 3-kinase inhibition as a cancer treatment. Endocr Relat Cancer **8**, 237-248 (2001).

105. Liu, S., Knapp, S. & Ahmed, A.A. The structural basis of PI3K cancer mutations: from mechanism to therapy. Cancer Res **74**, 641-646 (2014).

106. Workman, P., Clarke, P.A., Guillard, S. & Raynaud, F.I. Drugging the PI3 kinome. Nat Biotechnol **24**, 794-796 (2006).

107. Chang, F. et al. Involvement of PI3K/Akt pathway in cell cycle progression, apoptosis, and neoplastic transformation: a target for cancer chemotherapy. Leukemia **17**, 590-603 (2003).

108. Martínez-Gac, L. et al. Phosphoinositide 3-kinase and Forkhead, a switch for cell division. Biochem Soc Trans **32**, 360-361 (2004).

109. Arcaro, A. & Guerreiro, A.S. The phosphoinositide 3-kinase pathway in human cancer: genetic alterations and therapeutic implications. Curr Genomics **8**, 271-306 (2007).

110. Liang, J. & Slingerland, J.M. Multiple roles of the PI3K/PKB (Akt) pathway in cell cycle progression. Cell Cycle **2**, 339-345 (2003).

111. Galan, P.P. et al. in 51st The American Society of Hematology Annual Meeting and Exposition (New Orleans, LA; 2009).

112. Kawamata, N., Chen, J. & Koeffler, H.P. Suberoylanilide hydroxamic acid (SAHA; vorinostat) suppresses translation of cyclin D1 in mantle cell lymphoma cells. Blood **110**, 2667-2673 (2007).

113. Rosenwald, I.B. et al. Eukaryotic translation initiation factor 4E regulates expression of cyclin D1 at transcriptional and post-transcriptional levels. J Biol Chem **270**, 21176-21180 (1995).

114. Mamane, Y. et al. eIF4E--from translation to transformation. Oncogene **23**, 3172-3179 (2004).

115. Patricia Perez-Galan, C.C., Xiameng Sun, Federica Gibellini, Poching Liu, Nalini Raghavachari and Adrian Wiestner in American Association for Cancer Research Annual Meeting (Washington, D.C.; 2010).

116. Luo, X., Budihardjo, I., Zou, H., Slaughter, C. & Wang, X. Bid, a Bcl2 interacting protein, mediates cytochrome c release from mitochondria in response to activation of cell surface death receptors. Cell **94**, 481-490 (1998).

117. Vermeulen, K., Van Bockstaele, D.R. & Berneman, Z.N. Apoptosis: mechanisms and relevance in cancer. Ann Hematol **84**, 627-639 (2005).

118. Dhanasekaran, D.N. & Reddy, E.P. JNK signaling in apoptosis. Oncogene **27**, 6245-6251 (2008).

119. Oussenko, I.A., Holland, J.F., Reddy, E.P. & Ohnuma, T. Effect of ON 01910.Na, an Anticancer Mitotic Inhibitor, on Cell-Cycle Progression Correlates with RanGAP1 Hyperphosphorylation. Cancer Res **71**, 4968-4976 (2011).

120. Manoj Maniar, S.M.e.a. in American Association for Cancer Research Annual Meeting (Washington, D.C.; 2010).

121. Yusof, I. & Segall, M.D. Considering the impact drug-like properties have on the chance of success. Drug Discov Today **18**, 659-666 (2013).

122. Di, E.H.K.a.L. Drug-like Properties: Concepts, Structure Design and Methods, Edn. 1st Edition. (Academic Press, 2008).

123. Lipinski, C.A., Lombardo, F., Dominy, B.W. & Feeney, P.J. Experimental and computational approaches to estimate solubility and permeability in drug discovery and development settings. Adv Drug Deliv Rev **46**, 3-26 (2001).

124. Congreve, M., Carr, R., Murray, C. & Jhoti, H. A 'rule of three' for fragment-based lead discovery? Drug Discov Today **8**, 876-877 (2003).

125. Nakashima, S., Yamamoto, K., Arai, Y. & Ikeda, Y. Impact of physicochemical profiling for rational approach on drug discovery. Chemical & pharmaceutical bulletin **61**, 1228-1238 (2013).

126. Veber, D.F. et al. Molecular properties that influence the oral bioavailability of drug candidates. J Med Chem **45**, 2615-2623 (2002).

127. Clark, D.E. & Pickett, S.D. Computational methods for the prediction of 'drug-likeness'. Drug Discov Today **5**, 49-58 (2000).

128. Ritchie, T.J. & Macdonald, S.J. The impact of aromatic ring count on compound developability--are too many aromatic rings a liability in drug design? Drug Discov Today **14**, 1011-1020 (2009).

129. Di, L. & Kerns, E.H. Profiling drug-like properties in discovery research. Curr Opin Chem Biol **7**, 402-408 (2003).

130. Selleckchem (Selleck Chemicals, 2013).

131. Chahrour, O., Abdalla, A., Lam, F., Midgley, C. & Wang, S. Synthesis and biological evaluation of benzyl styrylsulfonyl derivatives as potent anticancer mitotic inhibitors. Bioorg Med Chem Lett **21**, 3066-3069 (2011).

132. Devillers, J. (ed.) Neural Networks in QSAR and drug design. (Academic Press, San Diego, CA; 1996).

133. Timothy J. Ritchie, S.J.F.M., Simon Peace,b Stephen D. Pickettc and Christopher N. Luscombec The developability of heteroaromatic and

heteroaliphatic rings – do some have a better pedigree as potential drug molecules than others? MedChemComm **3**, 1062 (2012).

134. Meanwell, N.A. Synopsis of some recent tactical application of bioisosteres in drug design. J Med Chem **54**, 2529-2591 (2011).

135. Lima, L.M. & Barreiro, E.J. Bioisosterism: a useful strategy for molecular modification and drug design. Curr Med Chem **12**, 23-49 (2005).

136. Pallela, V.R. et al. Hydrothiolation of benzyl mercaptan to arylacetylene: application to the synthesis of (E) and (Z)-isomers of ON 01910.Na (Rigosertib(R)), a phase III clinical stage anti-cancer agent. Org Biomol Chem **11**, 1964-1977 (2013).

137. Gert-Jan M. Gruter, O.S.A., Friedrich Bickelhaupt Nuclear versus Side-Chain Bromination of Methyl-Substituted Anisoles by N-Bromosuccinimide. Journal of Organic Chemistry **59**, 4473-4481 (1994).

138. Djerassi, C. Brominations with N-bromosuccinimide and related compounds; the Wohl-Ziegler reaction. Chem Rev **43**, 271-317 (1948).

139. Hathaway, B.A. Organic Chemistry the Easy Way. (2005).

140. Lu, T. et al. Discovery of (E)-3-((styrylsulfonyl)methyl)pyridine and (E)-2-((styrylsulfonyl)methyl)pyridine derivatives as anti-cancer agents: synthesis, structure-activity relationships, and biological activities. J Med Chem (2014).

141. Lu, T. et al. Discovery of (E)-3-((Styrylsulfonyl)methyl)pyridine and (E)-2-((Styrylsulfonyl)methyl)pyridine Derivatives as Anticancer Agents: Synthesis, Structure-Activity Relationships, and Biological Activities. J Med Chem **57**, 2275-2291 (2014).

142. Vogel, C., Kienitz, A., Hofmann, I., Muller, R. & Bastians, H. Crosstalk of the mitotic spindle assembly checkpoint with p53 to prevent polyploidy. Oncogene **23**, 6845-6853 (2004).

143. Duldulao, M.P. et al. Gene expression variations in microsatellite stable and unstable colon cancer cells. J Surg Res **174**, 1-6 (2012).

144. Herz, C. et al. Occurrence of Aurora A positive multipolar mitoses in distinct molecular classes of colorectal carcinomas and effect of Aurora A inhibition. Mol Carcinog **51**, 696-710 (2012).

145. Birk, M., Burkle, A., Pekari, K., Maier, T. & Schmidt, M. Cell cycle-dependent cytotoxicity and mitotic spindle checkpoint dependency of investigational and approved antimitotic agents. Int J Cancer **130**, 798-807 (2012).

146. Morse, D.L., Gray, H., Payne, C.M. & Gillies, R.J. Docetaxel induces cell death through mitotic catastrophe in human breast cancer cells. Mol Cancer Ther **4**, 1495-1504 (2005).

147. Wu, R., Hu, T.C., Rehemtulla, A., Fearon, E.R. & Cho, K.R. Preclinical testing of PI3K/AKT/mTOR signaling inhibitors in a mouse model of ovarian endometrioid adenocarcinoma. Clin Cancer Res **17**, 7359-7372 (2011).

148. M T. Burger, M.K., A Wagman, Z Ni, T Hendrickson, G Atallah, Y Zhang, K Frazier, J Verhagen, K Pfister, S Ng, A Smith, S Bartulis, H Merrit, M Weismann, X Xin, J Haznedar, C F. Voliva, E Iwanowicz, and S Pecchi Synthesis and in Vitro and in Vivo Evaluation of Phosphoinositide-3-kinase Inhibitors. ACS Medicinal Chemistry Letters, 34-38 (2011).

149. Xu, W.J. et al. Efficient inhibition of human colorectal carcinoma growth by RNA interference targeting polo-like kinase 1 in vitro and in vivo. Cancer Biother Radiopharm **26**, 427-436 (2011).

150. Hikichi, Y. et al. TAK-960, a novel, orally available, selective inhibitor of polo-like kinase 1, shows broad-spectrum preclinical antitumor activity in multiple dosing regimens. Mol Cancer Ther **11**, 700-709 (2012).

151. Valsasina, B. et al. NMS-P937, an orally available, specific small-molecule polo-like kinase 1 inhibitor with antitumor activity in solid and hematologic malignancies. Mol Cancer Ther **11**, 1006-1016 (2012).

152. Roberts, D. et al. Identification of genes associated with platinum drug sensitivity and resistance in human ovarian cancer cells. Br J Cancer **92**, 1149-1158 (2005).

153. Watanabe, N., Okochi, E., Mochizuki, M., Sugimura, T. & Ushijima, T. The presence of single nucleotide instability in human breast cancer cell lines. Cancer Res **61**, 7739-7742 (2001).

154. Airley, R. Novel anticancer agents. (John Wiley & Sons Ltd, 2009).

155. Janos Fischer, C.R.G. Drug Likeness and Analogue-Based Drug Discovery. (Wiley-VCH, 2006).

156. A Montalbano, P.D., P Barraja, A Lauria, G Cirrincione, G Dattolo and A. M. Almerico. Pyrimido[5,4-c]pyrrolo[2,1-a]isoquinoline: a new potential DNA-interactive ring system. Archive for Organic Chemistry **2002**, 264-273 (2003).

157. F. Javier Lopez-Jaramillo, F.H.-M.a.F.S.-G. Vinyl Sulfone: A Multi-Purpose Function in Proteomics, in Intergrative proteomics. (ed. H.-C.E. Leung) 301-326 (2012).

158. Salvi M, T.E., Cozza G, Negro A, Hanson P.I, and Pinna L.A Tools to discriminate between targets of CK2 vs PLK2/PLK3 acidophilic kinases. BioTechniques, 1-5 (2012).

159. Burkard, M.E., Santamaria, A. & Jallepalli, P.V. Enabling and disabling polo-like kinase 1 inhibition through chemical genetics. ACS Chem Biol **7**, 978-981 (2012).

160. Kothe, M. et al. Selectivity-determining residues in Plk1. Chem Biol Drug Des **70**, 540-546 (2007).

161. Cyprotex in http://www.cyprotex.com/admepk/in-vitro-permeability/caco-2-permeability/, Vol. 2014 (2014).

162. Ades, E.W. et al. HMEC-1: establishment of an immortalized human microvascular endothelial cell line. J Invest Dermatol **99**, 683-690 (1992).

163. Hotchkiss, K.A. et al. Inhibition of endothelial cell function in vitro and angiogenesis in vivo by docetaxel (Taxotere): association with impaired repositioning of the microtubule organizing center. Mol Cancer Ther **1**, 1191-1200 (2002).

164. Jacobs, J.P., Jones, C.M. & Baille, J.P. Characteristics of a human diploid cell designated MRC-5. Nature **227**, 168-170 (1970).

165. Kennedy, A.S. et al. Survival of colorectal cancer cell lines treated with paclitaxel, radiation, and 5-FU: effect of TP53 or hMLH1 deficiency. Int J Cancer **90**, 175-185 (2000).

166. Limame, R. et al. Comparative analysis of dynamic cell viability, migration and invasion assessments by novel real-time technology and classic endpoint assays. PLoS One **7**, e46536 (2012).

167. Collection), A.A.T.C., Vol. 2012 (ATCC (American Type Culture Collection), 2012).

168. Deer, E.L. et al. Phenotype and genotype of pancreatic cancer cell lines. Pancreas **39**, 425-435 (2010).

169. Yunis, A.A., Arimura, G.K. & Russin, D.J. Human pancreatic carcinoma (MIA PaCa-2) in continuous culture: sensitivity to asparaginase. Int J Cancer **19**, 128-135 (1977).

170. Dolinsek, T. et al. Multiple delivery of siRNA against endoglin into murine mammary adenocarcinoma prevents angiogenesis and delays tumor growth. PLoS One **8**, e58723 (2013).

171. Mul, F.P. et al. Sequential migration of neutrophils across monolayers of endothelial and epithelial cells. J Leukoc Biol **68**, 529-537 (2000).

172. A. Burgener, M.P., K. Coombs, D. Moffatt, N. Huzel, Dr Michael Butler in The European Society for Animal Cell Technology meeting, Vol. 1 200-203 (ESACT Proceedings, 2001).

173. Hendzel, M.J. et al. Mitosis-specific phosphorylation of histone H3 initiates primarily within pericentromeric heterochromatin during G2 and spreads in an ordered fashion coincident with mitotic chromosome condensation. Chromosoma **106**, 348-360 (1997).

174. Shahbaba, B. (ed. K.H. Robert Gentleman, Giovanni Parmigiani) 135-137/ 349 (Springer, New York; 2012).

175. Díaz, J.F., Valpuesta, J.M., Chacón, P., Diakun, G. & Andreu, J.M. Changes in microtubule protofilament number induced by Taxol binding to an easily accessible site. Internal microtubule dynamics. J Biol Chem **273**, 33803-33810 (1998).

176. Vasquez, R.J., Howell, B., Yvon, A.M., Wadsworth, P. & Cassimeris, L. Nanomolar concentrations of nocodazole alter microtubule dynamic instability in vivo and in vitro. Mol Biol Cell **8**, 973-985 (1997).

177. Chu, J.J. & Ng, M.L. Infectious entry of West Nile virus occurs through a clathrin-mediated endocytic pathway. J Virol **78**, 10543-10555 (2004).

178. Oussenko, I.A., Holland, J.F., Reddy, E.P. & Ohnuma, T. Effect of ON 01910.Na, an anticancer mitotic inhibitor, on cell cycle progression correlates with RanGAP1 hyperphosphorylation. Cancer Res (2011).

179. Mollinedo, F. & Gajate, C. Microtubules, microtubule-interfering agents and apoptosis. Apoptosis **8**, 413-450 (2003).

180. Sumara, I. et al. Roles of polo-like kinase 1 in the assembly of functional mitotic spindles. Curr Biol **14**, 1712-1722 (2004).

181. Schmit, T.L. & Ahmad, N. Regulation of mitosis via mitotic kinases: new opportunities for cancer management. Mol Cancer Ther **6**, 1920-1931 (2007).

182. Toyoshima-Morimoto, F., Taniguchi, E. & Nishida, E. Plk1 promotes nuclear translocation of human Cdc25C during prophase. EMBO Rep **3**, 341-348 (2002).

183. O'Connor, P.M. et al. Role of the cdc25C phosphatase in G2 arrest induced by nitrogen mustard. Proc Natl Acad Sci U S A **91**, 9480-9484 (1994).

184. Lindqvist, A., Rodriguez-Bravo, V. & Medema, R.H. The decision to enter mitosis: feedback and redundancy in the mitotic entry network. J Cell Biol **185**, 193-202 (2009).

185. van Vugt, M.A. & Medema, R.H. Getting in and out of mitosis with Polo-like kinase-1. Oncogene **24**, 2844-2859 (2005).

186. Toyoshima-Morimoto, F., Taniguchi, E., Shinya, N., Iwamatsu, A. & Nishida, E. Polo-like kinase 1 phosphorylates cyclin B1 and targets it to the nucleus during prophase. Nature **410**, 215-220 (2001).

187. Qian, Y.W., Erikson, E., Li, C. & Maller, J.L. Activated polo-like kinase Plx1 is required at multiple points during mitosis in Xenopus laevis. Mol Cell Biol **18**, 4262-4271 (1998).

188. Wendy J. Fantl, Y.-W.H., Edn. G01N33/53, A61K39/395, C12Q1/68, C12Q1/37, C12Q1/02, A61K38/16, A61K31/7088, C12Q1/48 (Nodality, Inc. A Delaware Corporation, USA; 2009).

189. Osaki, M., Oshimura, M. & Ito, H. PI3K-Akt pathway: its functions and alterations in human cancer. Apoptosis **9**, 667-676 (2004).

190. Sancak, Y. et al. PRAS40 is an insulin-regulated inhibitor of the mTORC1 protein kinase. Mol Cell **25**, 903-915 (2007).

191. Choi, J.H., Sancar, A. & Lindsey-Boltz, L.A. The human ATR-mediated DNA damage checkpoint in a reconstituted system. Methods **48**, 3-7 (2009).

192. Cohen, G.M. Caspases: the executioners of apoptosis. Biochem J **326 (Pt 1)**, 1-16 (1997).

193. Vermes, I., Haanen, C., Steffens-Nakken, H. & Reutelingsperger, C. A novel assay for apoptosis. Flow cytometric detection of phosphatidylserine expression on early apoptotic cells using fluorescein labelled Annexin V. Journal of immunological methods **184**, 39-51 (1995).

194. Soldani, C. et al. Poly(ADP-ribose) polymerase cleavage during apoptosis: when and where? Exp Cell Res **269**, 193-201 (2001).

195. Oliver, F.J. et al. Importance of poly(ADP-ribose) polymerase and its cleavage in apoptosis. Lesson from an uncleavable mutant. J Biol Chem **273**, 33533-33539 (1998).

196. Adams, J.M. & Cory, S. Bcl-2-regulated apoptosis: mechanism and therapeutic potential. Curr Opin Immunol **19**, 488-496 (2007).

197. Kim, R. Recent advances in understanding the cell death pathways activated by anticancer therapy. Cancer **103**, 1551-1560 (2005).

198. Yamaguchi, M. et al. Mutation of DNA primase causes extensive apoptosis of retinal neurons through the activation of DNA damage checkpoint and tumor suppressor p53. Development **135**, 1247-1257 (2008).

199. Mah, L.J., El-Osta, A. & Karagiannis, T.C. gammaH2AX: a sensitive molecular marker of DNA damage and repair. Leukemia **24**, 679-686 (2010).

200. Kan, Q., Jinno, S., Yamamoto, H. & Okayama, H. Chemical DNA damage activates p21 WAF1/CIP1-dependent intra-S checkpoint. FEBS Lett **581**, 5879-5884 (2007).

201. Xu, N. et al. Akt/PKB suppresses DNA damage processing and checkpoint activation in late G2. J Cell Biol **190**, 297-305 (2010).

202. Rodriguez-Jimenez, F.J. et al. FM19G11: A new modulator of HIF that links mTOR activation with the DNA damage checkpoint pathways. Cell Cycle **9**, 2803-2813 (2010).

Appendix I

Kinase inhibitory activity of TL-77 and ON01910.Na

Experimental procedure

Kinases of interest (Aurora-A, Aurora-B, CDK1/cyclinB and Plk1) is incubated with 8 mM MOPS pH 7.0, 0.2 mM EDTA, proper substrate, 10 mM MgAcetate and [γ-^{33}P-ATP] (specific activity approx. 500 cpm/pmol, concentration as required). The reaction is initiated by the addition of the MgATP mix. After incubation for 40 minutes at room temperature, the reaction is stopped by the addition of 3% phosphoric acid solution. 10 μL of the reaction is then spotted onto a P30 filtermat and washed three times for 5 minutes in 75 mM phosphoric acid and once in methanol prior to drying and scintillation counting. ATP concentration is used within 15 μM of the Km value for each kinase.

[Non-radioactive assay] PI3 Kinase is incubated in assay buffer containing 10 μM phosphatidylinositol 4,5-bisphosphate (PIP_2) and MgATP (concentration as required). The reaction is initiated by the addition of the proper substrate. After incubation for 30 minutes at room temperature, the reaction is stopped by the addition of stop solution containing EDTA and biotinylated phosphatidylinositol- 3,4,5-trisphosphate. Finally, detection

buffer is added, which contains europium-labelled anti-GST monoclonal antibody, GST-tagged GRP1 PH domain and streptavidin allophycocyanin. The plate is then read in timeresolved fluorescence mode and the homogenous time-resolved fluorescence (HTRF) signal is determined according to the formula HTRF = 10000 x (Em665nm/Em620nm).

Appendix Table 1. Kinases assay information

Kinase	Construct	Enzyme final concentration (µM)	Substrate	Substrate concentration	ATP concentration
Aurora-A(h)	Full length; I31F	0.0064	LRRASLG	200 µM	15 µM
Aurora-B(h)	Full length	0.0323	AKRRRLSSLRA	30 µM	10 µM
CDK1/cyclinB(h)	Full length	0.000662	Histone H1	0.1 mg/ml	45 µM
PI3 Kinase (p110a/p85a)(h)	Full length	0.000242	PIP2	10 µM	200 µM
PI3 Kinase (p110b/p85a)(h)	Full length	0.000333	PIP2	10 µM	200 µM
Plk1(h)	Full length	0.0974	Casein	1.25 mg/ml	70 µM

Results

Appendix Table 2. Kinase inhibitory activity of TL-77 and ON01910.Na

	Activity±SD (% Control)					
Sample	Aurora-A(h)	Aurora-B(h)	CDK1/cyclinB(h)	Plk1(h)	PI 3-Ka(h)	PI 3-Kb(h)
Control (Plus Enzyme)	100	100	100	100	100	100
Control(Blank)	/	/	/	/	0	0
TL-77 2μM	93±4	104±2	108	105±0	98±1	95±2
TL-77 4μM	95±6	106±7	111	105±3	98±1	94±1
TL-77 8μM	96±7	98±1	110	112±4	98±3	95±2
TL-77 16μM	112±3	94±6	103	101±7	98±2	95±1
ON01910.Na 0.03μM	104±0	100±4	111	100±4	99±0	96±0
ON01910.Na 0.06μM	108±1	103±4	110	107±4	98±0	97±1
ON01910.Na 0.12μM	98±4	102±2	109	104±2	98±0	99±0
ON01910.Na 0.24μM	105±5	99±2	102	100±2	97±2	98±1

Plk1 kinase inhibitory profile of ON01910.Na reported by Gumireddy et al

Plk1 expressed in the Sf9 cell line was purified. 10 ng of recombinant Plk1 was incubated with different concentrations of ON01910 in a 15 µl reaction mixture (50 mM HEPES, 10 mM $MgCl_2$, 1 mM EDTA, 2 mM Dithiothreitol, 0.01% NP-40 [pH 7.5]) for 30 min at room temperature. Kinase reactions were performed for 20 min at 30°C in a volume of 20 µl (15 µl enzyme + inhibitor, 2 µl 1 mM ATP), 2 µl of γ ^{32}PATP (40 µci), and 1 µl of recombinant Cdc25C (100 ng) or casein (1 µg) substrates. Reactions were terminated by boiling for 2 min in 20 µl of 2× Laemmli buffer. Phosphorylated substrates were separated by 18% SDS-PAGE. The gels were dried and exposed to X-ray film for 3–10 min.[53]

Appendix II

Awards:

Feb. 2013	Graduate School Travel Prize The University of Nottingham
Dec.2012	EORTC-PAMM fellowship to attend the EORTC-PAMM-BACR conference EORTC-PAMM group

Publications, patents and proceedings:

- **Lu, T.** et al. Discovery of (E)-3-((Styrylsulfonyl)methyl)pyridine and (E)-2-((Styrylsulfonyl)methyl)pyridine Derivatives as Anticancer Agents: Synthesis, Structure-Activity Relationships, and Biological Activities. J Med Chem **57**, 2275-2291 (2014).
- **Lu T.,** Laughton C. A., Wang S., Bradshaw D T. In vitro anti-tumour mechanism of (E)-N-(2-methoxy-5-(((2,4,6-trimethoxystyryl)sulfonyl)methyl)pyridin-3-yl)methanesulfonamide. Molecular Pharmacology, Accepted on October 14, 2014
- **Lu T.,** Wang S., Laughton C. A., Bradshaw D T. Abstract 3406: Evaluation of (E)-Styrylsulfonyl methylpyridine: A novel kinase inhibitor targeting mitotic pathways. AACR 104th Annual Meeting 2013; Washington, DC. Cancer Research: April 15, 2013; Volume 73, Issue 8, Supplement 1.
- Wang, S.; Chahrour, O.; **Lu, T.;** Hu, A. Compounds for treating proliferative disorders, International patent, WO2011161446. 21 June, 2011.
- **Lu Tiangong**. Review and prospect of Gecko anti-tumor action and its pharmacological mechanism, Chinese Journal of Medicine, Volume 9, periodical 6, 2009, ISSN1680-077X, CN98-0333/R

Conference presentations:

- Synthesis and evaluation of (E)-Styrylsulfonyl Methylpyridine: a novel mitotic kinase inhibitor
  Podium presentation
  7th Biological and medicinal chemistry symposium
  13 Dec. 2013. Cambridge, UK
- Evaluation of (E)-Styrylsulfonyl methylpyridine: a novel kinase inhibitor targeting mitotic pathways
  Poster presentation
  AACR conference 2013 (Abstract Number: 3406)
  6-10 Apr. 2013. Washington DC, US
- Evaluation of (E)-Styrylsulfonyl Methylpyridine: a novel mitotic kinase inhibitor
  Podium
  34th EORTC-PAMM-BACR Winter conference
  23-26 Jan. 2013. Cardiff, UK
- Discovery and Evaluation of (E)-Styrylsulfonyl methylpyridines as Novel Anti-cancer Agents
  Podium &Poster presentation
  UK-PharmSci 2012
  12-14 Sep. 2012. Nottingham, UK

Appendix III

In: Proceedings of the 104th Annual Meeting of the American Association for Cancer Research

2013 Apr 6-10; Washington, DC. Philadelphia (PA)

AACR; Cancer Res 2013;73(8 Suppl):Abstract nr 3406. doi:10.1158/1538-7445.AM2013-3406

Abstract 3406: Evaluation of (E)-Styrylsulfonyl methylpyridine: A novel kinase inhibitor targeting mitotic pathways.

Tiangong Lu, Shudong Wang, Charles Laughton, and Tracey Bradshaw.
University of Nottingham, Nottingham, United Kingdom.

ON01910.Na, a styryl benzylsulfone, is a Phase III stage, non-ATP competitive anti-cancer agent. It is multi-targeted, promoting selective mitotic arrest and apoptosis in cancer cells. Extensive Phase II/III trials conducted in patients with solid tumors and hematological cancers have proved its excellent efficacy and impressive safety profile. However, incomplete understanding of mechanisms of action and relatively low drug oral bioavailability remain obstacles to development. By modifying the structure of ON01910.Na, a novel class of (E)-Styrylsulfonyl methylpyridines was designed and synthesized. I report herein the evaluation of a selected compound, TL-77, (E)-N-(2-methoxy-5-((2,4,6-trimethoxystyrylsulfonyl)methyl)pyridin-3-yl)methanesulfonamide, as a potent small molecule inhibitor targeting mitotic pathways.

MTT assays were performed to assess in vitro anti-proliferative effects. In a panel of 10 tumor and 2 non-transformed human cell lines following 96 h exposure, TL-77 gave consistent GI_{50} values in the sub-micromolar range in tumor cells, whereas, it was non-toxic to non-transformed human mammary endothelial cells (HMECs). Cell cycle was analyzed by flow cytometry. TL-77 caused significant G2/M arrest $\geqslant$ 6 h, whereas ON01910.Na caused the same effect after longer exposure periods ($\geqslant$ 12 h). An OD-based tubulin polymerization assay allowed us to explain obstruction of cell division caused by TL-77. TL-77 retarded tubulin polymerization between 1μM and 6μM, intriguingly, microtubules were stabilizes at TL-77 concentrations > 8μM. Western blot analyses of cell lysates following treatment of cells with TL-77 revealed dose-dependent reduction of phosphorylated Cdc25c, a known substrate of Plk1 and/or Chk1/2, indicating Plk1 and/or Chk1/2 inhibition. Finally, dose- and time-dependent apoptosis triggered by TL-77, detected by Annexin-V assays, was closely associated with induction of caspase 3/7 activity. Importantly, pharmacokinetics studies in mice revealed that the oral bioavailability of TL-77 was optimized to 56% compared with 9% for ON01910.Na.

In summary, TL-77 is a potent anti-cancer agent. It disturbs tubulin during cell division, resulting in G2/M cell cycle arrest, followed by caspase-dependent apoptosis. TL-77 appears to share an analogous mechanism of action with ON01910.Na, but exhibits greater selectivity towards cancer cells and possesses superior oral bioavailability. Therefore, further evaluation of TL-77 as a promising anti-tumor agent is justified.